2019 Doctor Dissertation

Femtosecond Laser-Actuated High-Speed Cell Manipulation in a Microfluidic Chip

(フェムト秒レーザー誘起衝撃力を用いたマイクロチップ中での高速細胞操作)

Zhen-Yi Hong (洪振益)

Nara Institute of Science and Technology

Materials Science　Bio-Process Engineering Lab

（Main supervisor　Hosokawa Yoichiroh）

Submission Date: January. 8, 2019

Index

Chapter 1 Introduction

The rapidly developing single-cell research in the recent decade will be introduced, and a significant role of single-cell manipulation in the research will be elucidated along with its development bottlenecks in the first section. In the second section, to overcome the issues, microfluidic devices attract massive attentions from researchers worldwide to establish diverse manipulation methods on the devices, among which inspired us the potential of ultrafast laser for great improvements. Such potential of the ultrafast laser will be interpreted with its multiple advantages in the third section.

1.1 Single-cell manipulation

Cell is well-known as the most basic biological unit of structure and function that composes most of creatures on earth and is called "building blocks of life". An in-depth understanding on cellular behaviors and their properties serves as a scientific foundation in life sciences, pharmaceutical development, clinic diagnosis, and renewable energy, et. al [1,2]. Conventional cellular researches focus on the average response from a vast cell population, which is assumed to be a representative of a cell type. Unfortunately, clonal cells in an identical environment could even have different response to a same stimulation, which is due to stochastic nature of cell for fate-determining. This simplification can yield a misleading interpretation since cells with identical morphology and genes maybe actually heterogeneous and differ dramatically [3-6]. This heterogeneity can result from genetic drift, differences in cell development or cell cycle status, differences in cell age due to proliferation/passaging and non-genetic heterogeneity because of inherent stochasticity of cellular processes. Any cellular heterogeneity above can notably influence cell fate and decision making [7]. For example, a recent study on hormone-determined maturation process of unfertilized eggs (oocytes) revealed different results from a cell group and single cells [8]. The population data showed a graded dependence on the hormone concentration, while the single-cell data indicates a sharp yes-or-no switch. The single-cell research not just provides complementary information but uncovers the complex working mechanisms of biological system from cell level. This basic knowledge is necessary for understanding on tissues, organs, or even whole organism.

To have investigation on single cells in a ten-of-micrometers scale in general, it is the first step to have invisible hands to handle them from a cell population prior to cell analysis or further treatment. Plenty of manipulation tools for single cell have

then been employed such as micro-pipette [9-12], optical tweezer, magnetic tweezers and atomic force cantilever [13]. Especially, the optical tweezer, so-called laser trapping, was invented by Ashkin, the 2018 Nobel Prize winner in physics (Fig. 1a) [14]. It is a powerful tool with not only high spatial resolution for tiny objects even down to size range from ~20 nm to several micro-meters. This includes not only single cells but even organelles within cells. Ashkin applied this optical tweezer system to have long-term trapping of yeast and studied on cell division (Fig. 1b) [15]. He demonstrated a strong capability of optical tweezer with a three-dimensional object trapping and a manipulation speed up to 500 μm/s. Umehara's group utilized the optical tweezer to place and isolate one single bacteria in a micro-chamber for micro-cultivation, which enable the production of genetically identical bacteria for gene expression study by flowing different nutrients through the microfluidic system [16]. Optical tweezer offers a high resolution for single-cell trapping and widely applied to study on single cells [17], intra-cellular organelles [18], lipid vesicles [19, 20] and polystyrene or silica microspheres [21]. Unfortunately, the high-resolution property serves not only an advantage but also a drawback, which means a limited manipulation area owing to tight focusing requirements of laser [22]. What's worse, optical tweezer along with other single-cell manipulation tools are dramatically time-consuming to process a cell population one by one although it could facilitate acquirement of massive information. The manipulation throughput (efficiency) was improved by increasing the number of laser beam such as dual-beam laser [23] and vertical cavity surface emitting lasers (VCSEL) from Flynn's group [24, 25]. Sorrowfully, beam splitting had an issue of weak trapping strength, not to mention employment of multiple laser systems. Particularly, single cell research requires massive data to receive a statistically meaningful result on the contrast of the population method. Hence, a new manipulation tool of high throughput (efficiency) is critical for development of single cell research. This tremendous requirement boosts rapid development of "microfluidic device" in this decade.

(a) (b)

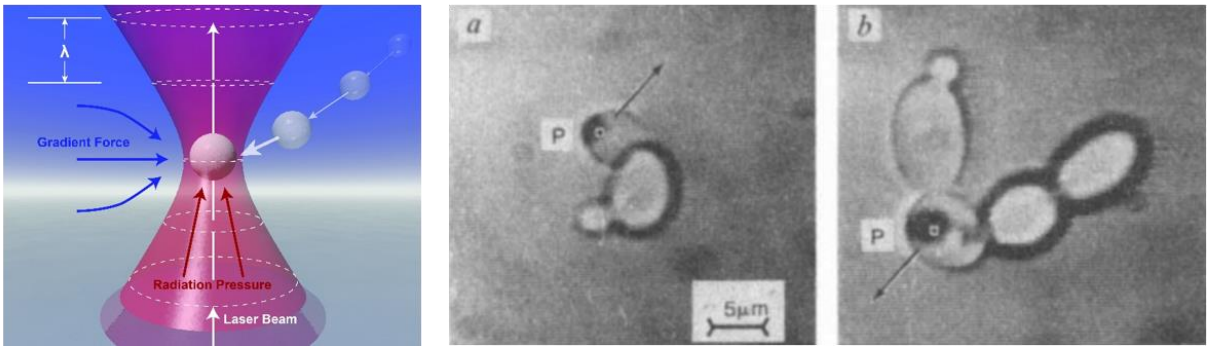

Fig. 1 (a) Illustration of optical tweezer for micro-particles at the focal point of a laser [http://padenroder.com/laser-tweezers/] (b) Long-term trapping of yeast for studying on cell division [15]

1.2 Single-cell manipulation in microfluidic chip

Microfluidics is an innovative research field which rapidly develops in the two decades. Back in 1908s, an inspiring concept, MEMS (micro-electro-mechanical system), was proposed as miniaturized micro-devices by exploring the distinct electronic properties under micro-scale for higher performance and more functions. The first microfluidic device, a gas chromatograph, appeared under development of silicon-based MEMS, then various microfluidic chips began to flourish since 1991 [26]. With a great development in 2006, George Whitesides, a leading researcher in this microfluidics field, interpreted microfluidic device as "the science and technology of systems that process or manipulate small (10^{-9} to 10^{-18} L) amounts of fluids (Fig. 2), using channels with dimensions of tens to hundreds of micrometers" [26]. With these unique microfluidic properties introduced in chapter 2, the microfluidic technique is then put into applications.

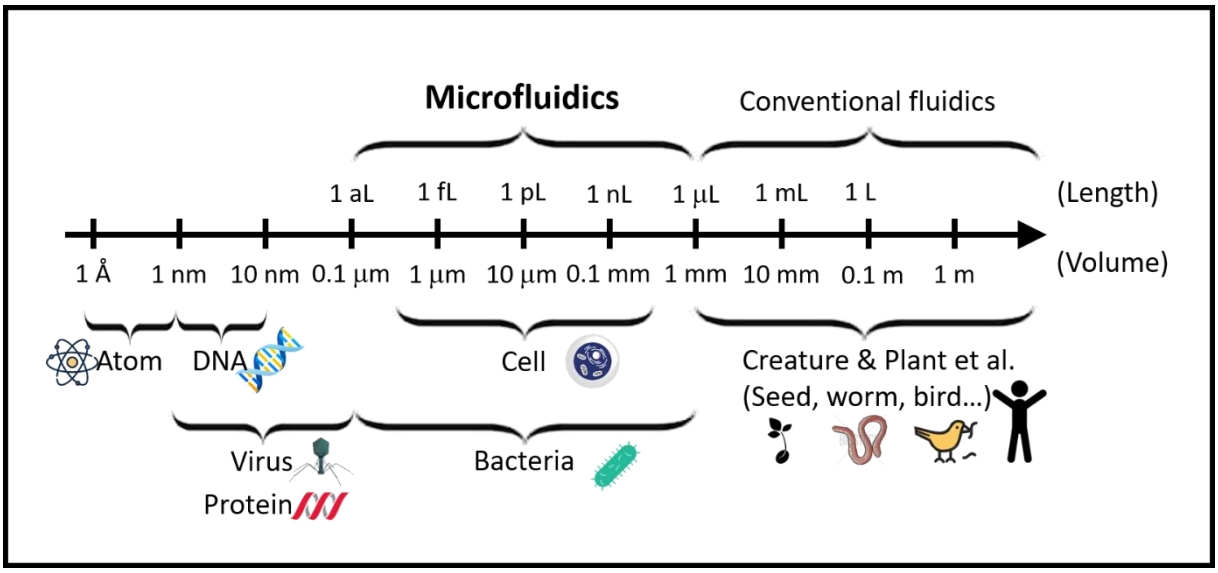

Fig. 2 Characteristic sizes of various devices and objects

Over the past two decades, micro-fluidic technique has a great development in the field of single-cell research, as micro-fluidic systems have the advantages of high efficiency, easy operation, small sample and reagent consumption, and dimension matching between channels and cells [27]. The micro-fluidic devices enable to perform single-cell monitoring, manipulation, treatment, analysis, et. al [28]. For instance, single-cell manipulation in a microfluidic system was realized for the first time in 1997 [29]. Since then, cell culture [30], cell separation [31], component analysis [32], and various operations on single cell were realized one by one and

optimized for their performance. In assistance of more and more powerful micro-fabrication techniques, the micro-fluidic devices are named as micro total analysis systems (μTAS) and lab-on-a-chip (Fig. 3), which means most of experimental operations could be conducted, automized and even integrated in such a small microfluidic chip. A microfluidic chip is designed diversely with channels, branches, valves, cavities and so on according to purposes. All the complicated channels could be regarded as roads. To drive all the samples toward their destination, it is essential component to have them make turns, which manipulation their flow direction by switching the flowing track. When it comes to automation, throughput (efficiency) is definitely one of the top important parameters. The speed of the microfluidic switch determines how fast each process can be passed on to the next step and in turn the final throughput of the microfluidic function in a given time duration.

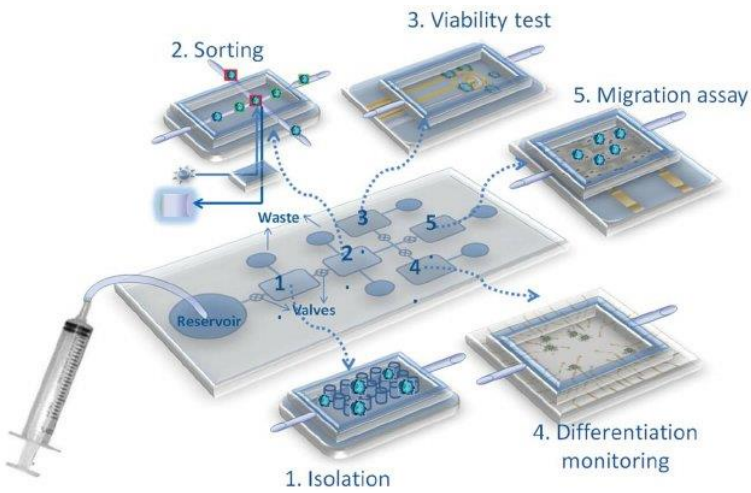

Fig. 3 Concept of lab-on-a-chip with various functions [28]

Although it could bring us high throughput and other benefits in assistance of microfluidic device, single-cell manipulation on a moving object is obviously a technical obstacle, not to mention targets with high-speed movement so as for a high throughput. A cell recognition for a triggering signal at the upstream is usually required to actuate the manipulating force aiming at the coming targets, but we will not discuss it since our research focuses on the development of manipulation system. To realize single-cell manipulation in a fluid, many tools and techniques were proposed and could be categorized into five groups based on type of their manipulating force, which are magnetic, optical, mechanical, electrical and other (Fig. 4).

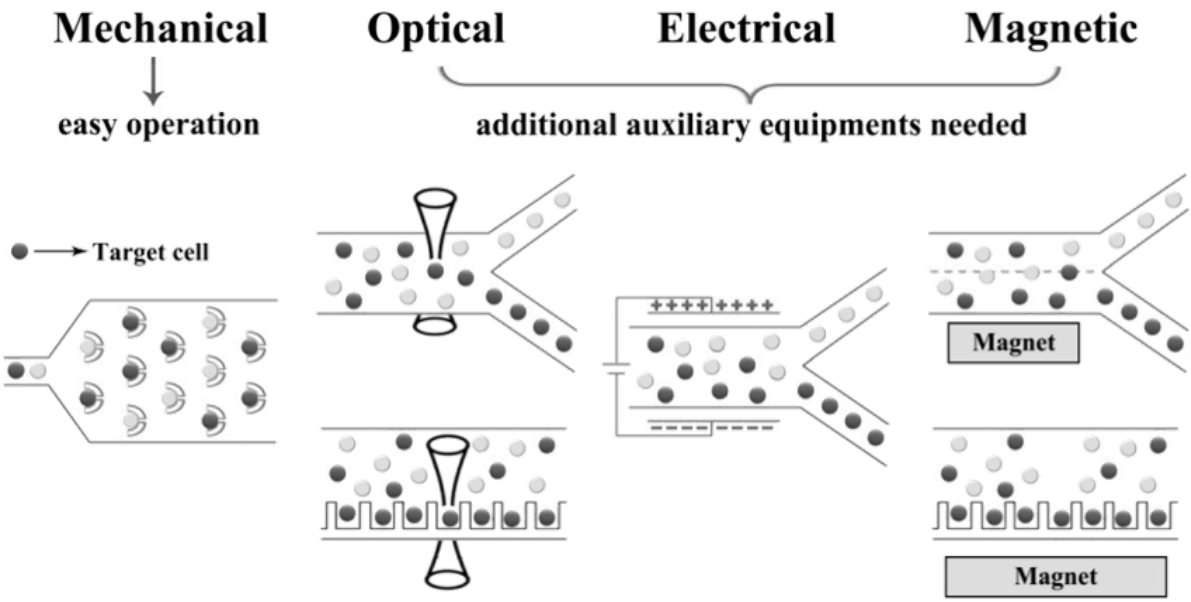

Fig. 4 Classification of single-cell manipulation methods in the microfluidic chip based on types of their manipulating forces

(1) Magnetic Forces

For magnetic manipulation, it is a common method that selectively attaches magnetic particles to targeted cells and manipulates them by tuning magnetic force field. Super-paramagnetic particles are the most popular material with diameter of 10–100 nm and this extremely tiny size is said to impose little influence on the cellular function and cell viability. Besides, this magnetic method has high specificity because binding factors for attaching onto cells of interest are highly selective. Taking immunology research for example, cells were incubated with antibody-coated paramagnetic particles before the manipulation process [33]. In spite of high specificity, it is highly restricted by a few types of binding factor, which makes magnetic manipulation method less applicable. To solve this problem, there is no shortcut but only cooperation with growing bio-chemistry for diverse binding factors to increase applicability of the magnetic manipulation.

(2) Electrical Forces

An electric field is a common tool for electric manipulation and gives rise to some approaches like electrokinetics and dielectrophoresis. Particularly, dielectrophoresis (DEP) is highly competent to have manipulation on objects of all dimension since most of materials exhibit dielectrophoretic properties in the presence

of an electric field. Dielectrophoresis is the electronic analog of optical tweezer [34, 35] and exerts its manipulation force on a neutral cell by a non-uniform electric field (Fig. 5). Strength and direction of the dielectrophoretic force relates to not only magnitude of the electric field but also size and frequency-dependent polarizability of a target [36]. With such selectivity, various applications have been demonstrated in a micro-fluidic chip, such as trapping of biological cells [37-40], sorting of blood cells [41], bacteria [42] and isolation of circulating cancer cells (CTC) from blood [43]. In case of identical responses to DEP force between a target and a non-target, the selectivity could still be retained in assistance of dielectric tagging through suitable surface binding [42, 44]. Nevertheless, these electric manipulation methods with electric field imposes undesired biological stress such as protein migration and clustering within the cells and so on.

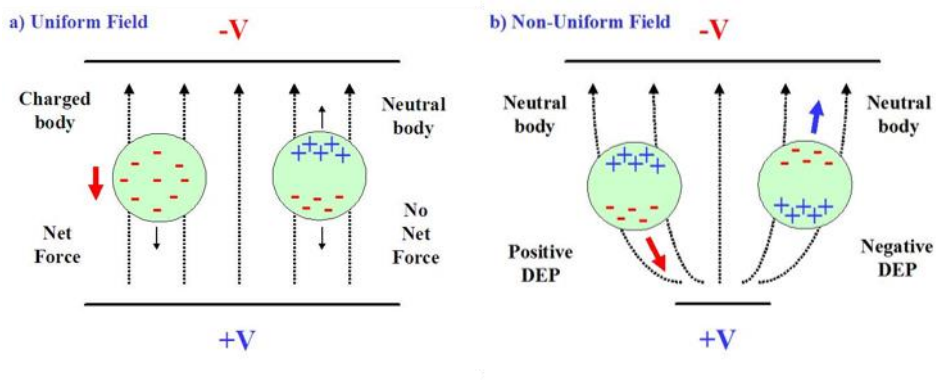

Fig. 5 Schematic illustration of dielectrophoresis (DEP) force [Course materials prepared by Jong Min Sung in Stanford University]

(3) Mechanical Forces

Among these forces, mechanical force is the most popular as a manipulation tool due to its easy operation without requirement of additional auxiliary instruments in comparison with other forces. Mechanical force is generated with the aid of specially-designed micro-structures inside the channel of microfluidic chip. Firstly, the micro-structures could trap targets directly with various designs like micro-grippers [45], micro-wells [46], micro-filters [47], micro-chambers [48], etc. VanDelinder and Groisman utilized a cross channel with smaller dimension to the main channel to extract white blood cells (WBCs) of smaller size from whole human blood [49]. With even higher trapping force and selectivity, Lee and Di Carlo made efforts on developing a U-shaped trapping microstructure array with surface modification [50].

Lin's group demonstrated trapping and positioning of single cells with sieve-like trap arrays in a microfluidic channel [51]. Secondly, the micro-structures also enable generation of microfluidic force to manipulate their flowing direction. For example, Di Carlo's group [52] reported a microfluidic force of a secondary flow arising in a curved rectangular micro-channel, which allocated micro-particles with different flowing position in the channel based on their size. Di Carlo's group also interrogated one of the of microfluidic forces, inertial lift force, to be a manipulation force and applied the size- and shape- dependency of this force to achieve a high-throughput label-free cell sorting and enrichment for isolation of circulating cancer cells (CTC) from whole blood sample [53]. Besides, a micro-vortex emerged in a micro-well was applied to pick up and trap cells according to cell size by the same research group [54].

In general, mechanical forces execute the manipulations on the basis of cell size no matter direct trapping by micro-structures or guiding of targets' flow direction by a microfluidic force around the micro-structures. This mechanical manipulation demonstrated a high-throughput, high reproducibility, high selectivity for cell size and no requirements of auxiliary tools like electric fields, magnetic fields, acoustic wave, lasers and so on. Although it could be a potential method for point-of-care diagnostics with its easy manipulation, it shows low specificity to conduct the manipulation just based on size of targets, which limits its applicability.

(4) Acoustic Forces

A surface-acoustic wave could serve as another non-contact tool to manipulate single cells in a microfluidic channel. The acoustic manipulation is implemented with an ultrasonic standing wave produced by a pair of interdigital transducers (IDT) while applying electricity. This ultrasonic standing wave induces acoustic radiation force [55] and was applied to cell positioning [56] and cell sorting [57] with advantages such as strong manipulation force, short actuation time and little damage to cells [58, 59]. Friend and Yeo has demonstrated a fast manipulation speed of 1–10 cm/s by this surface-acoustic wave [60]. Huang and his group applied this acoustic force to manipulate particles, cells and organisms like HeLa cells and C. elegans [61]. Weak points of this acoustic manipulation is size-dependency of the acoustic force, which means a shortage of specificity for samples composed of cells in similar size. This makes the acoustic manipulation less applicable as the mechanical manipulation who suffers from the same problem. In addition, a popular material for microfluidic chip,

Polydimethylsiloxane (PDMS), has been found to absorb acoustic energy, which heat up the PDMS quickly [62]. This is another drawback for the acoustic manipulation.

(5) Optical Forces

Recently, optical manipulation on biological species receives more and more interest due to transparent materials of microfluidic chip, non-contact and contamination-free manipulation process. Optical tweezer is a well-known technique for single-cell manipulation by trapping targets at the focal point of laser. With its natural properties of light, it is easy to combine optical tweezer with microfluidic systems, and this is the most common method for optical manipulation in microfluidic devices. Xiaolin Wang and his group proposed a transparent PDMS microfluidic system integrated with optical tweezer and applied such on-chip optical tweezer system to position yeast cells and human embryonic stem cells (hESCs) for selection and isolation [63, 64]. In contrast to trapping, a set of laser focuses was lines up to pull a target little by little toward its destination, which was named as laser guidance by Robert W. Applegate Jr's group [65]. Due to the weak trapping force of optical tweezer, it required a slow flow speed and a long working distance to have a stable trapping and a visible position change of a target, and this therefore highly limited the throughput of this on-chip optical tweezer.

To overcome the throughput issue, Pei-Yu Chiou and his group proposed a novel idea to conduct the manipulation with an impulsive force induced by a nano-second pulsed laser (ns-laser). As Fig. 6, they prepared a parallel channel as a flexible packet for nano-second pulsed laser to switch the flow direction of targets with a pushing force, which induced by the expanding packet as laser irradiation [66]. This method achieved a high throughput with characteristics of a pulsed laser, which could generate thousands of or even millions of pulses to actuate the manipulation of flow switching. With such powerful advantages, this pulsed-laser manipulation system was optimized for a throughput up to 45,000 cell/s with a high purity of 45% at the same time [67].

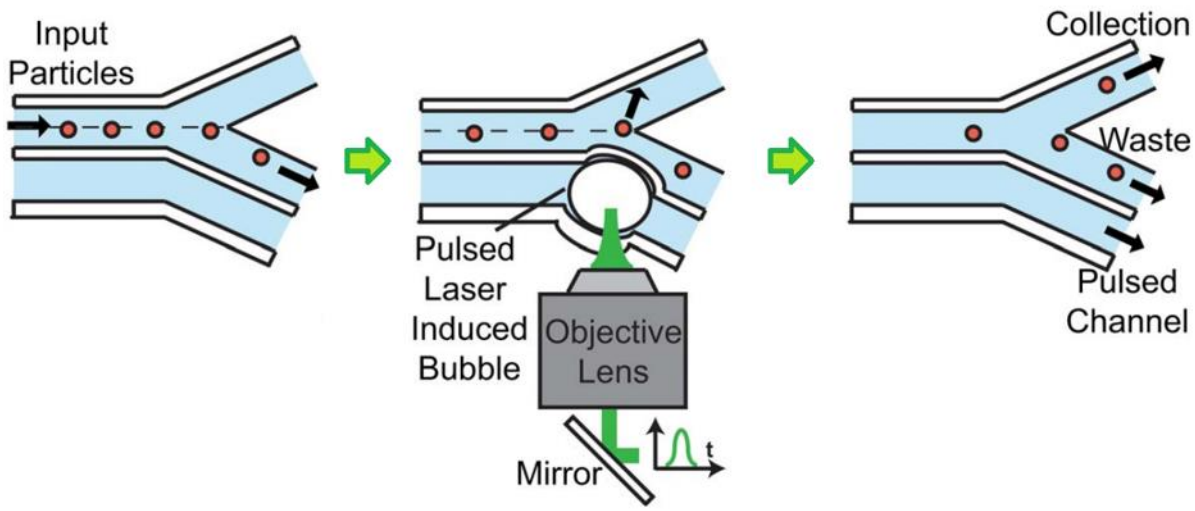

Fig. 6 An optical manipulation method with a nano-second pulsed laser proposed by Pei-Yu Chiou's group [66]

1.3 Ultra-fast pulsed laser

Discovery of laser has aroused a huge revolution for both scientific and technological applications, especially after realization of an intense ultra-fast pulsed lasers by Mourou and Stricktland, laureates of 2018 Nobel Prize in physics, in the 1980s [68, 69]. Highly intense and ultra-short laser pulses could be achieved in assistance of chirped pulse amplification technique and became a versatile tool for a wide variety of research fields. For example, with ultra-short laser pulse duration in a range of 10^{-12} – 10^{-15} seconds, instantaneous chemical reactions at the atomic level could be initiated and analyzed, which facilitates development of photochemistry and spectroscopy [70, 71]. In addition, an extremely high peak power within the ultrashort pulse duration could even induce strong nonlinear light-matter interactions, which brought up with new optical phenomenon, such as formation of spatio-temporal solitons [72, 73] and generation of coherent white light (white light laser [74]). The solitons behave as "solitary waves" that could propagate for a long distance with a constant shape and are capable of interacting with other solitons. The formation and propagation of solitons is greatly significant to exploit a potential technique in optical communications and optical computing. Furthermore, laser micromachining was advanced with the property of ultrashort pulse duration, which suppresses the heat accumulation issues like distortion and cracks to provide cleaner cuts for devices of higher performance. [75]

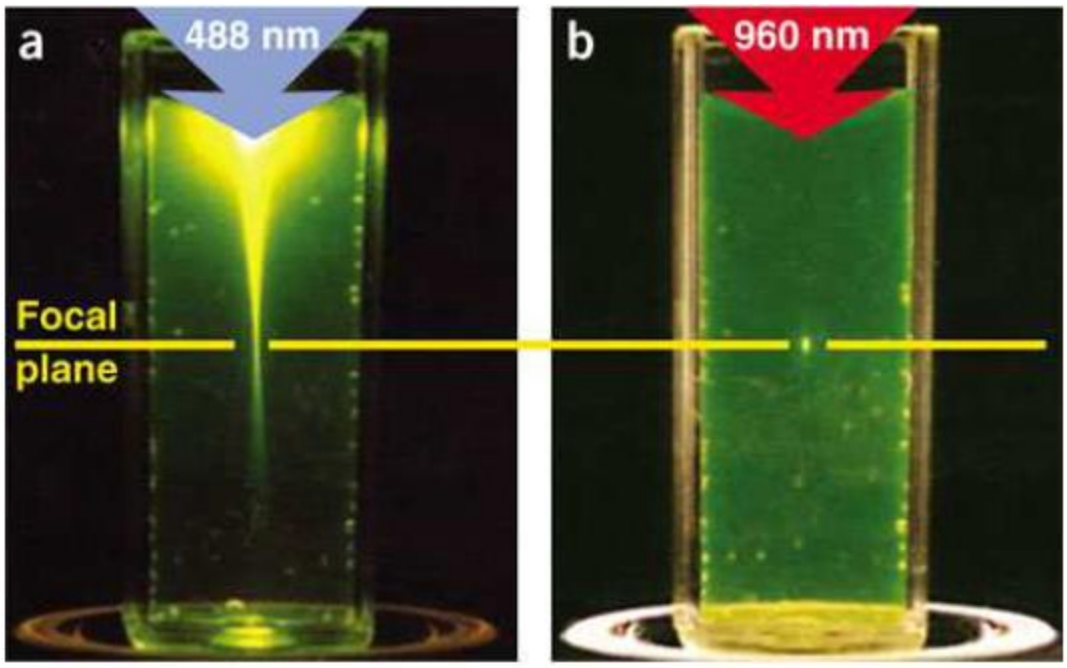

Fig. 7 Non-linear absorption with a pulsed laser [76]

In biological research field, the ultrashort pulse lasers are popular for its highly efficient non-linear absorption effect, which is strictly confined at the focal point for a precision beyond diffraction limitation [76, 77] (Fig. 7). This non-linear absorption has inspired multiphoton imaging for biology researches like two-photon excitation microscopy (TPEF) [78] and second-harmonic imaging microscopy (SHG) [79, 80]. Moreover, the ultrashort pulse lasers are particularly beneficial for biological and medical research with their common wavelength specification in near-infrared range, which has a high penetration depth in biological samples. In combination of this high spatial resolution and ultra-short pulses with intense peak power, the ultra-fast pulsed laser became an appealing manipulation tool for applications like laser ablation, which creates precise and confined damage on a small targeted spot, also called by laser surgery. A variety of biological and medical research were developed, ranging in scale from in vitro sub-cellular dissection of organelles [81-83] and chromosomes [84] to in vivo functional manipulation of animal organ such as eyes [85], skin [86], and teeth [87]. In this decade, the ultra-fast pulsed laser was even put into clinical applications like ophthalmology [88-89], dermatology [90], and otolaryngology [91].

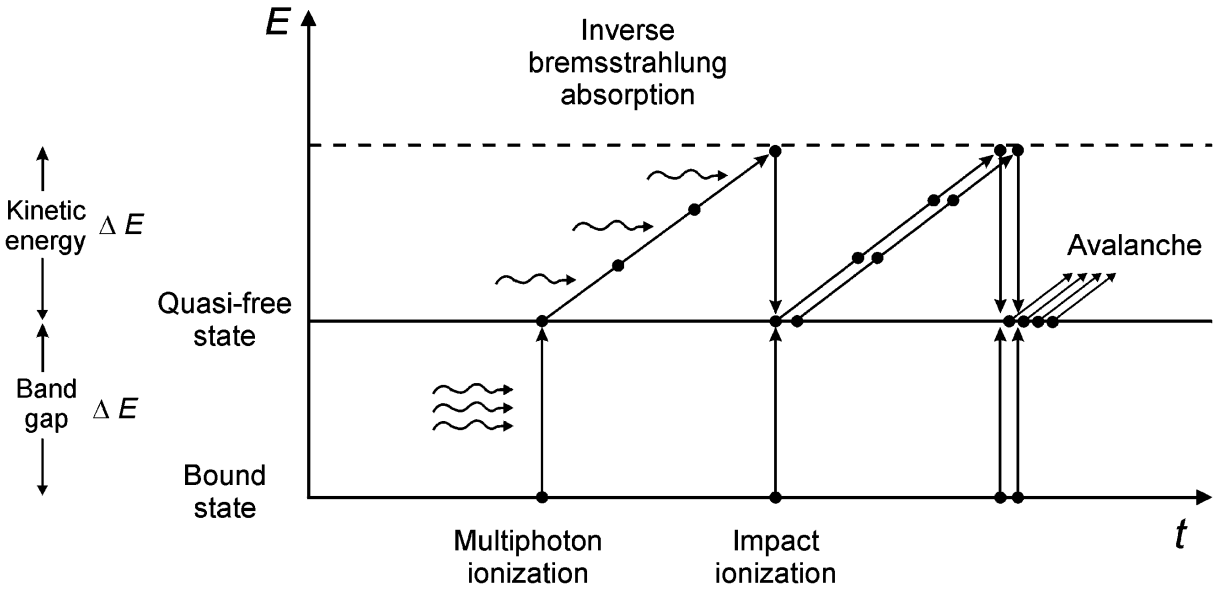

Fig. 8 Photonic mechanism induced by an ultra-fast laser [96]

Hence, for the widespread use of ultra-fast lasers in medical and commercial applications, a physical understanding of the interaction between the laser pulses and biological medium has been explored [92-95]. When an intense ultra-fast laser pulse is focused at a biological tissue or in a physiological medium, a plasma formation occurs with high density free electrons at the laser focal point under the strong electric

field of the laser (Fig. 8) [96]. An electron gains enough kinetic energy from the electric field of laser (photo-excitation) and escapes from confinement of local potential barrier of a molecule to be a free electron, which is called photo-ionization. This escaping electron is kept accelerating in the strong electric field of laser. As it accumulates enough kinetic energy, this speedy free electron would bring out another free electron by collision with an atom or a molecule, which is called impact ionization process. Repeatedly, these two free electrons absorb energy and make collisions again for more free electrons, which initiates an electron avalanche process to produce appreciable densities of free electrons as a plasma within a short time. The whole process of plasma formation takes place within tens of picoseconds [97]. This duration of plasma formation process is much shorter than the micro-second time scale of the heat evolution and diffusion, which correspond to a slow equilibrium process of intermolecular distance between medium molecules and a confinement of the vigorous molecules at the laser focal point. A confined stress is induced and propagates from the focal point to the surrounding medium with a sonic speed (> 1 μm/ns) as shock and stress waves. The stress propagation abruptly decreases hydrostatic pressure around the laser focus (< 1 atm) and induces its explosive vaporization without a considerable temperature increasing, which corresponds to the formation of a cavitation bubble (Fig. 9) [98]. The bubble expands and displaces the surrounding medium within a few microseconds. The combination of the stress wave and cavitation bubble gives rise to the impulsive force on an object around the laser focal point.

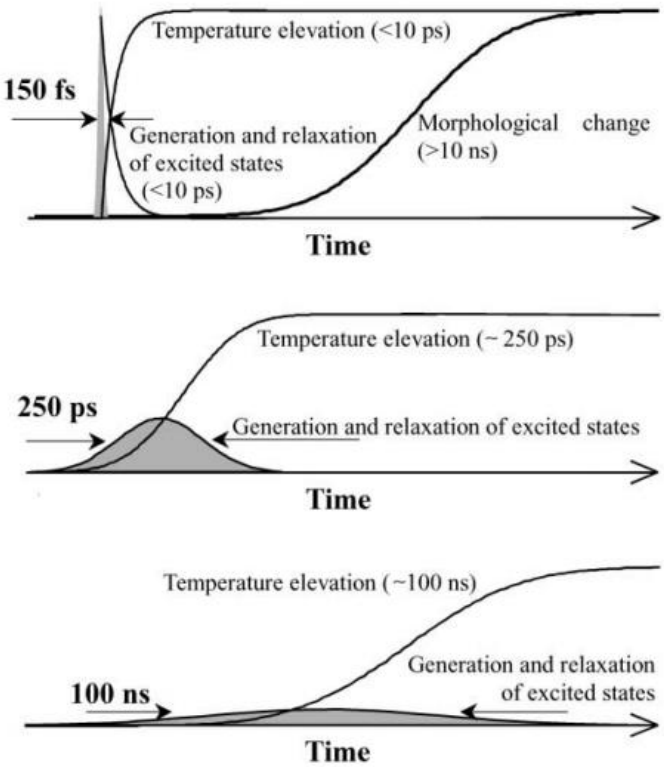

Fig. 9 Time evolution of photo-thermal processes and morphological change under laser pulses of difference duration [98]

Even as pulsed lasers, the mechanism of the ultra-fast induced impulsive force generation is thoroughly different from that of the nanosecond-pulsed induced impulsive force although the only difference between them is the pulse width (by six orders of magnitude). In the case of the nanosecond pulses, the processes of excitation and relaxation of electrons would occur simultaneously during the pulse duration (~ ns). This time duration provides enough time for the vigorous molecules to reach an equilibrium intermolecular distance with environmental molecules (Fig. 10) [98]. The stress is released out of the laser focal point through heat diffusion. As the amount of heat generation increases with the pulse energy, an explosive evaporation occurs and induced huge cavitation bubbles subsequently, whose expansion induces shock and stress waves. Therefore, the ultra-fast laser provides the localized impulsive force confined at the focal point, which possesses a high potential for cell manipulation.

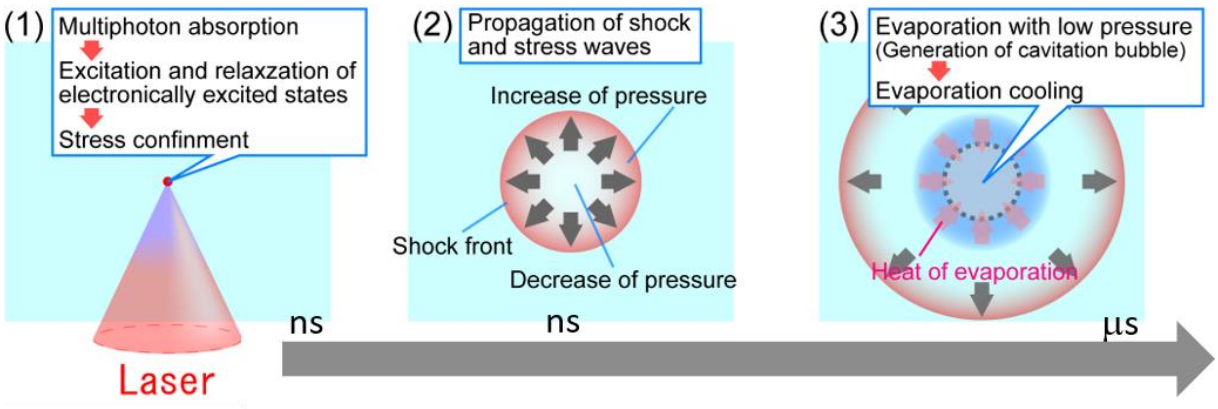

Fig. 10 Schematic of mechanism of cavitation bubble generation induced by an ultra-fast laser [98]

Our group has been studying on this impulsive force induced by a femtosecond pulsed laser (fs-laser). When a single intense fs-laser pulse is focused at a biological tissue or in a physiological medium, it has been proved that a cavitation bubble and a shockwave are generated, propagated away radially as an impulsive force to change the position of surrounding objects (Fig. 11). Furthermore, this fs-laser induced impulsive force was revealed with a magnitude in a micro-Newton scale by means of atomic force microscopy [99] and applied it to optical injection of impermeable materials into single cells [100] and nondestructive micro-patterning for controllable cell arrangement [101] and so on. On basis of all these advantages, the fs-laser is believed to facilitate the cell manipulation in the microfluidic chip.

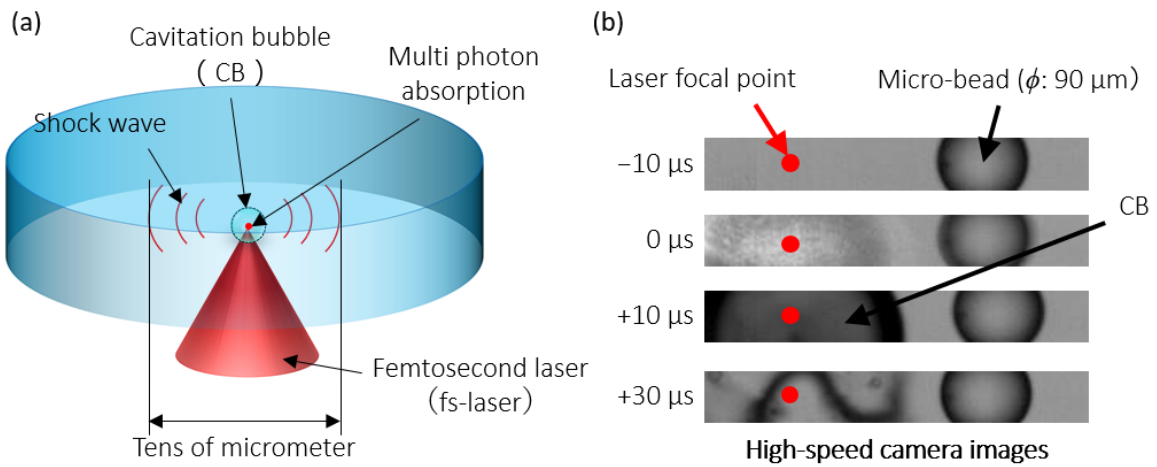

Fig. 11 (a) Illustrative scheme of an impulsive force generated by a fs-laser (b) Demonstration of an impulsive force to change the position of surrounding objects through a cavitation bubble and a shockwave (from our group)

1.4 Combination of microfluidic device and ultra-fast pulsed laser technology

Along with the rapid growth of single cell research, fast and efficient experimental protocols is notably significant for a massive data request and an increasing interest on special rare cells in a huge population to come to statistical results and meaningful conclusions. For instance, researches on circulating cancer or stem cells plays a key role toward detecting pathogenic factors of diseases in very early stage for disease prevention and therapy/drug development [102-104]. It was estimated that there is only one circulating cancer or stem cell in every 6 billion of cells, which is a 1 milliliter blood sample from a healthy person. This means an enormous amount of cells is required to be analyzed for isolation of enough targeted cells for early diagnosis. Under this background, automation received huge attention and led to an explosive development of microfluidic device techniques for high throughput. It is a tremendous revolution in biological and medical fields to diminish the requirements of time and human source for cumbersome experiment steps, which is like the industrial revolution to enable immense production in a short time by replacing labor force with automatic machines.

As its name said, the microfluidic devices employed a fluid as moving platforms for each single cells to avoid direct exposure to air and individually run down every experiment steps. With a great progress of fabrication techniques, it could realize any complex channel designs on the microfluidic devices and even integration with most of common experimental instruments, which is highly potential to realize all kinds of experiment steps and hence entitled as lab-on-a-chip.

Based on purposes of each experiment steps, it could be classified into sample preparation, manipulation, treatment and analysis prior to data acquisition. Researches of these four operations on the microfluidic chip has been widely studied on how to automize and give a high throughput (efficiency) in these two decades. Here, we focused only on the manipulation part, and lots of on-chip methods has been discussed above. Among them, the optical manipulation method is the most potential one since the manipulation force is independent from the target properties like size and polarizability. This makes the optical manipulation method much more applicable such as a sample containing targets and non-targets with a similar size. Besides, it is so versatile, for examples, cell analysis could be conducted on the basis of scattering light, fluorescence, etc. and cell treatment like optical injection is able to be performed in a microfluidic chip. What's more, optical tools are highly integratable

with penetration nature of light and ease-operable since it would be independent from the microfluidic chip without attaching or embedment.

As optical manipulation methods developed so far, two representative approaches were established on the basis of the optical tweezer and nano-second pulsed laser, which showed manipulation throughputs of 830 [105] and 45,000 [67] events/s respectively. In comparison with other methods in Table.1, the optical manipulation method is relatively low. Herein, we proposed a potential approach to boost the throughput of manipulation by utilizing a femtosecond pulsed laser with a high repetition rate. With a precise spatio-temporal control of the laser focal point at the vicinity of targeted cells, the propagating impulsive force is potential to change the flowing direction of the targets and conducted as quickly as its repetition rate, which is the amount of pulses produced within a second.

1.5 Structure of this thesis

The goal of my whole work presented in this thesis is to develop a powerful cell manipulation system with ultra-high throughput. Here below showed how I approached my goal step by step as described in the chapters below (Fig. 12):

Chapter 1: To introduce the required background knowledge for establishing and achieving the goal on the basis of understanding its requirements and significance

Chapter 2: To interpret how my manipulation system was constructed and working under the cooperation of various components

Chapter 3: Determination of critical manipulating parameters by using polymer micro-particles for my system to function correctly and precisely

Chapter 4: Performance evaluation of our manipulation system by using polymer micro-particles

Chapter 5: Pre-test of cell viability under the influence of the manipulating force

Chapter 6: Performance evaluation of our manipulation system by using mammalian cells

Chapter 7: Modification of the current system with additive micro-structures inside the microfluidic channel for better manipulating performance

Chapter 8: Conclusions and perspectives

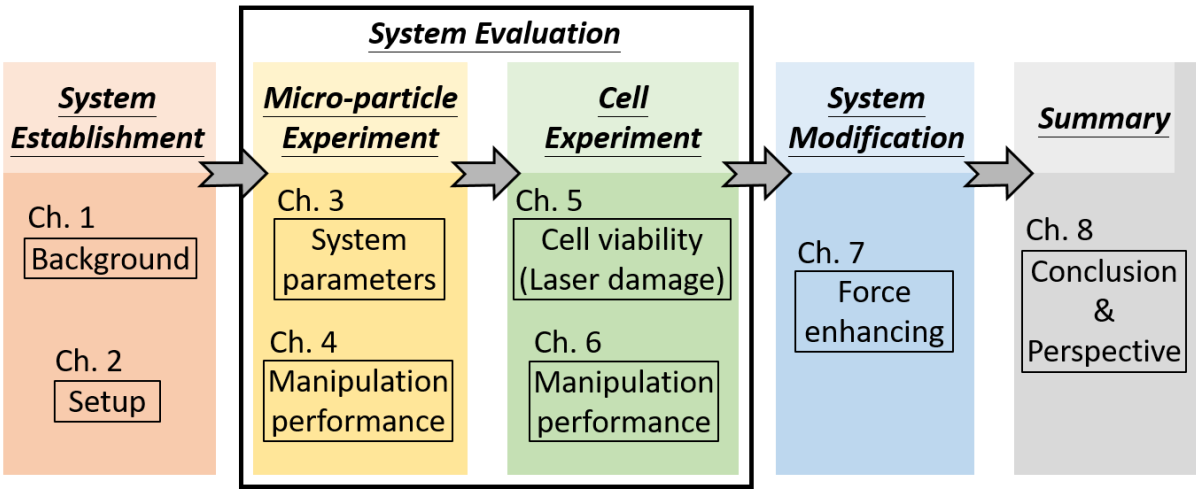

Fig. 12 Structure of this thesis

Chapter 2 Experimental setup

Our manipulation system will be introduced here for the working principles in the first section, whose components are classified into three groups in the following sections. In the section 2.2, optical setup is constructed to conduct the signal excitation/detection and the spatial control of manipulating force. In the section 2.3, a signal-processing circuit is designed to recognize targets according to their signals and actuate the manipulating force. In the section 2.4, the microfluidic devices are employed to serve as a sample transportation system and a manipulating platform.

2.1 Working principles of proposed manipulation system

Fig. 13 (a) shows the working principle of the cell manipulation with the fs-laser induced impulsive force. After a solution with particles is loaded into the microfluidic chip, particles are arranged into a single straight flow line at the center of the channel (To be discussed in later section). A probing laser with little bio-damage is focused on that flow line and excites specific signals from the particles passing through one by one for target recognition. As targets are detected, the signal triggers another manipulation laser in the downstream of the flow line, which is a femtosecond pulsed laser (fs-laser). With a proper time delaying, the targets come to the same position, where a single pulse triggered from the fs-laser is focused nearby. Those targets are pushed away to other flow lines, which leads them to collection port. On the contrary, non-targets without specific signals can not activate the above manipulating process. For more details, the focal positions of both the probing and manipulating laser is indicated in Fig. 13 (b). A relative position between these two lasers is noted as a critical setting for our manipulation system, which would be further discussed in the next chapter. The manipulating laser is at 13 μm downstream from the probing laser along with a distance of nearly 8 μm perpendicular to the center flow line.

To carry out our strategy for a new manipulation system, the fs-laser plays an important role. In Fig. 13(c), it briefly shows the pulses with different width (duration) such as nanosecond (10^{-9}) and femtosecond (10^{-15}), which are colored with red and blue. The red part means the energy to overcome the threshold of cavitation bubble generation. Then, the rest energy of the pulse in blue would provide for cavitation bubble generation and is related to the bubble size. With a narrower fs pulse, the energy threshold is overcome easily and the rest of energy tends to induce a small cavitation bubble, which is localized at the laser focal point. This may allow us to focus the fs-laser near the targets and load the force on the target specifically without influence on the neighboring particles in comparison with ns-laser (Fig. 13(c)). More

significantly, as described in chapter 1.3, a single fs pulse is actually much narrower than ns pulse as the difference of pulse width is six orders. A fs-laser could therefore provide much more pulses in one second (high repetition rate), which means more manipulating process can be conducted in one second (high manipulating throughput).

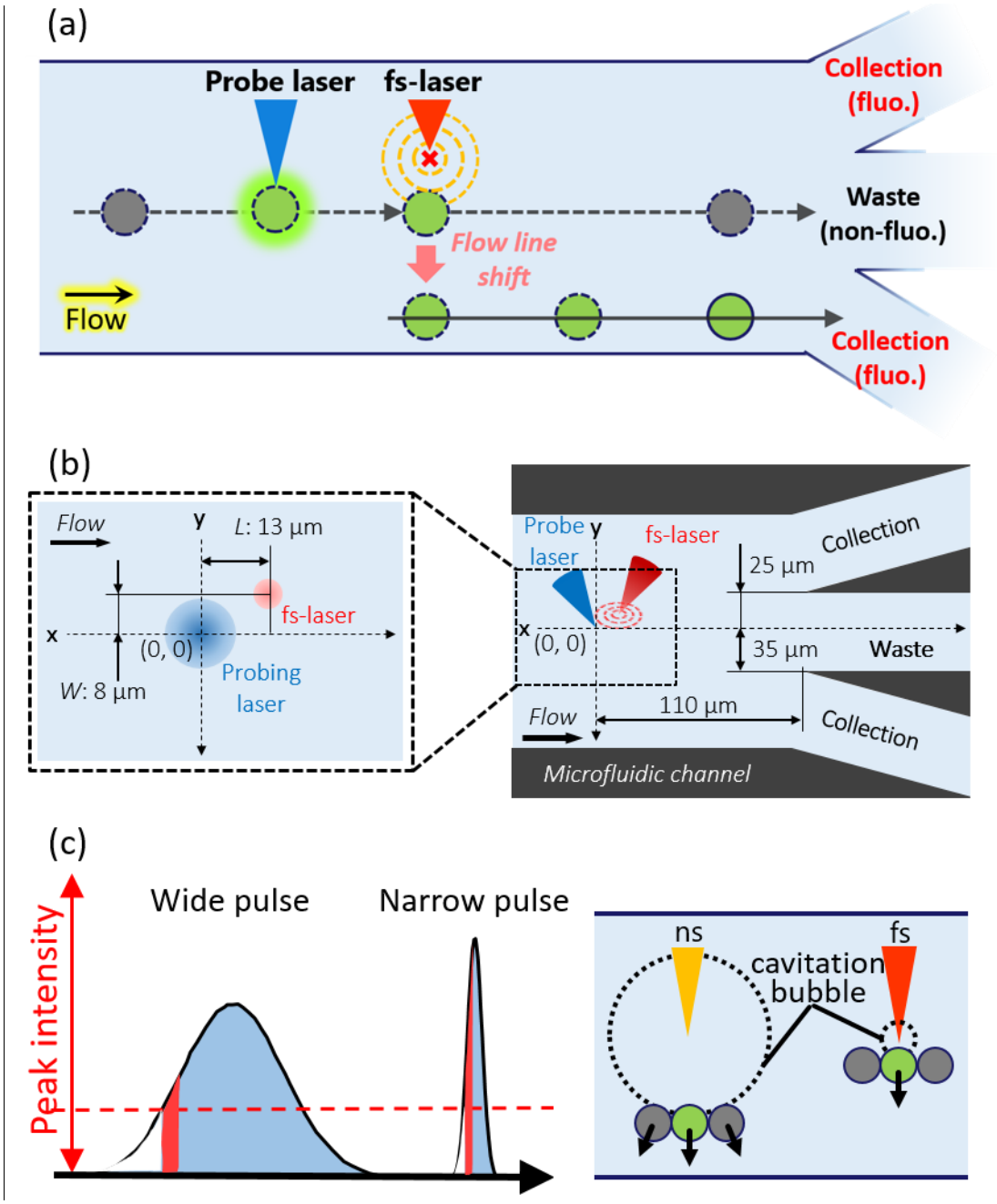

Fig. 13 (a) Illustrative scheme of our cell manipulation system (b) Details about the relative focal positions of both the probing and the manipulating lasers (c) Advantages of femtosecond laser (red: energy to overcome the threshold of cavitation bubble generation; blue: energy relative to cavitation bubble size)

2.2 Optical setup

The optical setup is classified into 3 parts according to their purposes: (1) bright field monitoring, (2) signal detection and (3) manipulation force actuation. All the 3 parts cooperated with an upright microscope (Olympus BX53) and a 20× objective lens (Olympus, Plan N, NA. 0.4) (Fig. 14).

(1) Bright field monitoring

A light source, mercury DPSS lamp (Olympus, U-HGLGPS), was employed to light up samples from the bottom side with a short-pass filter (Thorlabs, FESH0500) in order to reduce noise for signal detection. The transmitting light was collected by the objective lens and reflected by a dichroic mirror (Thorlabs, DMLP490R) towards a high-speed camera (Ametek, Phantom V1211). Bright field images were obtained with a high capturing rate over 100,000 frames/s, which allowed us monitor the manipulating process and evaluate manipulating performance of this system.

(2) Signal excitation and detection

A diode-pumped solid-state laser (Spectra-Physics, Excelsior 488, 50 mW, CW) with 488 nm wavelength was utilized as a probing laser to excite specific signals from targets, which was fluorescence in this thesis. This probing laser was modified with a pair of collimating lens to expand the beam size, which fully fitted in the back port of the objective lens for NA. 0.4. Then, it was reflected by a dichroic mirror to pass through the objective lens and focused onto the center flow line as mentioned in chapter 2.1. After the fluorescence was emitted, it would pass through a laser notch filter (488 nm), a band-pass filter (510–550 nm) and a spatial filter to remove other background noises for a high signal-to-noise ratio. This fluorescence signal sensed by a photomultiplier tube (Hamamatsu Photonics, H10722-210) and transformed into an electrical signal for further signal recognition by a home-made circuit.

(3) Manipulating force actuation

After signal recognition, the signal-processing circuit would electrically trigger an Ytterbium fs-laser amplifier (Spectra-Physics, Spirit One, 400 fs, 1 MHz, <8 μJ/pulse). One single pulse is released out from a pulse train of 1 MHz and coupled with the probing laser by a dichroic mirror. Following the same optical route of the probing laser with a little tilt, this single pulse was focused into the flowing streams of the micro-fluid chip as showed above. In principle, the throughput limitation of

our system is equal to the repetition rate of the fs-laser, 1,000,000 events/s, which means there will be one particle to be manipulated in every micro-second by single pulses. Unfortunately, there are other relative factors such as particle size and flow velocity, the manipulating resolution of the impulsive force (manipulating capability on small objects) and the life-time of cavitation bubble (disturbance on the impulsive force by the air inside the bubble). The particle/cell size and flow velocity will be selected before experiment, and the manipulating resolution and the life-time of cavitation bubble will be surveyed in this research. All these factors influenced one another. Following the previous researches (optical tweezer and ns-laser) [67, 105], a similar estimation method for "maximum" throughput of a system was employed in this research. By removing the variant of particle concentration with a perfect-aligning condition of particles (Fig. 24(h)) as a standard, the throughput is defined as the flow velocity to be a dividend, and the dividor is selected on the basis of a comparison among other factors mentioned above, which will be investigated later.

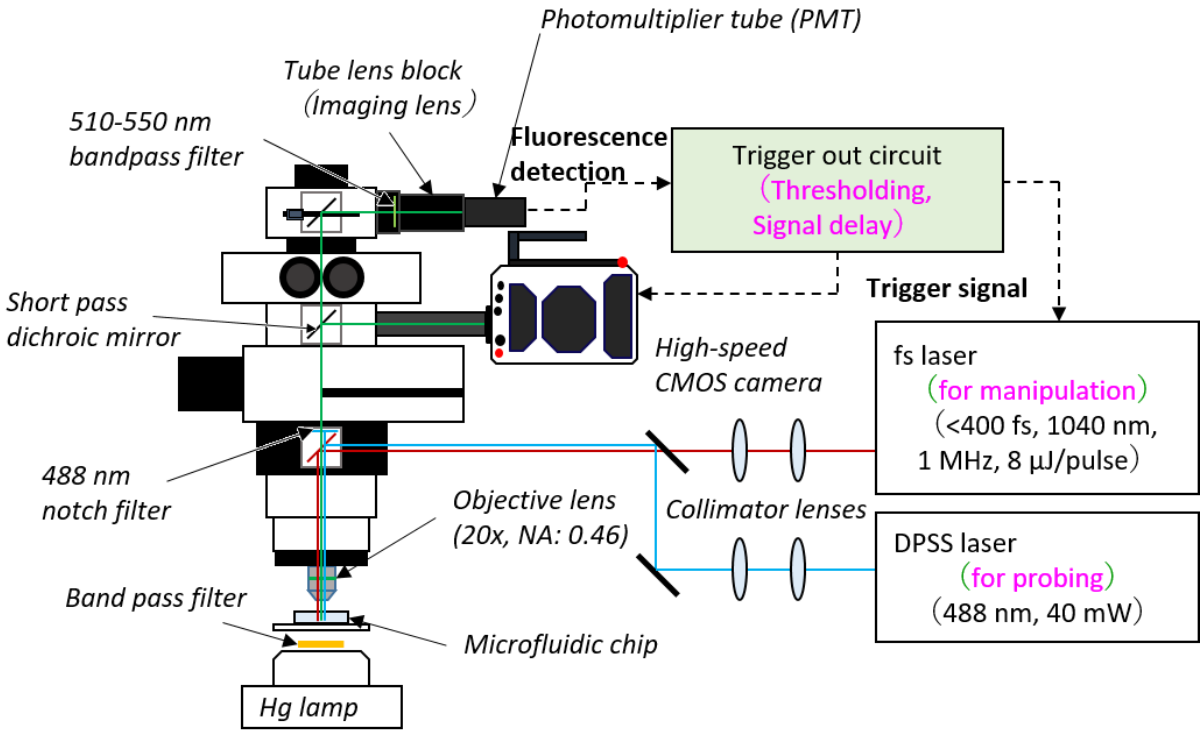

Fig. 14 Illustrative scheme of our system setup for manipulation

2.3 Signal-processing circuit

Based on the effort of previous graduate student, a signal-processing circuit was designed and fabricated to have judgements on the electrical signals from the PMT for target recognition and manipulating force triggering. In connection with an oscilloscope as an operating interface, the electrical signals could be monitored, and a threshold could be set to judge which signals came from our targets. Since the fluorescence was treated as a difference between targets and non-targets in this thesis, an optimal threshold was decided by testing intensity relation between electrical and fluorescent signals.

Fig. 15 is a time chart about working principles of the circuit. A fluorescence from a target induces a time delaying of 13 μs, which is estimated based on the flow velocity of 1 m/s and the 13 μm distance between the probing and manipulating lasers at the flow direction (W: 13 μm). As soon as the time delaying finished, an electrical signal is delivered to fs-laser system and trigger a pulse picker inside to pick up a coming single pulse on the pulse train for irradiation. With the pulse train of 1 MHz repetition rate, there is an uncontrollable jitter less than 1 μs, which equals to 1 μm fluctuation of targets' position. Whether this jitter of fs-laser irradiating timing influences the manipulating performance will be examined and discussed later.

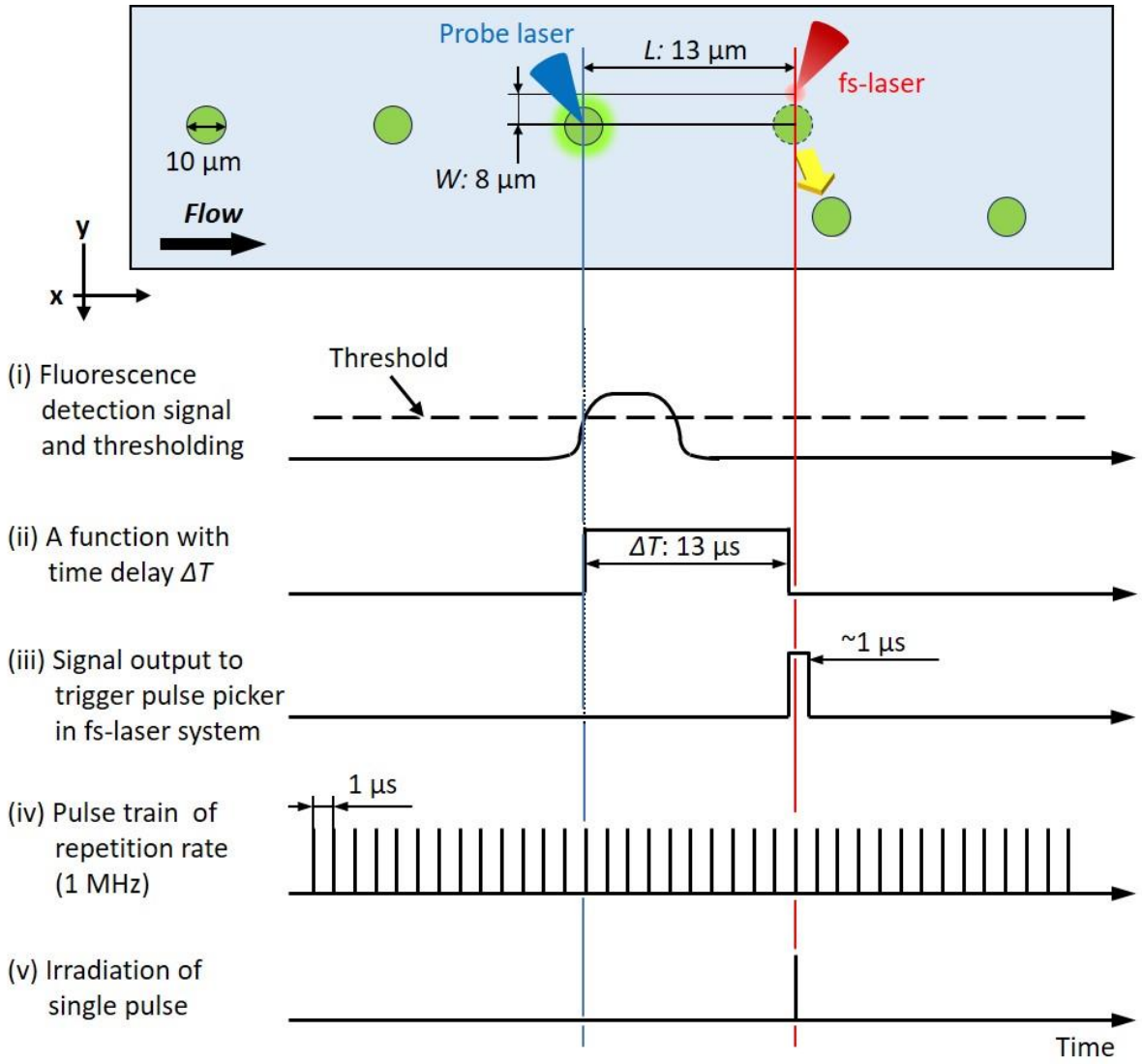

Fig. 15 Time chart of the working principles for a precise manipulating force triggering

2.4 Microfluidic chip

The microfluidic chips were used as a working platform for fs-laser actuated manipulation in this study and fabricated with developed methods in the references [4-18]. The chips were set under the microscope and connected with a syringe pump for loading sample solution containing suspended particles/cells.

Glass/silicon-assembled microfluidic chip

The glass/silicon-assembled microfluidic chip is illustrated as Fig. 16(a) and fabricated by Prof. Arai's group in Nagoya University. There is one inlet as upstream on the left, and a channel branch is created for cell manipulation as it goes downstream. At this branch point, there are one central waste channel and two side collection channels. As the waste channel goes straight to one exclusive outlet, the two collection channels beside would merge toward the other outlet.

The glass-based microfluidic chip is composed of three layers (Fig. 16(a)): the channel layer made of a silicon plate (20 mm x 80 mm x 0.2 mm) is sandwiched by two cover layers at the top and bottom made of borosilicate glass plates (20 mm x 80 mm x 0.3 mm). In the middle layer, the microchannel is fabricated in methods of conventional photolithography and deep reactive-ion etching (DRIE) techniques. The height of all the channels is 200 μm. The width of the main channel is 200 μm and branched into the central waste channel and the two side collection channels. The width of the waste and collection channels is 70 and 60 μm respectively, between which is a angle of ~5° to compose the total channel width of 200 μm. The angle between the two collection channels and the waste channel is symmetrically 10 degrees. The base, cover, and middle layers are packaged (fused) by anodic bonding without any intermediate layers. The chip's position is controlled by a motorized translation stage with a precision of 1 μm.

The introduced cells are 3D-positioned in the center of the main channel by an acoustic aligning force [31 50, 51] produced by the piezoelectric transducer (PZT) attached to the microfluidic chip (Fig. 16(a)). By applying high-frequency high voltage to the piezoelectric element, acoustic standing waves as shown in Fig. 16(b) is generated in the fluid due to vibration of the piezo element [31]. The flowing particles inside the channel are gradually aligned into a single line at the node of the standing wave (the center of the channel) under the influence of the acoustic radiation force [15]. (Fig. 16(c)) In cooperation with the symmetric design of micro-channels (one central waste channel and two side collection channels), the single line that the

particles flow on is located at the center of the micro-channels under the acoustic focusing wave induced by the vibration of the piezo-meterial.

The piezoelectric transducer (PZT) plate (width: 20 mm, length: 40 mm, resonance frequency: 3.67 MHz) (C203, Fuji Ceramics) is soldered with two lead wires on the backside. The PZT plate is driven by an AC voltage with frequency and amplitude of 3.69 MHz and 80 V, which is provided by a function generator (FG-274, TEXIO) and a voltage amplifier (HSA4101, NF Corporation). The frequency and the amplitude are always optimized based on empirical results as long as the chip was re-assembled or a new chip was recruited because the amount and position of adhesive PZT attachment may affect the vibration condition. In addition, the ability to tightly aligning the cells into one flow line without assistance of hydrodynamic forces prevents the cells from being diluted by sheath flow [50, 51] This means that the cells could be densely packed into the flow line compared with conventional hydrodynamic methods. This would facilitate the speed of cell manipulation.

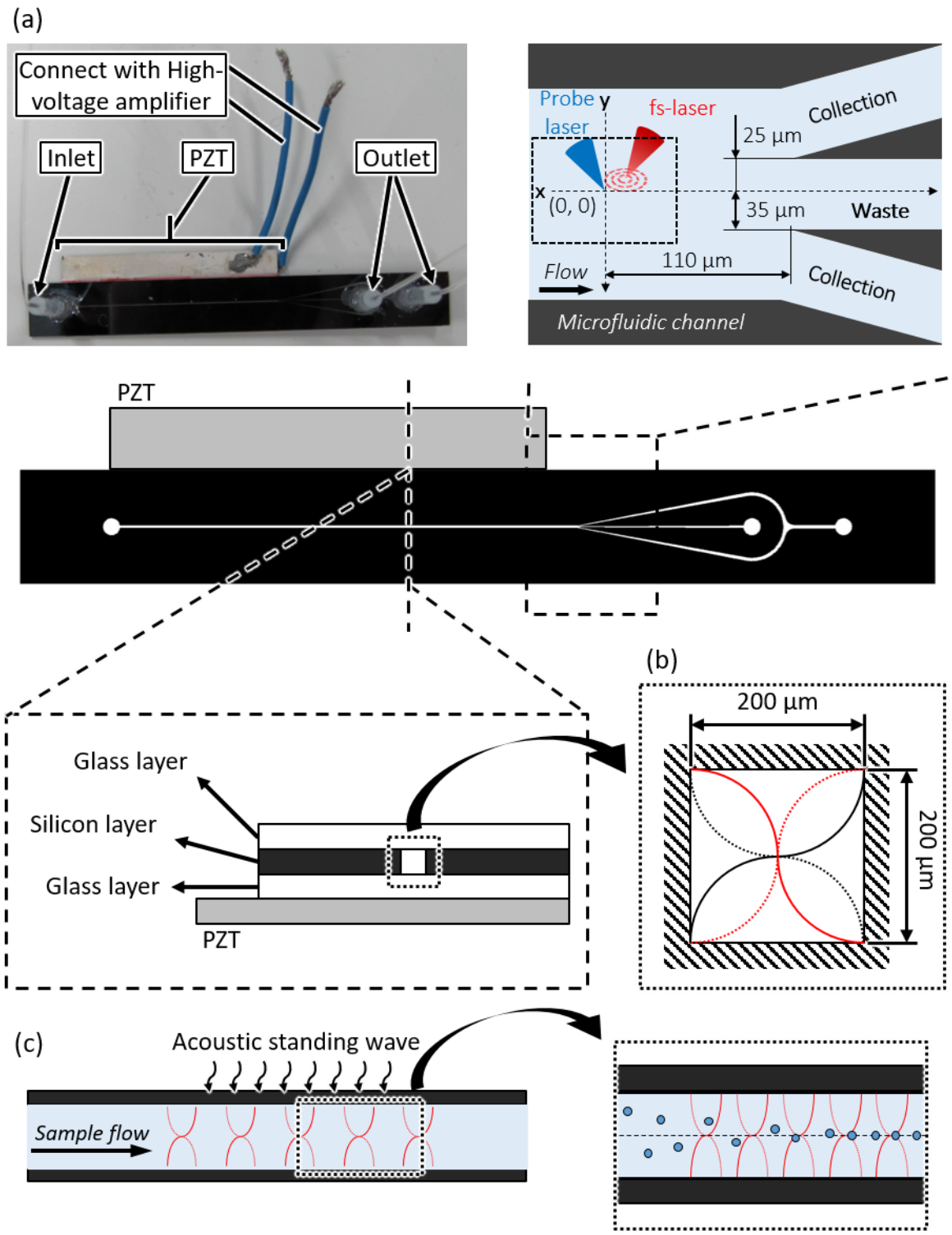

Fig. 16 (a) Topview and structure of the glass/silicon-assembled microfluidic chip (b) Cross section view of acoustic standing waves induced by a piezoelectric element (c) Lateral view of acoustic standing waves for a particle aligning process

Chapter 3 Determination of manipulating parameter with micro-particles

To realize the proposal of our system, there are still a few settings that have to be explored first to complete establishment such as flow line control of samples, good irradiation timing and proper intensity of manipulating force. To explore these settings in this chapter, micro-particles with fluorescence coating and homogeneous size of 10 μm are employed as a phantom of cell because cells are more complicated with properties of size, stiffness, shape etc.

3.1 Method

3.1.1 Sample preparation

Solution with pure fluorescent particles

A medium of 20% blocking reagent was prepared by diluting the commercial product (N102, NOF Co.) in pure water (Milli-Q, EMD Millipore Co.) and served as a particle-carrying medium to avoid aggregation. In this medium, 10 μm polystyrene polymer particles with fluorescence (FluoresbriteTM, Polysciences) were added and mixed by a Vortex mixer for 1 minute. Concentration of the particles was measured by a cell counter plate (DHC-F01, NanoEnTek) and adjusted to be $2\sim3 \times 10^5$ particles/ml. This particle-containing medium was shaken by the Vortex mixer for 1 minute again to have the particles evenly spread. At last, a filter (EASY strainer 40 μm - sterile, Greiner bio-one) with 40 μm pores were employed to remove big particle clots in prevention from clogging in the microfluidic chip.

3.1.2 Experimental steps and setup

Fig. 18 showed the experimental setup. The solution with micro-particles (ϕ: 10 μm) prepared above was loaded into the micro-channel of the glass/silicon-assembled chip (as introduced in chapter 2.4) by a syringe pump in a flow rate of 2400 μl/min, which was measured and equal to a flow velocity of 1 m/s. This chip was set on a motor-driven stage under the upright microscope. In an ideal case, the targeted particles would stay strictly on the center flow line with a stable flow velocity of 1 m/s. With a perfect timing of irradiation, the targeted particles be located at 8 μm far from center of the fs-laser induced impulsive force a direction perpendicular to the flow. From the signal detection to the manipulation, the whole process took place at the branch region of the channel, which was monitored by the high speed camera with

frame rate of 100,000 or 240,000 frame/s. Based on the high-speed images, coordinates of all targeted particles just before and after shooting were recorded, and the data were summarized as the distribution of particle's flow line shift in perpendicular direction of the flow.

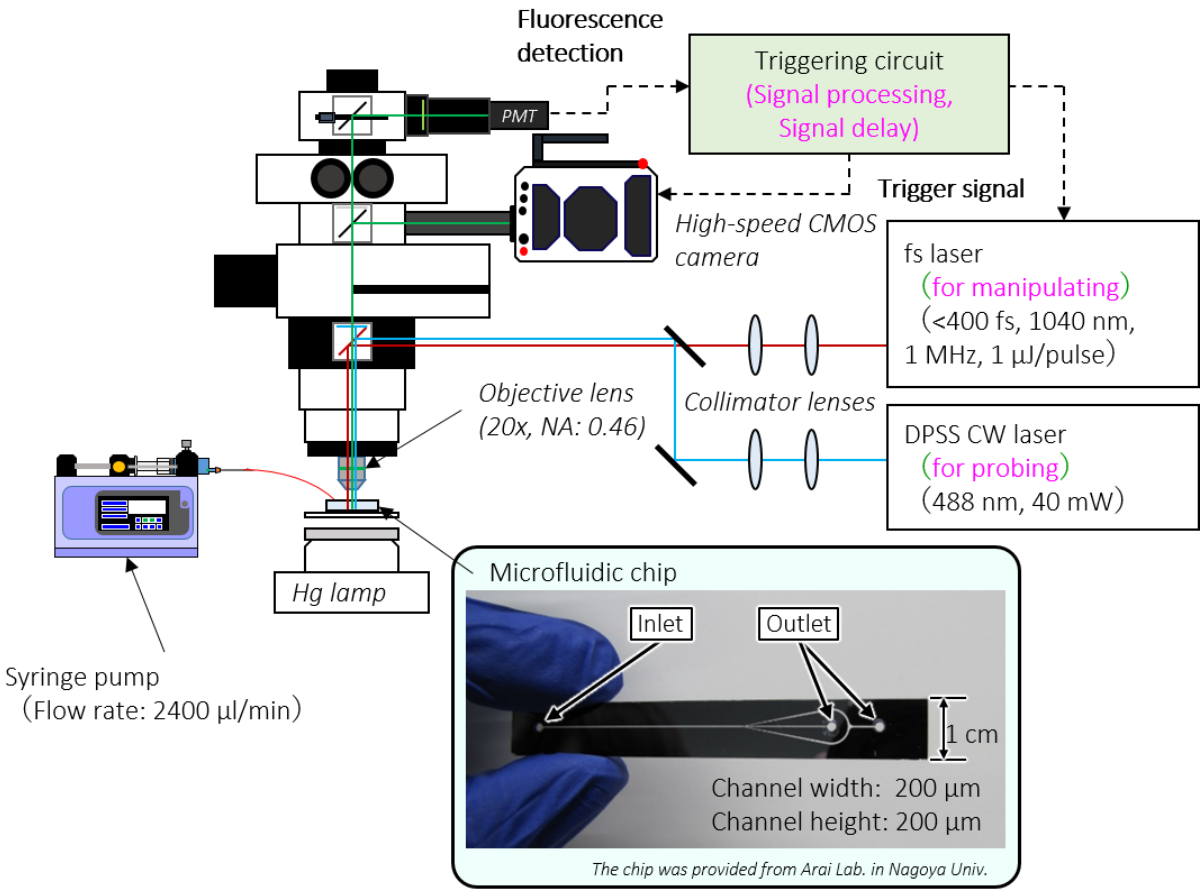

Fig. 17 Illustrative scheme for microfluidic setting onto our manipulation system

3.2 Demonstration of manipulating

In Fig. 19, the high-speed image sequence shows a demonstrative case of manipulation process on a fluorescent particles from particle detection to particle redirection with pulse energy of 0.6 μJ/pulse. A fluorescent particle follows the center flow line (Fig. 19(a)) and is excited for fluorescence emission as passing through the probing laser (Fig. 19(b)). A single pulse is irradiated and a cavitation bubble is observed a motion change of the target in a direction perpendicular to the flow, which is defined as Y direction (Fig. 19(c)). The targeted particle is then calmed down and followed another flow line in Fig. 19(d) with a total flow shift of ΔY. Afterwards, the targeted particle enters the collection port instead of the original channel for waste port (Fig. 19(e)).

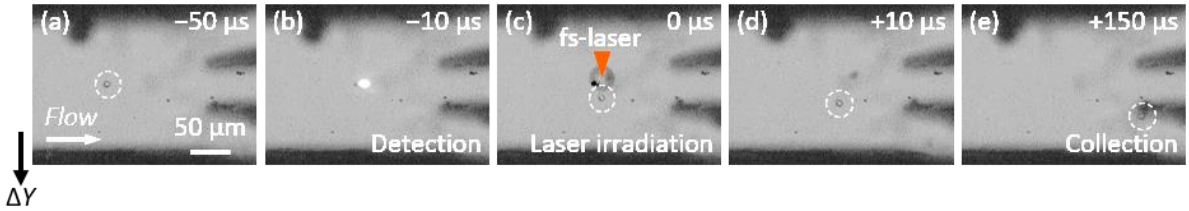

Fig. 18 High-speed image sequence for a demonstrative case of manipulation process on a fluorescent particles from particle detection to particle redirection with pulse energy of 0.6 μJ/pulse

Here, a sample contained pure fluorescent particles was utilized. The focal point of the excitation laser was referred as original point, (0, 0), and located on the center flow line. Distance from flow lines of particles to the center flow line was taken as ΔY (Fig. 20(a)). By statistics, the spatial distribution of ΔY before and after fs-laser irradiation was then obtained (Fig. 20(b)). In Fig. 20(b), particles entering the collection port were showed as red, and other particles entering the waste port were showed as blue. All of particles are indicated to receive the impulsive force for a change of ΔY, but only half particles were successfully sent into the collection port, which pointed out a requirement of stronger impulsive force.

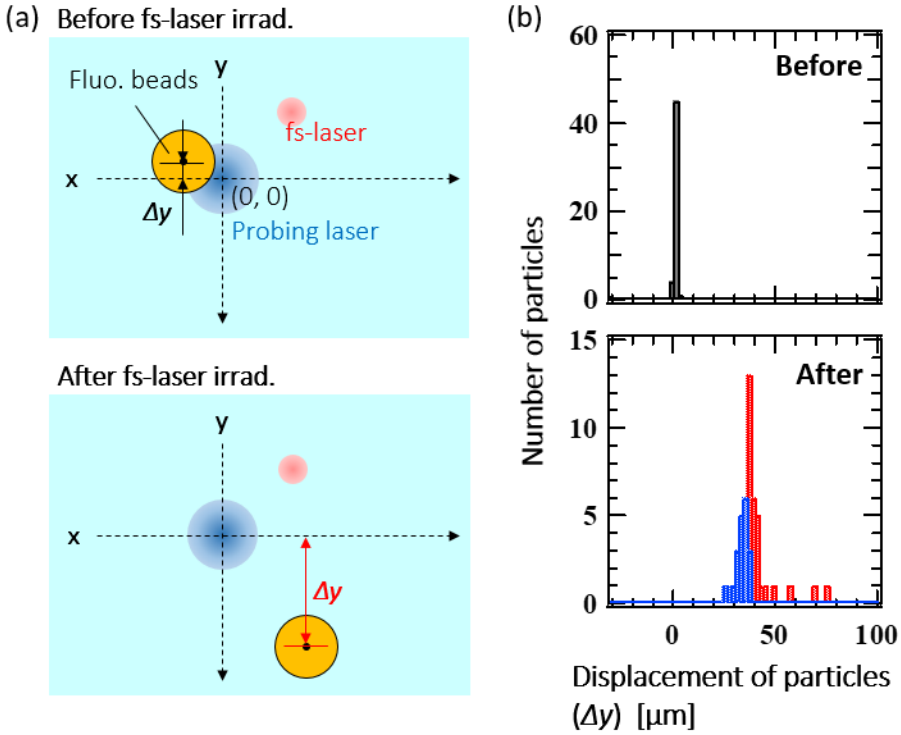

Fig. 19 A preliminary result of manipulation on a fluorescent particles (a) Evaluation parameters (b) Particle flow line positions before and after the manipulating process

3.3 Time delaying (ΔT)

As the circuit designed for signal processing and fs-laser triggering in our manipulation system, there would be a time delaying (ΔT) required between detecting signal and fs-laser irradiating. At a high flow velocity of 1 m/s, an improper time delaying by 1 μs longer could make target move downstream for 1 μm more. This would weaken the net imposed impulsive force by an increasing laser-to-target distance and have a different force-imposing angle. Not to mention longer/shorter more than over 10 μs, which would let targets slit away or even mis-manipulate the next coming object. To have the fs-laser precisely irradiate and impose the impulsive force on the targets, a proper time delaying is required by a well tuning for a good irradiating timing.

Here, only pure fluorescent particles was loaded into our system and supposed to be collected without any loss after manipulation process. We define a parameter, success rate, which indicates a percentage of targeted particles collected back through our manipulating force. To determine the optimal timing for fs-laser irradiation, we investigated the success rate as a function of the time delaying (ΔT). Fig. 21 showed the success rate changing with the time delaying (ΔT) at a pulse energy of 1 μJ/pulse. A peak of success rate was located at the time delaying (ΔT) of 10~15 μs and reached 100% to collect all the targeted particles back. The optimal timing for fs-laser irradiation was set as 13 μs as a middle point of the peak apex, This is consistent with our estimation that particles should take 13 μs to move from the detection point to manipulating point based on the distance (L) of 13 μm and the particle flow velocity of 1 m/s. In addition, this consistency suggests little influence on the manipulating performance caused by the 1 μs jitter of fs-laser timing (mentioned in chapter 2.3). Furthermore, the success rate decreased to 0% when ΔT was smaller than 8 μs or larger than 22 μs. The 14 μs time interval between 8 and 22 μs was equivalent to 14 μm (14 μs × particle velocity 1 m/s). This means an estimation of spatial resolution to be smaller than 14 μm for the fs-laser induce impulsive force under this current setting. On the other hand, this also suggests that this 14 μm over one 10 μm particle may impose some influence on the particles neighboring the targets.

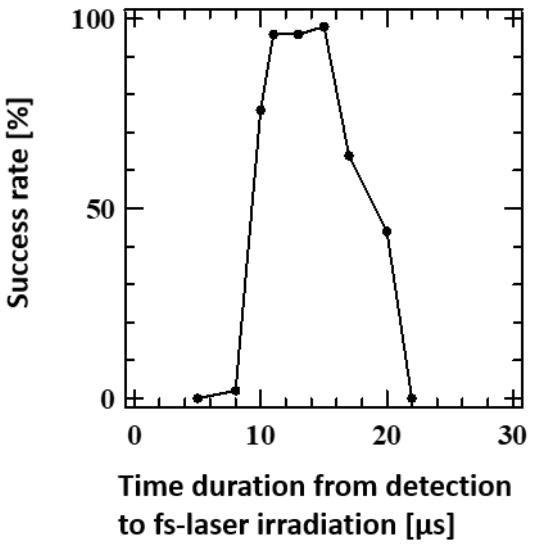

Fig. 20 Dependence of the success rate on the time delaying (ΔT) under a pulse energy of 1 μJ/pulse

3.4 fs-laser focal position based on flow line fluctuation

Apart from the proper time delaying, performance of the acoustic aligning was another important requirement prior to conducting the whole manipulation process. This determined how precise the targets passed through the detection laser and was positioned for a good exposure to the impulsive force. If a bad aligning performance, it will lead to poor fluorescence excitation and force loading onto the targets. Here, a sample contained pure fluorescent particles was utilized. The aligning performance under a flow velocity of 1 m/s is shown by the black bars in the histograms in Fig. 21, which represented the flow line distribution of particles along the flow. Based on the Guassian distribution, the standard distribution (σ) of the particle flow line position is 1.25 μm. Unfortunately, the distribution increased with the flow speed since diffusion force of particles would strengthen and get out of the control by the acoustic aligning force. Moreover, the flow line distribution over 2.5 μm would make part of particles too close to the fs-laser focus or even ablated by the fs-laser. For this reason, we set the flow velocity at 1 m/s as a limit for our current high-throughput manipulation. By the way, according to particle radius (5 μm) and the sum of the aligning stream width of 2σ (2.5 μm), the focal point of the fs-laser was hence set to be nearly 10 μm away from the center flow line of particles, which could keep 95 % (totally 4σ in the range of ±2σ) of particles from direct fs-laser irradiation.

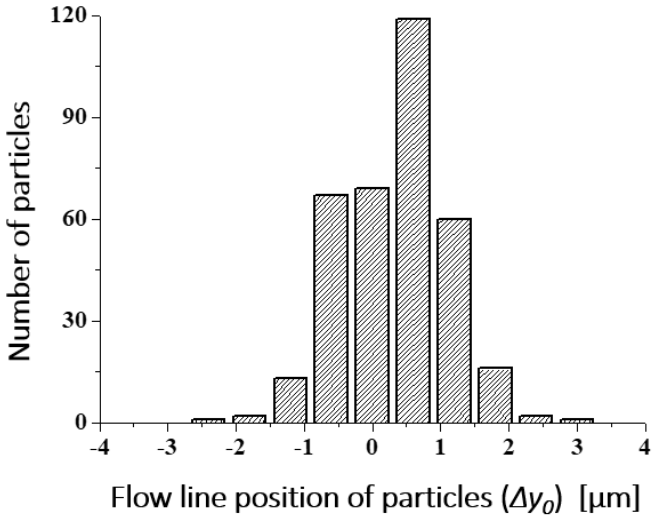

Fig. 21 The distribution of flow line position of particles before the fs-laser irradiation

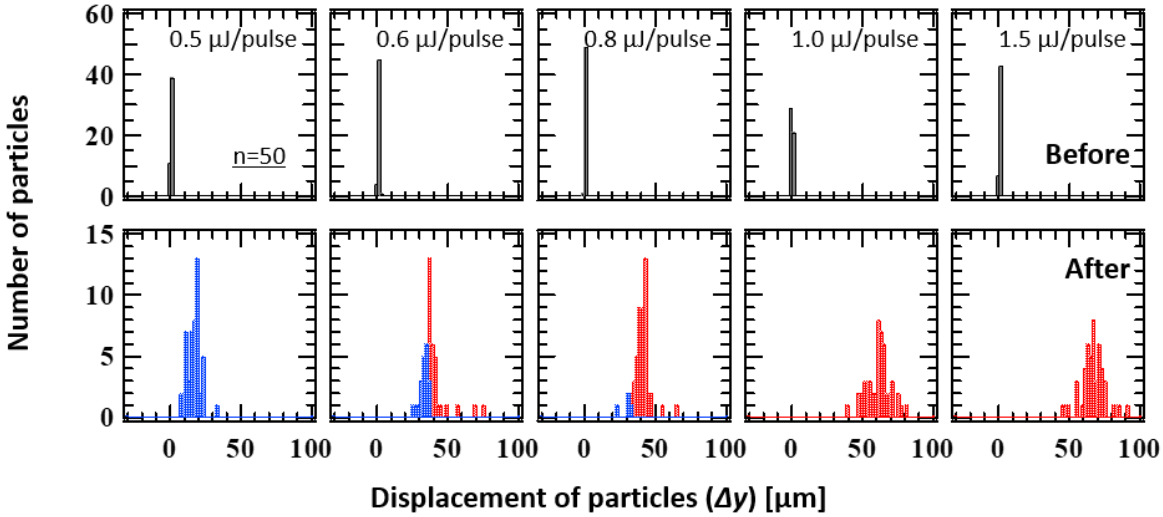

Fig. 22 Particle flow line positions before and after the manipulating process under various pulse energies

3.5 Laser pulse energy

Colored bars in the histograms of Fig. 22 showed the position distributions of the particle flow line before and after fs-laser irradiation with different pulse energy. Here, only pure fluorescent particles were utilized. Depending on the observation, we divided particles into two groups: particles going to the central waste channel (blue bars), and others going to the lower collection channel (red bars). The success rate was calculated as the portion of particles in collection port over total particles. With 0.5 μJ/pulse, all the flow lines of particles shifted as the fs-laser irradiation, which was weak and make few particles go to the waste port for a collection of zero (Fig. 22). Fortunately, more and more particles went to collection port shown as red bars when we increased the pulse energy. This dependency of success rate on the pulse energy was plotted as Fig. 23. At 1 μJ/pulse, the success rate reached 100% with all the particles in the collection port. This indicates switching the destination of particles could always succeed with pulse energy over 1 μJ/pulse. As a logical consideration that higher pulse energy would lead to stronger cell damage and even disturbance to the next manipulation event, we set the optimal sorting pulse energy as low as 1.0 μJ/pulse with 100% success rate retained.

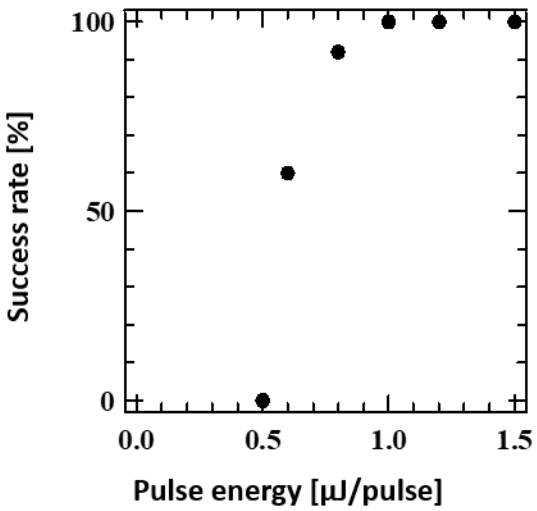

Fig. 23 Pulse energy dependence of the manipulating success rate

3.6 Summary

In this chapter, we have demonstrated the feasibility of our proposed manipulation system with fluorescent micro-particles at a flow velocity of 1 m/s. Our system succeeded in detecting fluorescence signals from particles, triggering the fs-laser and manipulating flow direction of the particles. The optimal working conditions has been determined from the results. The fs-laser focal point was set ~10 μm away from the center flow line, and the time delay was 13 μs to precisely impose the manipulating force to all the particles, which achieved the success rate of 100% to collect all the particles.

Chapter 4 Performance evaluation with micro-particles

Now our manipulation system has enabled to precisely impose the manipulating force to all the particles and achieved the success rate of 100% with pulse energy of 1 μJ /pulse to collect all the particles in previous chapter. To begin the performance evaluation on our system, a mixture sample of both fluorescent and non-fluorescent particles was employed to simulate the complexity of real cell samples, which commonly contained various cells. The fluorescent and non-fluorescent particles acted as targets and non-targets, respectively. In this chapter, under the disturbance of non-targets, the purpose is to verify some crucial parameters such as purity, success rate, throughput and so on.

4.1 Method

4.1.1 Sample preparation

Solution with particles of both fluorescent and non-fluorescent

Dilute the commercial product in pure water for a medium of 20% blocking reagent. Then, 10 μm fluorescent particles were added into a 10 ml blocking medium and mixed by the Vortex mixer for 1 minute. Again, 10 μm non-fluorescent particles were added into a 10 ml blocking medium and mixed by the Vortex mixer for 1 minute. Particle concentration of both particle-containing solutions was measured by a cell counter plate and adjusted to be $2\sim3\times10^6$ particles/ml, which is a high concentration in order to have the short distance among flowing particles for realization of high throughput. These two particle-containing solutions were mixed in a fraction of 1:20 (fluorescent : non-fluorescent). The fluorescent particles served as targets that should enter the collection port; vice versa, those non-fluorescent ones were regarded as non-targeted that should enter the waste port. The low portion of fluorescent particles suggests a realistic situation that targets often occupied only a small part of a sample. At last, this mixed solution was shaken by the Vortex mixer for 1 minute again and put through a filter (EASY strainer 40 μm - sterile, Greiner bio-one) with 40 μm pores to remove big particle clots in prevention from clogging in the microfluidic chip.

4.1.2 Experimental steps and setup

The experimental steps and setup as described in chapter 3.1.2 were utilized in this chapter with a different sample prepared above.

4.2 Manipulation on particles of high concentration

Fig. 24 demonstrated the manipulating process on the mixture sample of both the fluorescent and non-fluorescent particles. The fluorescent and non-fluorescent particles flowed on the center flow line together with random order and distance between one another. A fluorescent particle in Fig. 24(a) came into our sight and was tightly sandwiched by two non-fluorescent particles. Only the fluorescent particle was excited by the probing laser and detected by the signal-processing circuit (Fig. 24(b)). With the optimal time delay, the impulsive force was actuated, and it pushed the fluorescent particle with a slight influence on the two non-fluorescent particles beside (Fig. 24(c)). As this fluorescent particle was moving away from the center flow line, another fluorescent particle was detected again, which brought a non-fluorescent particle attaching behind (Fig. 24(d)). This second fluorescent particle also actuated the impulsive force for a flow direction change, which left the neighboring non-fluorescent particle on the original flow line at the center of the channel (Fig. 24(e)). The two targeted fluorescent particles were then observed to have flow line shifting in the y direction and enter to the collection port (Fig. 24(f)). These two consecutive case in a row suggests a potential of high-resolution of our manipulating force, which would particularly facilitate manipulating on highly compact particles in a condensed sample for achieving a high throughput. With a highly concentrated sample of 3×10^6 particles/ml compared with previous chapter, packed particles like the case above were checked in advance by recording the amount of particles with particle-to-particle interval below 10 μm (Fig. 24(g)). There were indicated to be nearly 100 similar cases within 3 seconds under 2400 μl/min, which was estimated to have thousands of packed particles in 1 ml solution. In this chapter, we focused on the manipulation of those packed particles with the particle-to-particle interval within 10 μm for performance evaluation in an extreme condition that all particles are aligned perfectly on the central line of the micro-channel (Fig. 24(h)).

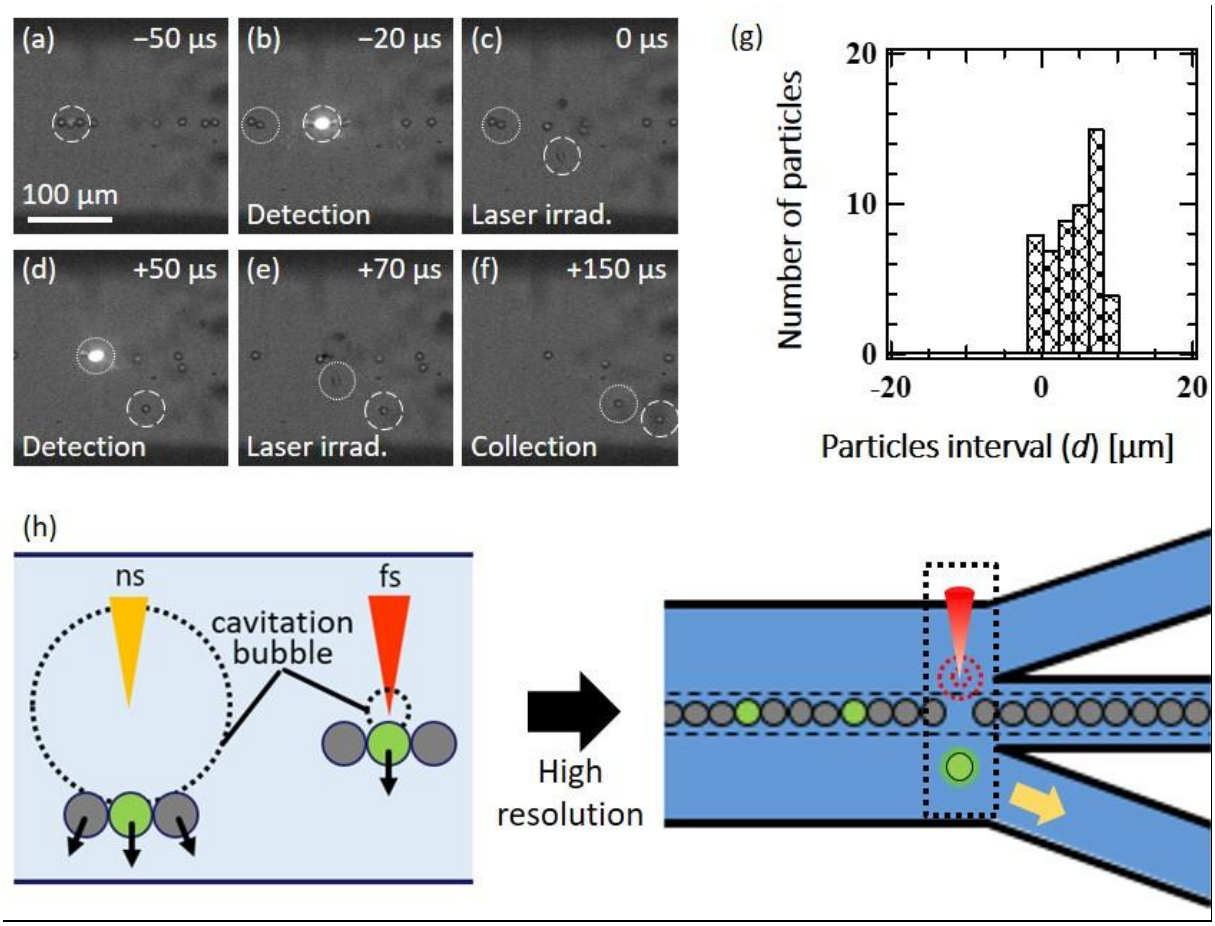

Fig. 24 (a-f) A demonstrative case of the manipulating process for the mixture sample of both the fluorescent and non-fluorescent particles. (g) Distance distribution of particle-to-particle interval in a high-concentration sample (h) An illustration of the perfect particle aligning for estimation of theoretical throughput

Take the manipulating with pulse energy of 0.6 µJ/pulse for example, the evaluation method was to record the flow line position of both the fluorescent and non-fluorescent particles before and after irradiation (Fig. 25). The center flow line, where the probing laser focused on, was referred as the standard flow line, where all the particles should follow. The flow line position before and after irradiation was indicated as the relative distance from the center flow line (Δy) in the y direction (Fig. 25(a)). The flow lines before irradiation were showed as the black bars for all the particles (Fig. 25(b)), and those after irradiation were plotted separately for the fluorescent and non-fluorescent particles. After irradiation, the non-fluorescent particles entering the collection and the waste port were illustrated as orange and green bars respectively (Fig. 25(b)); on the other hand, the fluorescent ones were recorded in red and blue bars (Fig. 25(b)). The results reported that most of the non-

fluorescent particles went to the waste port in spite of a slight flow line shift after the irradiation, but a few fluorescent particles were lost in the waste port in this pulse energy of 0.6 μJ/pulse.

In addition, the non-fluorescent particle in front of the first fluorescent target in Fig. 25(b) was actually pushed a little bit and went to attach with another non-fluorescent particle even forwards. In contrast, the non-fluorescent particle behind the second fluorescent target in Fig. 25(d) was rarely influenced after fs-laser irradiation. This is consistent with the results mentioned in chapter 3.3. Even though, the influenced non-fluorescent particle still went to waste port after irradiation, so more performance evaluation is required and will be showed in next section.

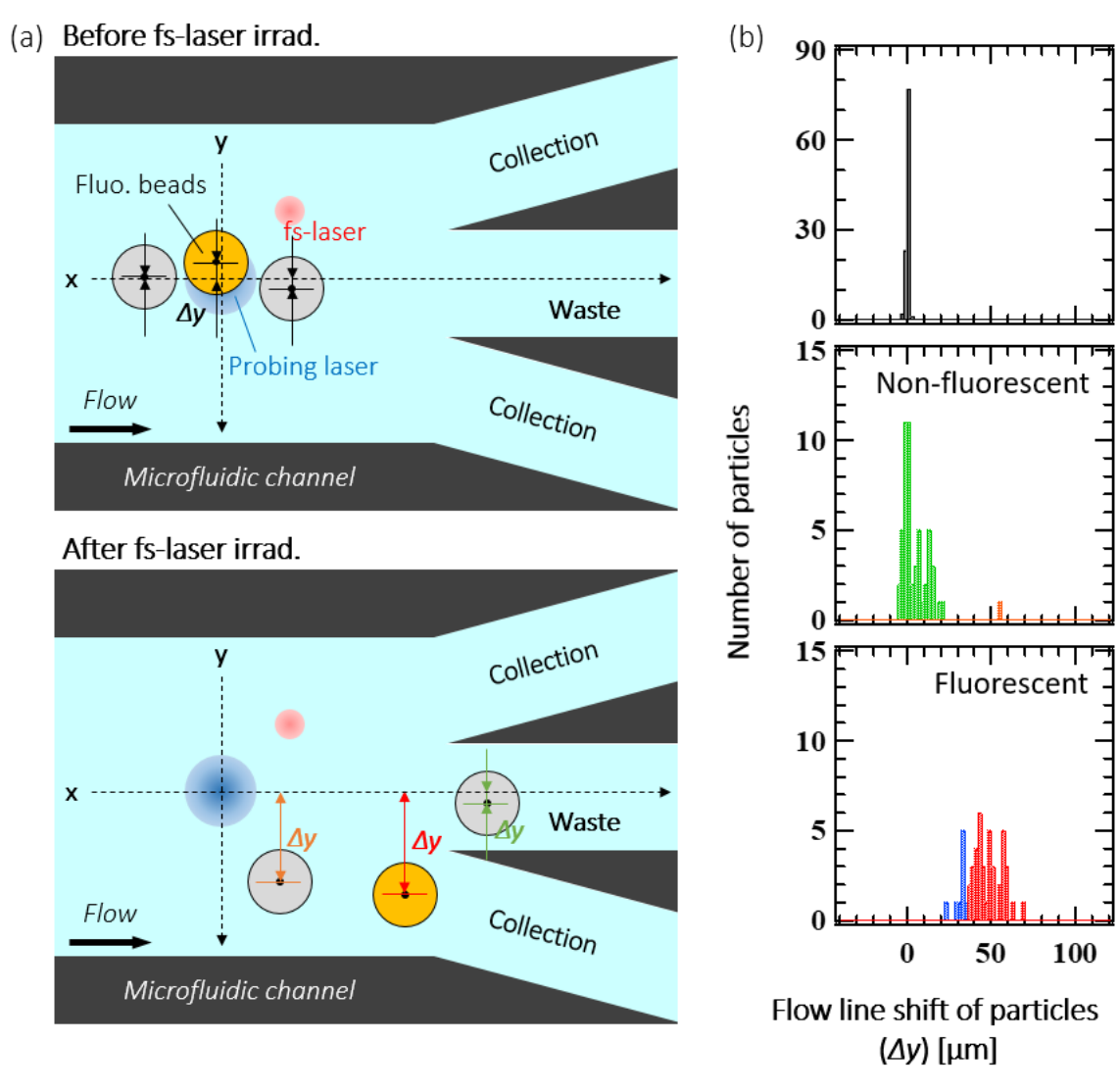

Fig. 25 A preliminary result of manipulation on a fluorescent particles (a) Evaluation parameters (b) Particle flow line positions before and after the manipulating process (orange and red: collected particles; green and blue: wasted particles)

4.3 Power dependence of manipulation

To optimize the success rate and purity for our manipulation system, we investigated the flow line shift of the fluorescent and non-fluorescent particles under conditions of different pulse energies from 0.5 to 1.5 μJ/pulse (Fig. 26). With 0.5 μJ/pulse, there were more than half fluorescent particles lost in the waste port but a few non-fluorescent particles collected as impurity, which attributed to the short particle-to-particle interval. As the pulse energy increased, the Δy of both the fluorescent and non-fluorescent particles increased. Surprisingly, not only the success rate but also the purity increased with the pulse energy and reach 100% as the pulse energy was over 1 μJ/pulse. This suggests both the targeted fluorescent particles and the neighboring non-targeted ones received a weak impulsive force of similar level with low pulse energy. Nevertheless, only the targeted fluorescent particles were brought into a region for a strong impulsive force as a threshold distance increasing with the pulse energy. Even though the non-targeted particles were influenced, they still went to waste port and remained the high purity rate. As the energy is kept increasing over 1.5 μJ/pulse in the future, it may have purity dramatically decreased at a specific energy. In addition, the threshold of success manipulating on the polymer micro-particles was revealed as the flow line shift of 35 μm, which would determine the destination of targets after irradiation.

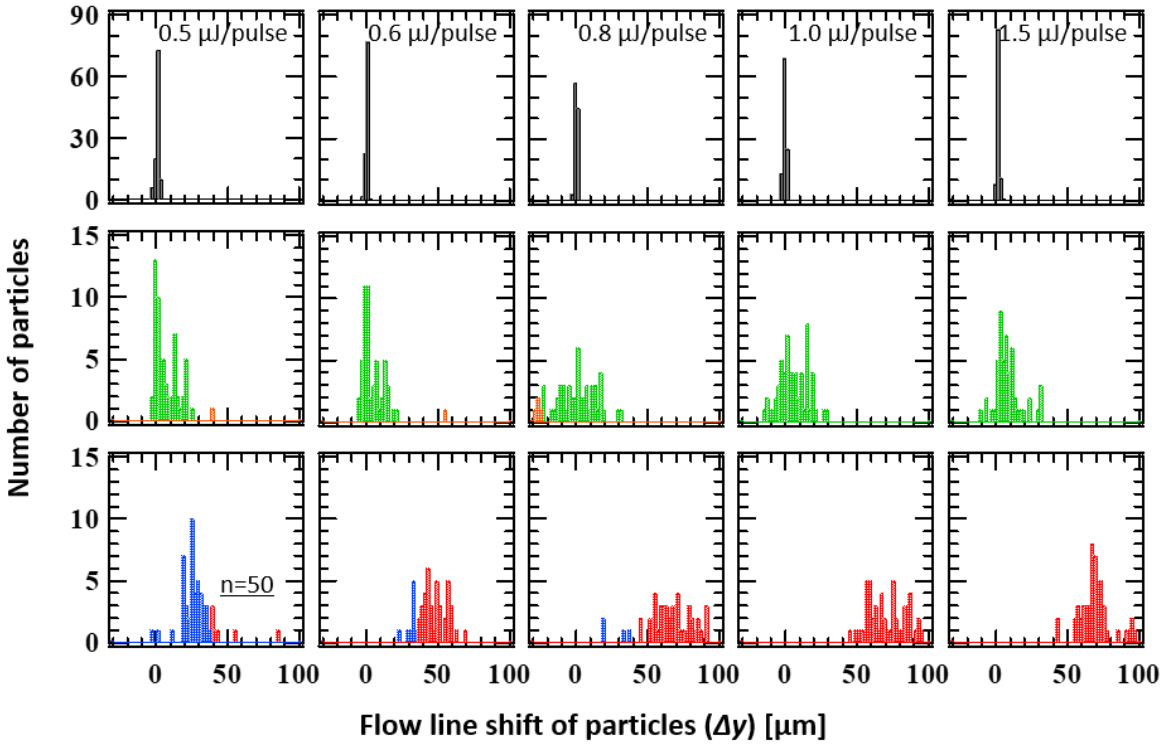

Fig. 26 Particle flow line positions before and after the manipulating process under various pulse energies

In addition, as the case of pulse energy of 0.8 μJ/pulse in Fig. 26, we observed an interesting case that the Δy of a few non-fluorescent particles became minus (orange bars) after irradiation, which means to be pulled toward the focal point of the fs-laser. Their motion dynamics are checked based on the high-speed images (Fig. 27). There was one fluorescent particle followed by a non-fluorescent one with a short particle-to-particle interval of 2 μm in Figure 27(a). The fluorescent particle followed the manipulating procedure with signal detection and flow line shift to the collection port (Fig. 27(b-h)). Unexpectedly, the flow line of the following non-fluorescent particle tilted after irradiation and went to the upper collection port. This may result from the collapse of the fs-laser induced cavitation bubble, which generated a pulling force to have the particle move toward laser focal point in the minus direction of the y axis. This was supported by another study on the dynamics of the fs-laser induced cavitation bubble in our group, which has indicated a pulling force following the impulsive force because of the collapse of the fs-laser induced cavitation bubble. To make the manipulating force high precision and reproducibility, the in-depth understanding on the fs-laser induced phenomenon in a fluid is required in the future.

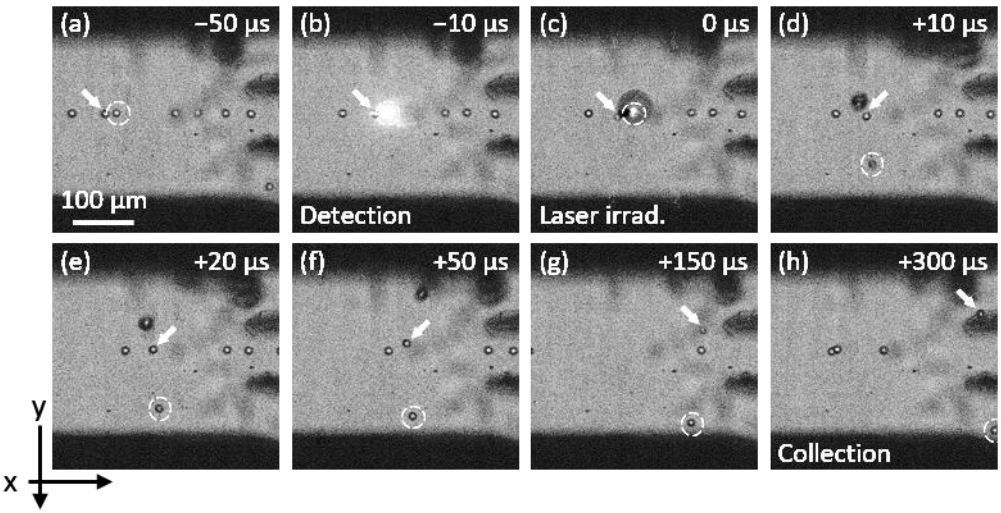

Fig. 27 A demonstrative case of the manipulating process for the mixture sample of both the fluorescent and non-fluorescent particles with a pulse energy of 0.8 μJ/pulse

4.4 Throughput estimation

Based on the high spatial resolution reported in chapter 3.2.2, the impulsive force had influence only in a range shorter than 13 μm on the center flow line at the optimal pulse energy of 1 μJ/pulse. This means this force could leave particles out of this range unaffected. Furthermore, the manipulating on tightly-packed 10 μm particles with 100% purity in this chapter (as showed in Fig. 24(a)) narrowed down the spatial resolution to 10 μm. In addition to the spatial resolution, the time cost for each manipulating process was critical to the throughput as well and defined as the life time of the fs-laser induced micro-phenomenon from one single pulse. For instance, if the cavitation bubble induced by previous pulse did not collapse yet, the next coming pulse would focus in air inside that bubble, which would fail to have another impulsive force for manipulation, not to mention a disturbance on the aligning of the laser focal point by the bubble. By increasing the imaging speed of camera, we could capture one image in every 4.2 μs (Fig.28). The laser-induced phenomenon was captured in only one image, which suggests a life span of ~4 μs or even shorter. Within this 4 μs, all the 10 μm particles just moved on the center flow line by 4 μm, which is smaller than the spatial resolution of manipulation. In other words, the laser-induced phenomenon including cavitation bubble disappear, and a single manipulating process finishes with no influence left on the next manipulating process. In comparison among particle size (10 μm), spatial resolution of manipulating (<10 μm) and life-time of cavitation bubble (<4 μs, equal to 4 μm at the 1 m/s flow velocity), the particle size is the largest to serve as the dividor in the throughput estimation.

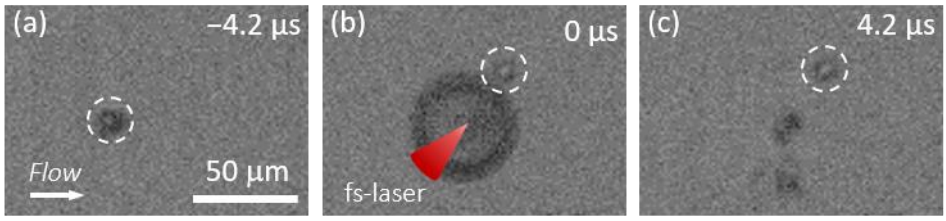

Fig. 28 High-speed images of the instant manipulating procedure with a fs-laser.

In combination of high spatial resolution, fast manipulating process and high repetition rate, the maximum throughput of manipulation could be estimated as 100,000 events/s for 10 μm particles in a flow velocity of 1 m/s under the compactly-packing condition of particles as shown Fig. 24(g). This have exceeded the existing optical manipulating methods in a microfluidic chip.

4.5 Summary

We have demonstrated our system could manipulate a highly concentrated sample containing both targeted and non-targeted particles in the high-speed fluid. The success rate and the purity was measured to be as high as 100% to manipulate all and only the targeted particles. In the meanwhile, our system achieved a high throughput of 100,000 events/s estimated to exceed the existing optical manipulating methods in a microfluidic chip, whose throughput is 830 (optical tweezer) [105] and 45,000 (nanosecond laser induced impulsive force) [67] events/s.

Based on the short life span of the manipulating process, it allowed our system with a potential throughput up to ~200, 000 events/s by increasing the flow velocity. In addition, the pulling force was observed under pulse energy of 0.8 μJ/pulse and necessary to have further investigation on the dynamics of fs-laser induced phenomenon for reproducibility of stable manipulating force.

Chapter 5 Pre-test of cell viability under the influence of the manipulating force

Now that we received a great manipulating performance with the high throughput of 100,000 particles, which supported the great performance of our high-speed cell manipulation system. The next step toward application is to manipulate real cells for usability evaluation of our system. Taking the complicated properties of cells into consideration, we first evaluated the impact of the manipulating force on the cells on top of simple cell-culturing dishes before manipulating cells with our system.

5.1 Method

5.1.1 Cell sample preparation

C2C12 mouse myoblast cells were grown in a common cell culture medium, which is DMEM (Dulbecco's modified eagle medium) supplemented with 10% FBS (fetal bovine serum) and antibiotics (100 units/ml penicillin, 0.1 mg/ml streptomycin), at 37˚C with 5% CO2 in flasks. The cells at 80~90% confluence were washed with phosphate-buffered saline (PBS), which is a buffer solution with balanced salt, and then detached from the flask surface by trypsin treatment (Fig. 29(a)). After collecting cells by centrifugation, the medium was replaced by the PBS buffer solution with isometric 0.1% trypan blue, which could only penetrate those cells with damaged membrane and bond with intracellular protein for contrast alteration to indicate dead cells. The cells with the PBS/trypan blue medium were put in a micro-chamber, consisting of a silicon rubber sandwiched between slide glass and cover slip (Fig. 29(a)). The cells were then kept in this medium for one-hour experiment, whose control experiment without the laser irradiation showed little damage (remained at survival rate of ~99%) induced by the one-hour exposure to the medium containing trypan blue stain.

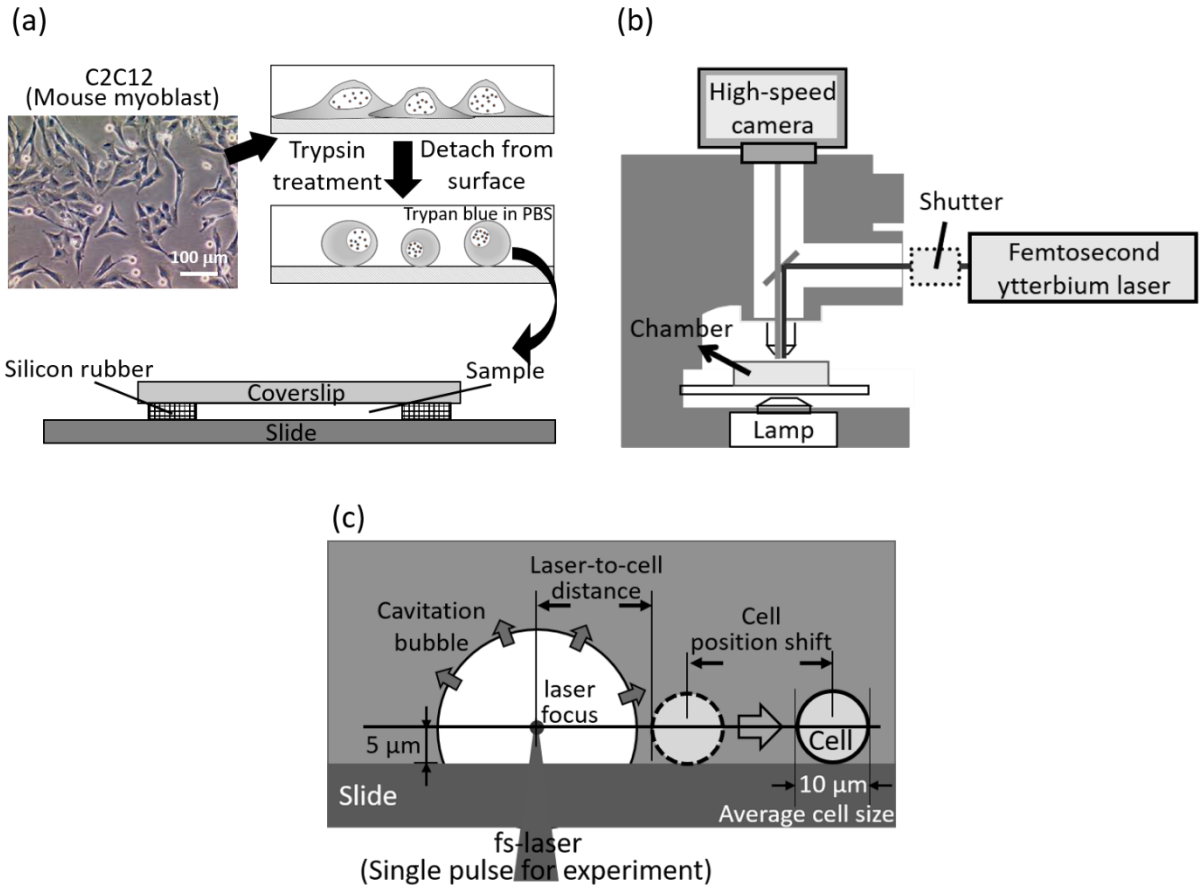

Fig. 29 Illustrative scheme for the procedure of the cell sample preparation and the sample setting onto our manipulation system (a) Preparation of suspended C2C12 cells in micro-chamber. (b) Experimental setup of the laser irradiation system (c) Geometrical relation between laser focal point, cavitation bubble, and C2C12 cell. The height of the laser focal point from the substrate surface was tuned to be 5 µm, which is nearly equal to average radius of the cells.

5.1.2 Experiment steps

The sample chamber was placed on the same upright microscope. Laser pulses from the same amplified femtosecond Yb laser system (400 fs, 1040 nm, <1 MHz, <8 µJ/pulse) were introduced into the microscope and focused in the chamber through the same 20× objective lens (NA. 0.4) (Fig. 29(b)). The laser pulse energy and the pulse repetition rate was controlled by the laser system. For this experiment, single laser pulses were picked up from the pulse train with repetition rate of 16 Hz by a mechanical shutter (Sigma Koki, Σ-65GR) with gate time of 62.5 ms and focused in the vicinity of target cells by controlling the motorized stage. The threshold pulse energy of the cavitation bubble generation was 0.3 µJ/pulse in both PBS buffer

solutions with and without the trypan blue. Although the trypan blue has a possibility to enhance the light absorption of the medium and the generation process of the cavitation bubble, the concentration would be too low to affect these processes.

As average radius of the cells was about 5 μm, laser focal position in the optical axis was adjusted to be 5 μm upper than the substrate by tuning the collimator lenses (Fig. 29(c)). The penetration of the trypan blue into the cell was checked by bright field image before and 5 minutes after the laser irradiation. In addition, cavitation bubble generation and the following position shift of the cell were observed by a high-speed camera (Ametek, Phantom V1211) with frame rate of 240,000 fps.

5.2 Cell motion induced by the manipulating force

A representative case with high-speed bright field images before and after the laser irradiation are shown in Fig. 30. We observed cavitation bubble generation immediately after the laser irradiation. There were three cells located around the laser focal point with different distances between cell membrane and the laser focal point ($D_{laser\text{-}to\text{-}cell}$). Only the nearest cell near the laser focal point was pushed away from the laser focal point along with the appearance of cavitation bubble. Although the rest two cells stayed at the same position before and after the laser irradiation, they actually received a pushing force as the cavitation bubble generated as we increased the imaging speed, and a pulling force was induced to have the two cell come back to the original position as the cavitation bubble collapsed. This is consistent with the results in a study of our group on the relation between micro-particles motion and the fs-laser induced cavitation bubble.

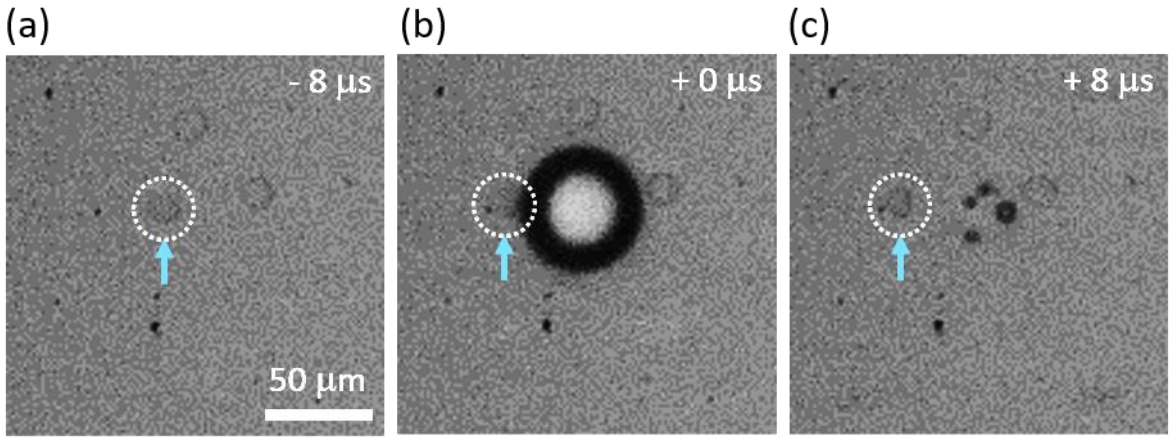

Fig. 30 High-speed images of the laser-induced cavitation bubble and the position shift of C2C12 cells (dotted circles) before and after the manipulating process

5.3 Cavitation bubble induced by the fs-laser

Hence, it is suggested that the cell motion strongly depended on spatial and temporal behavior of the cavitation bubble. The dependency of bubble size and life time on the pulse energy was explored. Take the pulse energy of 1.5 and 0.9 μJ/pulse for example, the high-speed images showed that the bubble size at 1.5 μJ/pulse was larger than that at 0.9 μJ/pulse (Fig. 31(a)). The bubble at 1.5 and 0.9 μJ/pulse appeared in two and one images respectively under a frame rate of 240,000 frames/s. This could be estimated to have a longer bubble life time of 8 μs at 1.5 μJ/pulse than that of 4 μs for 0.9 μJ/pulse. The pulse energy dependence of maximum diameter and life time of the cavitation bubble were recorded and shown in Fig. 31(b). The maximum radius and life time of the cavitation bubble increased with the laser pulse energy.

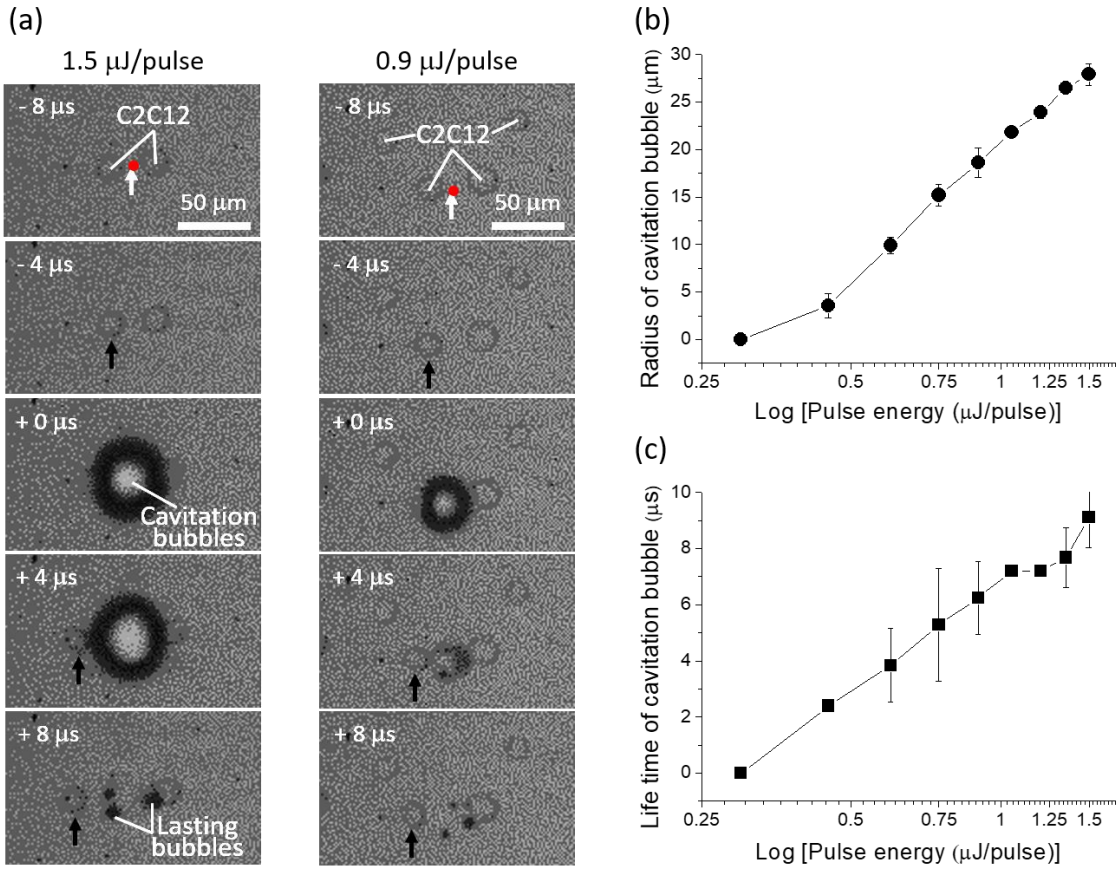

Fig. 31 (a) High-speed images of the laser-induced cavitation bubble and the position shift of C2C12 cells (shadowed circles) around the laser focal point (white arrows). The time origin (0 μs) is immediately after the laser irradiation. The laser pulse energy is 1.5 (left) and 0.9 (right) μJ/pulse respectively. (b, c) Pulse energy dependences of maximum radius (b) and life time (c) of cavitation bubble. Solid and dotted arrows indicate the experimental condition at 1.5 and 0.9 μJ/pulse respectively

5.4 Cell position shift and viability

The laser-induced position shift of the cell was estimated as a function of the difference between cell positions before the laser irradiation and at 4 ms after the laser irradiation when position shift was totally stopped, and plotted as a function of the distance between the laser focal point and the cell edge ($D_{laser\text{-}to\text{-}cell}$) in Fig. 32(a). The $D_{laser\text{-}to\text{-}cell}$ was tuned to be within a range from 0 (direct shot on cells) to 60 (around twice the cavitation bubble size) μm. The maximum position shift, when the laser focal point nearly contacts with the cell, was about 50 and 25 μm at 1.5 and 0.9 μJ/pulse respectively. The position shift was decreased with increasing the $D_{laser\text{-}to\text{-}cell}$. The obvious position shift was observed in the $D_{laser\text{-}to\text{-}cell}$ shorter than the radius of the cavitation bubble (arrows in Fig. 32(b)). This means that the main factor to induce the position shift is impact of the cavitation bubble to the cell. The amplitude of the fitting curve at 1.5 μJ/pulse (solid line) was about 1.8 times larger than that at 0.9 μJ/pulse (dotted line), which is similar with the difference of 1.7 times between pulse energy of 1.5 and 0.9 μJ/pulse. This indicates the cell position shift is almost proportional to the pulse energy, which supports the result in chapter 4.3. Even though those non-fluorescent particles near the targets also receives the impulsive force, their flow line shift is still much lower and insufficient to go to collection port.

Previously, in the experiment using the Ti:sapphire laser, we have also confirmed that the force due to impact of stress wave and cavitation bubble is linearly increased with the laser pulse with the laser pulse energy around the threshold of cavitation bubble generation [106]. Since the laser light is absorbed by multiphoton process, the absorption has strong nonlinearity against the irradiated pulse energy. If a certain percentage of the absorbed energy is converted to the energy to drive the stress wave, it is difficult to explain the liner dependence. Conversely, it is known that the nonlinear absorption is saturated when the pulse energy is extremely high because of absence of the ground-state molecule and the absorption is dominated by excited-state molecule, which can be excited by single-photon absorption. This behavior has been explained in terms of plasma absorption [107] and multi-cyclic absorption [108]. In such excitation condition, the energy absorbed by the solution is considered to be almost proportional to the input laser pulse energy.

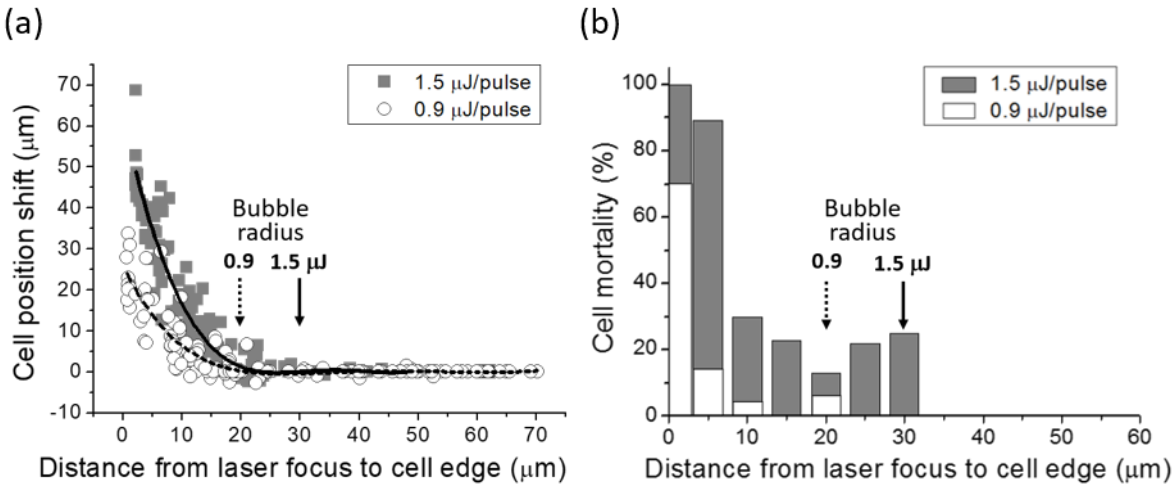

Fig. 32 (a) The dependence of cell position shift on distance between laser focus and cell edge. (b) The distance dependence of cell mortality. Cells tested in (a) were categorized into living and dead ones as a function of the distance and summarized in histogram (b). Solid and dotted arrows in (a) and (b) indicate the maximum radius of cavitation bubble at 1.5 and 0.9 μJ/pulse respectively. Each bar represents a distance range of ±2.5 μm from the central value except the first bar, which showed the results in the distance of 0~2.5 μm

The cell viability after the laser irradiation was evaluated cell-by-cell based on the cell mortality according to result of trypan blue staining, whose distance dependence was categorized (Fig. 32(b)). When the $D_{laser\text{-}to\text{-}cell}$ was shorter than 10 μm, the cell mortality was extremely high, which indicates the cells received strong damage. The damage decreased drastically in the $D_{laser\text{-}to\text{-}cell}$ longer than 10 μm. There was a threshold $D_{laser\text{-}to\text{-}cell}$ for the viability, above which the cell had no damage. The threshold $D_{laser\text{-}to\text{-}cell}$ was in good agreement with radius of the cavitation bubble, which was estimated from the Fig. 32(b). The cell mortality rate of 1.5 μJ/pulse was higher than that of 0.9 μJ/pulse at the same distance. More strictly to say, the rate had obvious nonlinear dependence on the pulse energy.

At 0 μm $D_{laser\text{-}to\text{-}cell}$ (0~2.5 μm), the mortality rate was 100% and 70% at the pulse energies of 1.5 and 0.9 μJ/pulse respectively. The very high cell mortality rate would be due to laser ablation of the cell at the laser focal point. Even when the laser did not directly focus on the cell, high cell mortality rate was observed at the $D_{laser\text{-}to\text{-}cell}$ less than 5 μm. In this condition, the cells may be destroyed by impact of the stress wave and the cavitation bubble. In addition, free-electrons generated at the laser focal point reacts with the buffer solution and produce oxidative species [109],

which is accumulated at the surface of the cavitation bubble in the generation process. An accidental cell death can be induced by exposure of the concentrated oxidative species with impact of cavitation bubble. In the interval between the seriously-damaged distance and the threshold distance in Fig. 32(b), main factor of the accidental cell death is speculated to be due to the impact of the cavitation bubble, while the impulsive force of the cavitation bubble and oxidative species at the bubble surface are distributed during the bubble expansion.

At the 5 μm $D_{laser\text{-}to\text{-}cell}$, the cell mortality rate of 1.5 μJ/pulse was over 6 times larger than that of 0.9 μJ/pulse. In the $D_{laser\text{-}to\text{-}cell}$ ranging from 5 μm to the value equivalent with the cavitation bubble radius, although the mortality rate of the former pulse energy was about 20 %, that of the latter was about 5% (low cell mortality). Obviously, there is strong nonlinearity in the pulse energy dependence, although the position shift of the cells (Fig. 32(a)) is almost proportional to the pulse energy. In the balance control between the cell viability and the cell position shift, the optimal condition for the cell sorting is that 15 μm position shift is induced with 10 % cell death when the laser at 0.9 μJ/pulse is focused from 5 μm $D_{laser\text{-}to\text{-}cell}$.

For instance, the minimum requirement for the cell manipulating is that the position shift is larger than the cell size, which is 10 μm in diameter for the C2C12 cell. Conclusively, in the present experiment, the optimal condition for the cell sorting is that 15 μm position shift is induced with 10 % cell death when the laser at 0.9 μJ/pulse is focused from 5 μm $D_{laser\text{-}to\text{-}cell}$, whose condition is quite close to that in chapter 4 for particle manipulation. Although the 10 % cell death is low, the 15 μm position shift is too small to have cells meet the requirement of flow line shift threshold (35 μm) for successful manipulating according to the results in chapter 4. This suggests the fs-laser induced impulsive force has a very different interaction with cells and the artificial polymer micro-particles.

5.5 Summary

In the on-dish experiments, we evaluated cell viability and position shift of C2C12 cells when the fs-laser was focused in the vicinity of the cell for usability elucidation of the fs-laser induced impulsive force as a manipulating force on single cells. The cell position was shifted with the impact of the cavitation bubble and meanwhile damaged by the cavitation bubble. Although both the position shift and the cell damage were increased with the irradiated laser pulse energy, the pulse energy dependency showed different behaviors. In the balance between the cell viability and the cell position shift, an optimal condition for the manipulation of the C2C12 cell is disclosed as the fs-laser with 0.9 μJ/pulse is focused at the $D_{laser\text{-}to\text{-}cell}$ of 5 μm, which is close to the current laser condition of the system (0.9 μJ/pulse at the $D_{laser\text{-}to\text{-}cell}$ of 3 μm) Therefore, the cell viability and displacement with current laser condition are estimated to be 30% and 20 μm. In comparison with the results of micro-particles in the chapter 4, the 20 μm cell displacements not able to overcome the threshold of flow line shift (35 μm in Fig. 26) for collection of targeted cells. A low success rate of manipulation is therefore predicted as the cell manipulation is conducted.

Chapter 6 Performance evaluation with cells

In comparison of the results in the chapter 4 and the on-dish experiments in the chapter 5, the optimal laser condition is almost the same to be ~ 1 μJ/pulse at the $D_{laser\text{-}to\text{-}cell}$ of 5 μm for manipulation of micro-particles and cells. Unfortunately, under this optimal laser condition, our manipulation system are predicted to have a poor manipulation performance of low success rate that cell may fail to arrive the collection port with a limited flow line shift (20 μm), which is less than half of the flow line shift threshold (35 μm). Even so, this on-chip experiment is still required to evaluate and confirm the manipulating performance of our current system, which would allow us to list out existing problems.

6.1 Method

6.1.1 Cell sample preparation

With the same culture method as mentioned in previous chapter, C2C12 cells were grown on a 6 cm dish with DMEM medium supplemented with 10% FBS and antibiotics at 37˚C with 5% CO_2. To test detect C2C12 cells in the manipulation system, a fluorescent labeling process was required as the procedure below. CMFDA (ViVidFluor Cell Green CMFDA, Wako, λ_{ex} = 492 nm, λ_{em} = 516 nm) was used as a fluorescent reagent, which is permeable to cell membrane and accumulated in the cytoplasm.

The cells at 80~90% confluence on the dish were washed by PBS and then added 2 ml fresh culture medium complemented with a CMFDA/Acetonitrile solution to be a final concentration of 10 μM. The dishes were put back to an incubator for 2 hours at 37˚C, and washed by PBS prior to a trypsin treatment with detach cells from the surface. After collecting cells by centrifugation, the trypsin solution was replaced by the PBS buffer solution, where the suspended cells were kept for the on-chip manipulating experiment. Concentration of the fluorescence-labeled C2C12 cells the was measured by a cell counter plate and tuned to be $\sim 1 \times 10^5$ cells/ml. In this experiment, all the suspended cells underwent the fluorescent labeling process, which means every cell is our target and should be collected by our system.

6.1.2 Experiment steps

The experimental setup as described in chapter 3.1.2 were utilized in this chapter with a different sample prepared above. The on-chip samples were measured for their cell density and viability right after preparation. After manipulating process, the sample was separated by the collection and the waste port into two tubes for the measurement of cell density and viability again.

6.2 Cell manipulating in the microfluidic chip

The cell manipulating in the microfluidic chip was first demonstrated in Fig. 33. The fluorescence emission was observed at the focal point of probing laser (Fig. 33(b)), and the impulsive force was generated (Fig. 33(c)) to have the flow line of the targeted cell shift to the collection port eventually (Fig. 33(d-f)). In this experiment after manipulation by our system, two tubes of solution from the collection ports and the waste port were analyzed by a cell counting plate.

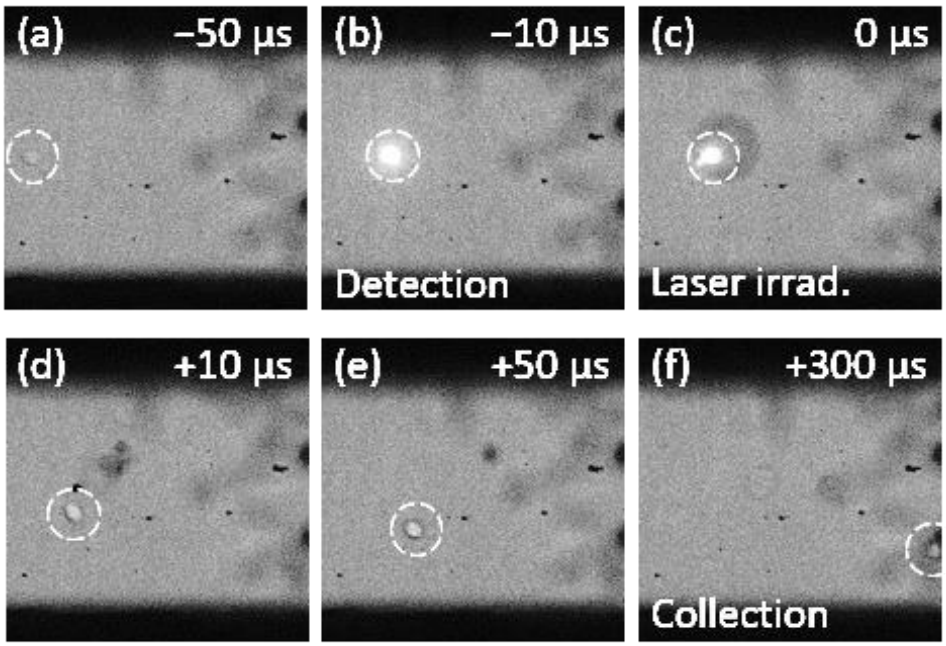

Fig. 33 A demonstrative case of the manipulating process for living C2C12 cells

6.3 Success rate

Different from the evaluation based on the high-speed videos for particles in chapter 4, the success rate here was evaluated based on the portion of the collected cells in the prepared cell amount after the manipulation by our system. There were 1.3×10^5 and 2.5×10^5 cells in the collection tube and waste tube respectively, which was deducted for the success rate of 21.7% according to the total cell amount of 6×10^5 cells in the prepared sample before manipulation. This low success rate is consistent with the prediction of the on-dish experiment and is much lower than other existing methods (Table 1), not to mention taking the purity into consideration as we employ complex sample (containing both targets and non-targets) in the future. With the high-speed imaging, a case of failed manipulating was showed as Fig. 34. It was noted that the targeted cell had a morphology deformation instead of flow line shift after exposure to the impulsive force, and recovered to round shape after hundreds of microseconds (Fig. 34(c-f)). The flow line of this targeted cell was rarely changed, and the targeted cell entered the waste port then. The cell deformation indicates a critical influence of the different characteristics between cells and artificial polymer micro-particles. Stiffness of cells is generally lower than polymer particles, especially the C2C12 cells we employed. As the nature of C2C12 cells, they are adherent cells that grow into a big population by leaning and attaching to one another, so the stiffness is lower compared with that of suspension cells such as blood cells. This low stiffness makes cells absorb the impulsive force through deformation. In addition, the deformation would cause unpredictable flow motion of cells such as falling trajectory of leaves, and this would decrease not only the success rate but also the purity.

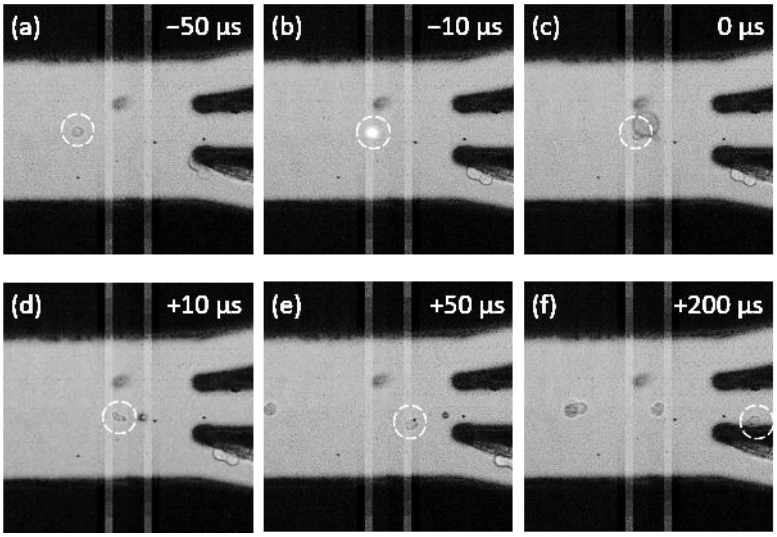

Fig. 34 A demonstrative case of a "failed" manipulating process for living C2C12 cells since the cell softness.

In addition, the total cell amount from both the collection ports and the waste port is inconsistent with that in the prepared sample before manipulation. This means we may lose nearly 40% cells in our system or during the analysis procedure, and suggests a huge problem of cell clogging in the microfluidic chip, which is serious and common for all the cell manipulation system currently. The cell clogging in the chip was confirmed after the experiment under microscope and cleaned out.

To confirm this problem, we repeated this experiment again with another sample of smaller volume. This time, there were 1×10^4 and 3×10^4 cells in the collection tube and waste tube, which was calculated for the success rate of 33.3% according to the total cell amount of 1.2×10^5 cells in the prepared sample before manipulation. With careful experiment operations, there was nearly 40% cells was lost again, which indicates this cell clogging would easily occur.

Another cause of the low success rate was the failure of thorough fluorescence labeling, which made part of cells carry little or insufficient fluorophores to actuate the manipulating process. A labeling failure case was showed as the following cell, which should have emitted fluorescence because it was prepared and operated in the same experimental procedure with the leading cell (Fig. 35). Therefore, the success rate here was underestimated since some cells actually emitted the weak fluorescence as non-targets, which conflicts with our expectation.

6.4 Cell viability

Cell viability in the prepared samples was confirmed before experiments and kept in a high level of 100% nearly. As mentioned above, we repeated this experiment twice, and the cell viability in the prepared samples was 100% and 93% for the first and second time. To confirm the cell damage induced by the high-speed flow and the acoustic aligning in the microfluidic chip, we made reference samples, which were loaded into the microfluidic chip without actuation of the manipulating force. The reference samples were tested for a cell viability of 87.3% and 97.5%. In comparison, average cell viabilities of the prepared and reference samples were 96.5% and 92.4% respectively, which were in a similar level and suggest little cell damage from the high-speed flow and the acoustic aligning.

Cell viability in the collection tube was 84.6% and 58.3% for the experiments of the first and second time, which was 71.5% in average. The cell viability was decreased from 92.4% (reference cells) to 71.5% (collected cells). This indicates that the manipulating force induced a cell mortality of ~20%, which is consistent with the results from the on-dish experiment under the optimal laser condition. However, the large difference of cell viability in the experiments of the first and second time was 26.3%, which suggests another issue of instability. This could result from the disturbance on acoustic aligning, which was induced by the cell clogging with an increasing distribution of cell flow line position before manipulation. The amounts of cells passing through the focal point of fs-laser were therefore increased to be directed ablated.

6.5 Throughput estimation

The same estimation method of throughput for micro-particle manipulation in the chapter 4 was followed here for cell manipulation in the microfluidic chip. A manipulating example of two tightly-neighboring cells was showed in Fig. 35. There was no space between the leading cell and the stalker cell. After fluorescence emission from the leading cell, the manipulating force still succeeded kicking the leading cell only to the collection port. This precise manipulating case on the cells of ~10 μm suggests the spatial resolution of manipulating is smaller than 10 μm. With the same estimation method, maximum throughput is retained at 100,000 events/s under 1 m/s flow velocity under the perfectly-aligning condition of particles as shown Fig. 24(g)

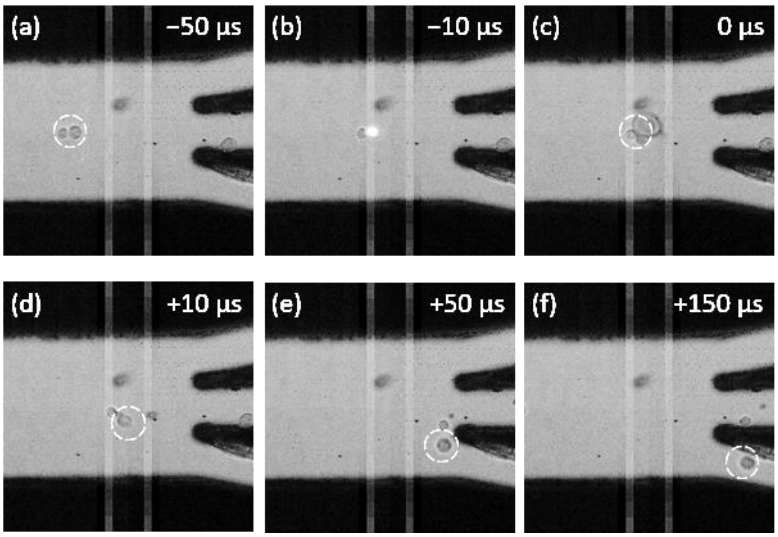

Fig. 35 High-speed images of a successful manipulating procedure for two cells with little space between each other.

6.6 Issues of proposed system

(1) Issues of target detection

This issue mainly results from the ineffective fluorescence labelling process, which made plenty of targeted cells carry insufficient fluorophores to be mis-judged as non-targets. Although our objective focuses on the manipulating force, an effective fluorescence labelling is still important for us to rule out the number of variants and narrow down the major cause of the low success rate in the on-chip experiments. The fluorescence labelling protocol will be adjusted by optimizing the incubating method or the incubation time. As the adhesive C2C12 cells tends to grow into clusters, there may be shielding from one another to stop the fluorophore loading. A suspended C2C12 by the trypsin treatment for aggregation reduction would be a good step to make cells exposed to the fluorophores more thoroughly for a better fluorescence labelling process. This may provide an effective fluorescence labelling with small intensity fluctuation for our future evaluation of the system.

(2) Issues of manipulating force

The issue of the soft cell membrane diminishing the manipulating force directly relates to the feasibility and usability of our optical manipulation system. As our objective to apply the system on the biological research and even clinical use, it is inevitable to manipulate cells, which are soft and flexible in general. Either increasing the pulse energy or a smaller $D_{laser\text{-}to\text{-}cell}$ could provide a stronger force for cell manipulation. Unfortunately, there is a confliction for these two solutions with the cell viability. If we increase the pulse energy or decrease the $D_{laser\text{-}to\text{-}cell}$ to enhance the manipulating force, the low cell viability under the optimal laser condition would decrease again with a dramatic drop, which would even rule out the potential of practicality of our manipulation system. This is the most serious problem to put our system into application. One potential solution is to decrease the flow line shift threshold by making the waste port narrower and the shape of branch structure sharper. This may improve the low success rate issue even though the small flow line shift of cells after manipulating. Therefore, our system possesses high potential to realized the high-speed cell manipulation in the near future.

(3) Issues of microfluidic chip

The cell clogging may not only reduce the success rate but even stop the system from functioning. The cell clogging would bring up various influences depending on

the clogging area and position. For instance, the clogging in the output channels of collection and waste ports would slow down the local flow velocity and induce an obstructing force to disturb the microfluidics upstream. The center flow line under the acoustic aligning would be deflected and have an increasing fluctuation. The center flow line deflected either away or close to the fs-laser focal point will lower the success rate and the cell viability respectively, not to mention a giant clogging to completely seal the waste port could produce a mis-leading result of 100% success rate. Coating on the inner surface of micro-channels to reduce the attachment of cells may reduce or even prevent the cell clogging.

6.7 Summary

In this chapter, we obtained the preliminary evaluation on the manipulating performance on cells. The success rate was as low as 27.5%, which means only one fourth targeted cells or so were collected back. The cell viability was decreased to 71.5% after the manipulating process, which is consistent with the results from on-dish experiments under the optimal laser condition. Most important of all, the maximum throughput was estimated according to the spatial resolution of the manipulating force and remained to be 100,000 events/s under 1 m/s flow velocity for 10 μm C2C12 cells. In spite of the low success rate and the moderate cell viability, a potential to achieve a high-speed manipulating is still kept for our system with the high throughput. As the current issues of the system listed above, it is still a long way to put our manipulation system into application prior to solving all the issues, especially the diminishing of the manipulating force by cell softness.

Chapter 7 Modification of the microfluidic channel with additive micro-structures

To improve the low success rate and moderate cell viability, we proposed a new manipulating strategy to have a stronger manipulating force, which is competent for diverse cells and particles and have lower cell damage at the meanwhile. Our strategy is to move the focal point away from the target into a micro-structure like a cavity, which is expected to enhance the manipulating force (Fig. 36(b)). In this strategy, the manipulating force will be a jet flow, where a fast fluid is pushed out from the cavity by the fs-laser induced impulsive force. Hence, the jet flow is expected to overcome the issue of cell softness and flexibility.

In this chapter, the feasibility of this strategy would be first tested, and the dependency of the jet flow intensity on the cavity size and shape would be further explored to pave the path toward a potential manipulating method.

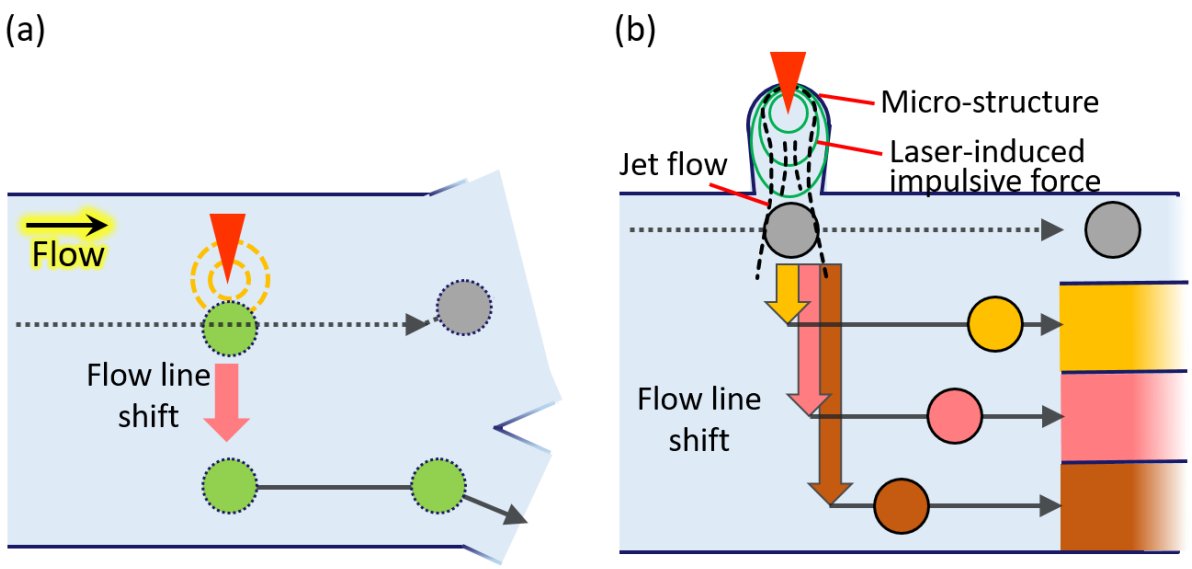

Fig. 36 Illustrative scheme of (a) our current cell manipulation system (b) concept for system modification

7.1 Method

7.1.1 Sample preparation

Solution with pure fluorescent particles

A medium of 20% blocking reagent was prepared by diluting the commercial product in pure water and served as a particle-carrying medium to avoid aggregation.

In this medium, 3 μm polystyrene polymer particles with fluorescence were added and mixed by a Vortex mixer for 1 minute. Concentration of the particles was measured by a cell counter plate and adjusted to be $2\sim3\times10^5$ particles/ml. This particle-containing medium was shaken by the Vortex mixer for 1 minute again to have the particles evenly spread. As last, a filter with 10 μm pores were employed to remove big particle clots in prevention from clogging in the microfluidic chip.

7.1.2 Experimental steps and setup

To test the feasibility of our new manipulating strategy with additive micro-structures, we prepared a new microfluidic chip. A glass microfluidic chip (Fig. 37 (b)) was designed with a software AutoCAD by myself and fabricated by wet-etching method with HF acid in assistance of Prof. Yaxar in our group. The channel in our microfluidic chip is composed of one inlet, one outlet and a main channel (Length: 3 cm, Width: 30 μm, Height: 10 μm). The micro-structures are located at the center of the bridge channel with nearly 1 mm space between one another, which is two-order larger than micro-structures to prevent any fluidic turbulence in between. The micro-structures could be categorized into three factors, which are bottom width, structure length as well as angle of its entrance. Especially, the angle of entrance means the angle between the main channel and the micro-structures shown as Fig. 37 (c). There are three shapes depended on the angle: Normal, Open and Close. The Normal shape is 90 degree. The Open shape is 105 degree (>90 degree), in contrast, the Close shape is 85 degree (<90 degree).

To evaluate this new manipulating force, the same experimental setup without a probing laser in the on-dish experiment of chapter 5 was employed (Fig. 37 (a)). The other microfluidic chip with new design was set on a movable stage under an upright microscope in assistance of a jig for fixation. With the syringe pump, the 3 μm polystyrene particles were introduced into the channel with flow velocity of 0.2 m/s. In this chapter, single laser pulses were picked up from the pulse train with repetition ration of 16 Hz by a mechanical shutter (Sigma Koki, Σ-65GR) with gate time of 62.5 ms and focused at the position inside the additive micro-structures by a 40× objective lens (Olympus, Plan N, NA. 0.8). The laser pulse energy and the pulse repetition rate was controlled by the laser system. Particle motion before and after the fs-laser irradiation was observed by high-speed imaging with a frame rate of 240,000 fps.

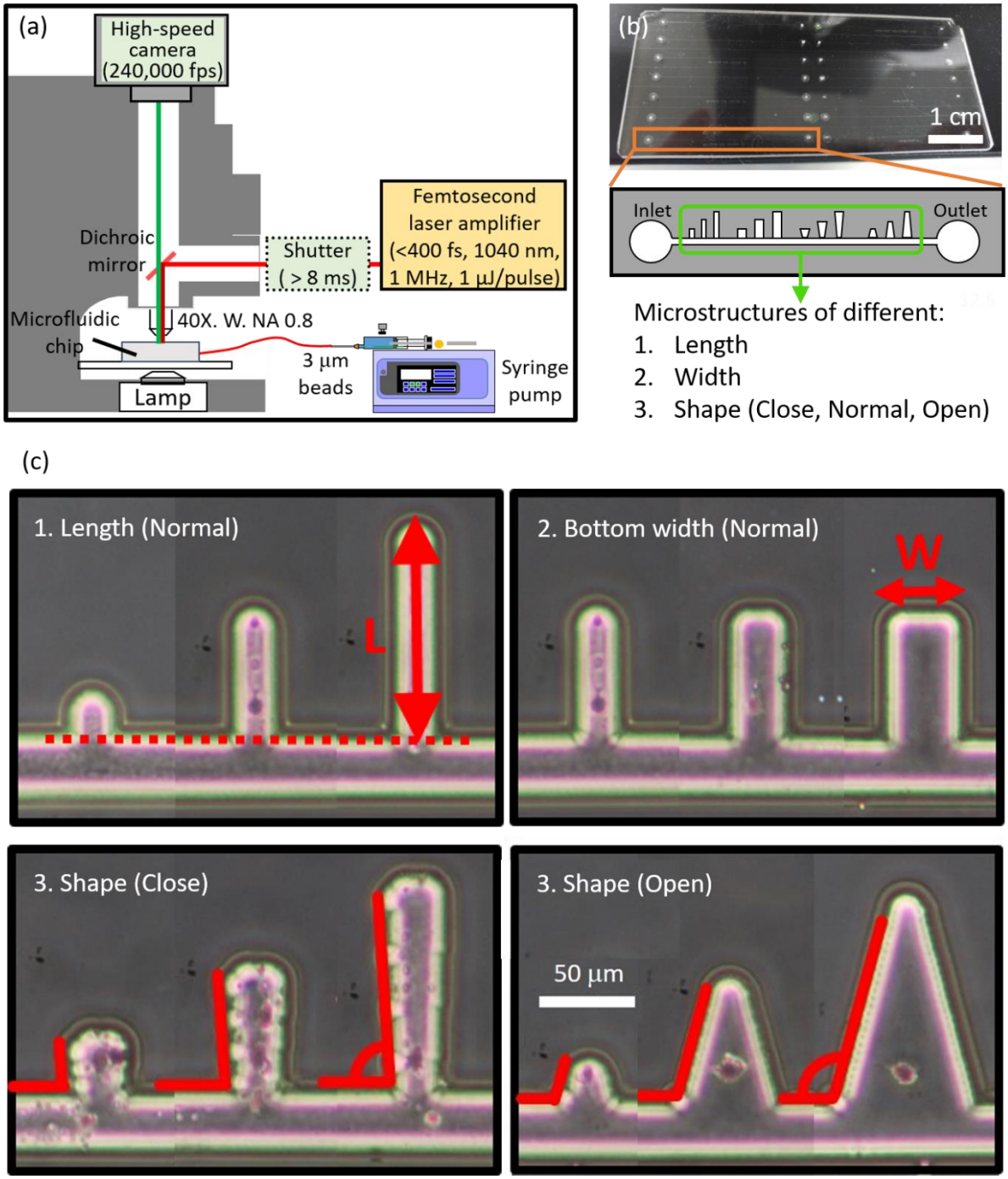

Fig. 37 (a) Experimental setup (b) Pictures of the microfluidic chip and (c) the micro-structures added inside the channel

7.2 Demonstration of particle manipulation

With high-speed imaging, the fs-laser induced phenomenon in the cavity of micro-structure was observed (Fig. 38). At the moment of fs-laser irradiation, an invisible and fast flow along with the a few bubbles was generated as (Fig 38). The bubbles were considered as lasting bubbles that came from the collapse of the fs-laser induced cavitation bubbles, and it assisted to indicate the invisible and fast flow which was named as jet flow in this experiment. In addition, the middle one of three coming particles was strongly pushed away by the jet flow, which served as the manipulating force in our proposal. The other two particles beside stayed nearly on their original flow line, which indicates a potential spatial resolution of this new manipulating force.

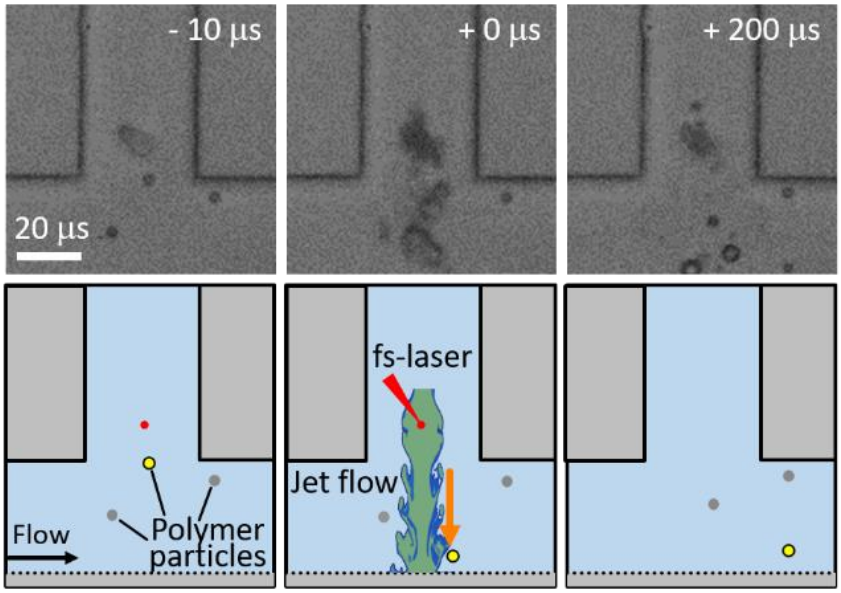

Fig. 38 High-speed image sequence for a demonstrative case of manipulation process on a fluorescent particle with the modified manipulating force by the micro-structure

7.3 Effect of micro-structures

Prior to an investigation on the micro-structures of various size and shape, we first attempted to confirm our expected force enhancing effect. We compared the fs-laser induced phenomenon inside and outside the micro-structures by setting the same relative distance of 10 μm between targets and the fs-laser focal point in the direction perpendicular to the targets' flow line (Fig. 39). Without the assistance of our designed micro-structures, the flow line of a targeted particle was slightly deflected away from the focal point of fs-laser by ~2 μm only. In contrast, with our micro-structures and the same laser-to-particle distance, the targeted particle was strongly pushed away by the fs-laser induce jet flow and received a large flow line shift. This suggests a force enhancing when this comparison was repeated with the optimal laser condition determined in the previous chapter. This force enhancing may result from the reflection and focusing of the radial impulsive force into a directional force by the micro-structures like a concave mirror redirecting the light source at the focus point.

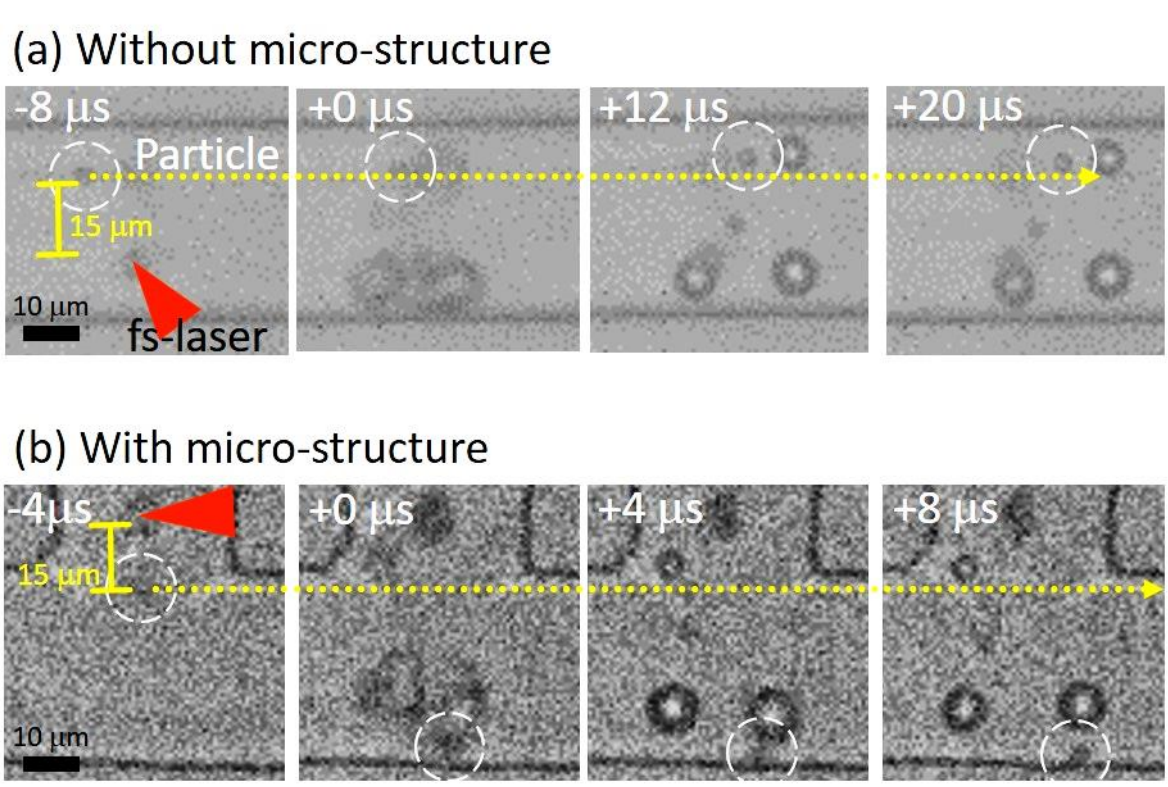

Fig. 39 Demonstrative cases of manipulation process on fluorescent particles (a) without and (b) with the designed micro-structure

7.4 Dependency of laser focal position

The dependency of laser focal position inside the micro-structures was first surveyed as soon as we confirm the force enhancing effect of our micro-structures. The pushing force intensity of the jet flow was evaluated based on the flow line shift of the targeted micro-particles. The force intensity as the fs-laser was focused at different positions was then measured with analyzing the flowing targets located in the front yard of the micro-structures as red dashed squares in Fig. 40. Two of the micro-structures were selected here and both of their results indicated the similar tendency that the force intensity is higher when the focal point of the fs-laser approached the entrance of the micro-structures. Beyond our expectation, this tendency is opposite to our expectation, that fs-laser focusing near cavity bottom of the micro-structures is more effective to pushing the fluid outward the cavity for a stronger jet flow. According to our proposal, the particles would be expected to flow along with the channel wall. This position at 10 μm from the entrance of the micro-structures was equal to the $D_{laser\text{-}to\text{-}cell}$, which would provide a high cell viability in line with the results of the on-dish experiments in chapter 5 and serve as a potential laser condition for this new system to have stronger manipulating force and retain the cell viability meanwhile.

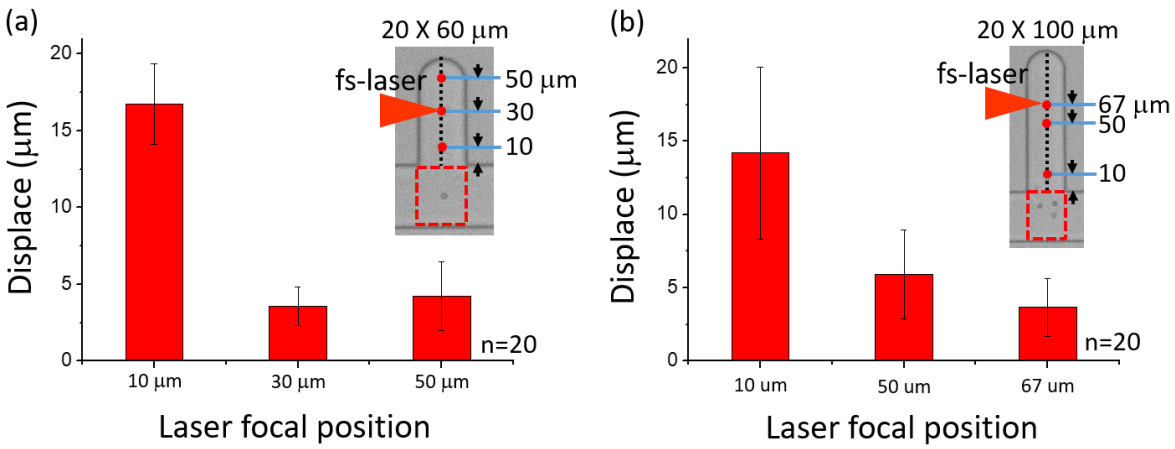

Fig. 40 Particle displacement by the jet flow with different laser focal positions inside the micro-structure (Width×Length) of (a) 20×60 μm and (b) 20×100 μm in normal shape

7.5 Optimization of micro-structure parameters: size and shape

Based on those results above, 10 μm away from the structure entrance was a potential position, which is hence set as a standard to compare the force of the jet flow under those micro-structures with various size and shape. In this experiment, only the particles within a region of 5 μm width in front of the micro-structure were analyzed to keep the laser-to-particle distance of ~10 μm. The flow line shift of these particles was measured by recording the flow line position before and after the irradiation. An average and a standard deviation of the flow line shift were calculated as a representative of the force intensity for each micro-structures. This was then plotted as a function of the force intensity generated by the micro-structures with various size and shape (Fig. 41).

As the normal-shape micro-structures shown in Fig. 41(a), there were three colors for the structure width of 20, 30, 40 μm respectively, and revealed the dependency of the force intensity on the structure length with fitting lines. The results of 20 μm-width group, the force intensity as well as its standard deviation increased with the structure length. In case of the 30 μm wide micro-structures, it showed a positive dependence with a larger flow line shift and a steeper slope compared with those of the 20 μm-width group. It means a longer structure did provide stronger jet flow but induce more instability of the manipulation at the same time. On the other hand, the larger structure width not only strengthens the jet flow but also raises the enhancing effect of the structure length without increasing of jet flow instability, which suggests the width factor play a dominant role over the length. As we increased again the structure width to 40 μm, the fitting line was turned into nearly horizontal and the standard deviations became huge and independent to the structure length. This indicates the structure width of 40 μm as a threshold width, over which would decrease the enhancing effect of the structure length and induce high instability of the jet flow although the force intensity was still remain at a high level.

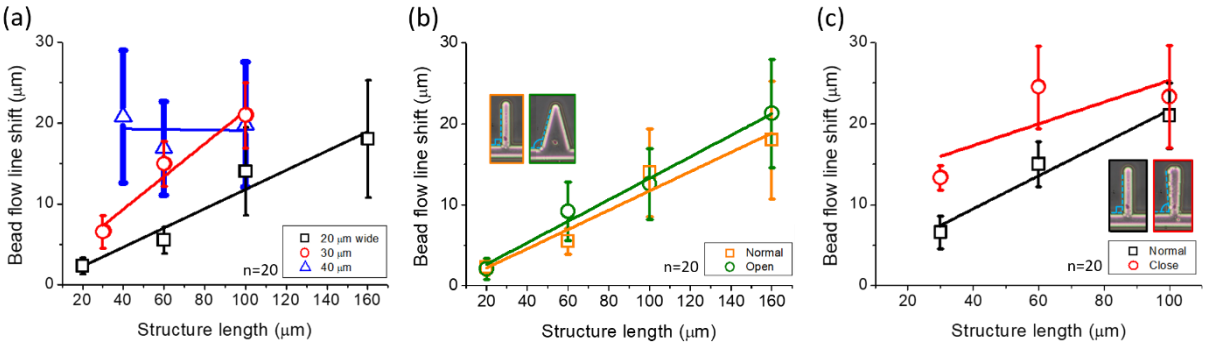

Fig. 40 Manipulating performance comparison of the jet flow induced in micro-structures of various (a) width and length and (b) the open shape (c) the close shape

Next, we compared the micro-structures of different shapes. In Fig. 41(b), the fitting lines of normal-shape and open-shape micro-structures showed a quite similar level for all the slope, deviation and magnitude. This indicates the open-shape barely benefited the force enhancing, which made no difference between the normal- and open- shape. On the contrary, in Fig. 41(c), the close-shape micro-structures had a fitting line with a larger magnitude but a smaller slope and a larger standard deviation. This denotes the force enhancing and the jet flow stability decreased as structure length increased, which means a confliction of enhancing effect between factors of the close-shape and the structure length. The close-shape can only benefit without a side-effect of the jet flow instability when the micro-structures are short. Totally, the structure size is the key factor for such force enhancing effect. We think it is highly relative to the process of the fs-laser induced cavitation bubble, particularly the structure width. A limited space was suspected to suppress the cavitation bubble generation, which was reported to be critical for manipulation in the on-dish experiments (chapter 5). The impulsive force was therefore diminished, which failed the jet flow activation. Conversely, an enough space allowed the cavitation bubble generation and impulsive force propagation for the jet flow activation (Fig. 42). In addition, in spite of the limited benefits of the close-shape, it is still expected to squeeze out the jet flow like a nozzle for high spatial resolution, which is the crucial character to realize a high-speed manipulation system. For the future work, we would have further investigation with a bigger channel first because the flow line shift in this chapter is always smaller than 20 μm, which is limited by the narrow channel of 30 μm. Then more structures and the flow dynamics during the entire manipulating process would be explored. Manipulation on particles and cells will be conducted

afterwards step by step toward applications.

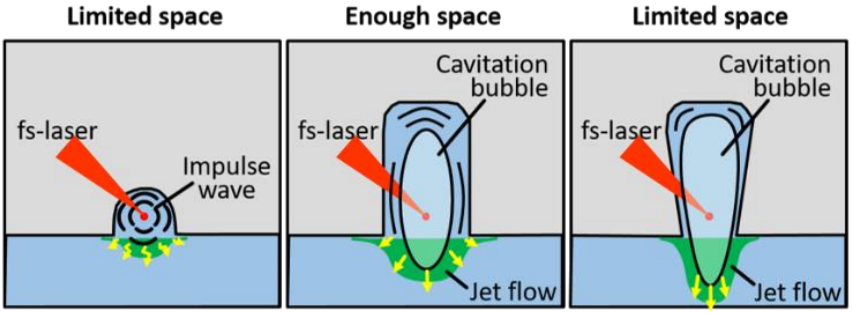

Fig. 42 Illustrative Schemes of the jet flow generation in the micro-structures of various sizes and shapes

7.6 Summary

In this chapter, we confirmed the feasibility of our proposal for a new manipulating force, and investigated the characteristics of our designed micro-structures. The force enhancing ability of the micro-structures of various size and shape was preliminary evaluated based on the flow line shift of flowing particles and summarized as Fig. 43. The magnitude of the force enhancing was strongly depended on the not only size and shape of the micro-structure but also the fs-laser focal position. Among factors relative to size and shape, the structure width is indicated to be the dominant factor on the force enhancement. The fs-laser focal position near the structure entrance showed a stronger force, which is an interesting topic to interrogate the working principles. In the future, to bring such micro-structures into application, further study on the activating process of the jet flow force will be conducted to provide a stronger manipulating force of both high directionality and spatial resolution for high-speed manipulation. The structure width of 30 μm would be the best starting point we disclosed here for the next step.

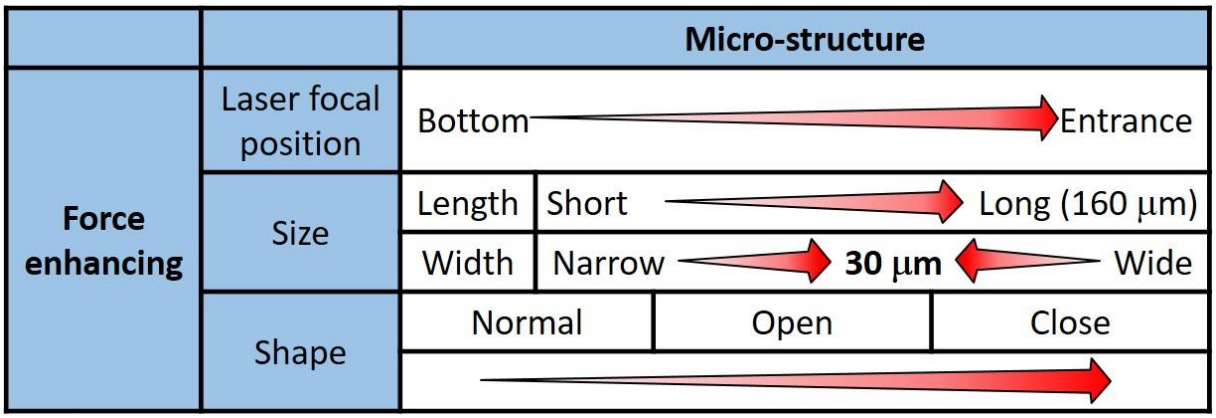

Fig. 43 Dependence of the jet flow (modified impulsive force) on the micro-structures of various sizes and shapes

Chapter 8 Conclusion and Perspective

The objective of this research focus on establishing a high-speed cell manipulation system to overcome the low throughput issue of the existing optical manipulation systems. The manipulation system is constructed in combination of techniques: positioning of micro-objects in the microfluidic, high-speed fluorescence detection circuit and a femtosecond laser induced impulsive force and a microfluidic chip. With cooperation among each element, our manipulation system achieve both high success rate and high purity to be 100%, which allow to collect all the targeted polymer micro-particles without impurity. On this basis, the maximum throughput was estimated to be 100,000 events/s. In comparison with the existing optical cell manipulation system (Table. 1), our system shows a great potential of higher purity (>99%) and throughput (100,000 events/s), which is higher than that of the ns-laser system by 2 times. The remained issues of our manipulation system for application of real cells is that the success rate drops to 27.5%, and the cell viability was 71.5% only. Fortunately, owing to the innate advantage of the fs-laser for high spatial resolution, the estimated maximum throughput was retained to be 100,000 events/s. Therefore, in the last chapter, a new manipulating force by modifying the fs-laser induced impulsive force to overcome the issue of low success rate and low cell viability was proposed and investigated for its feasibility. Our results demonstrate a potential of force enhancing for stronger manipulating force, and the basic characteristics has been investigated as a foundation stone toward the next step for cell manipulation in the future. The whole system establishing process was briefly concluded below chapter by chapter.

Chapter 1 introduced the requirement of high-speed manipulation for single cell research and the existing manipulation system. The low throughput and other drawbacks in each existing manipulation system were listed out and compared. With my knowledge and specialization at the femtosecond pulsed laser, the potential of this laser to improve the throughput and overcome the drawbacks was notice and described as my motivation.

Chapter 2 described the composition of my manipulation system and explained the functions of each element. Based on these elements, the working principle of the entire manipulation system was illustrated on the basis of cooperation of each elements.

In Chapter 3, the manipulating process based on my proposed working principle was successfully demonstrated to prove the feasibility of my manipulation system.

Further, parameter settings for a good cooperation among the working elements was explored and determined in order to have the manipulating process to be carried out correctly and precisely.

In Chapter 4, the manipulation system was preliminarily evaluated with the artificial micro-particles of high homogeneity for the first step. Both the success rate and the purity reached as high as 100%. Significantly, the maximum throughput was estimated to be 100,000 events/s with the high spatial resolution of my manipulating force, 10 μm. This suggests the potential of our system to overcome the low throughput issue of the existing manipulation systems. Moreover, the fast manipulating process of less than 5 μs was reported to potentially boost the maximum throughput up to 200,000 events/s.

In Chapter 5, before manipulating cells with our system, the cell damage and displacement induced by the manipulating force was evaluated on the simple dish outside of our system. Not only the dependence of the position shift and the cell damage on the $D_{laser\text{-}to\text{-}cell}$ was revealed, but also the optimal laser condition for cell manipulation could be disclosed to be the fs-laser with 0.9 μJ/pulse focused at the $D_{laser\text{-}to\text{-}cell}$ of 5 μm under the balance between the cell viability and the cell displacement. Such optimal laser condition is consistent with that for micro-particles in the Chapter 4, which revealed smaller displacements induced by the manipulating force for cells. This brings above a prediction that cells would fail to arrive collection port for a poor success rate of cell manipulation.

In Chapter 6, cells were employed to assess the applicability of my manipulation system for biological researches. It is a negative result that a low success rate of 27.5% and low cell viability of 71.5% was performed as our prediction in the previous chapter. Fortunately, the estimated maximum throughput was kept to be 100,000 events/s with the high spatial resolution of 10 μm, which could be taken as the nature advantage of the fs-laser as a manipulating force.

In Chapter 7, a new manipulating force, jet flow, was generated in assistance of additive micro-structures and proposed to overcome the poor manipulating performance on cells. The jet flow was confirmed for a potential to be a stronger manipulating force than the femtosecond laser induced impulsive force. Then, a basic investigation on the jet flow characteristics was conducted for the intensity dependency of the jet flow on the additive micro-structures of various size and shape was investigated. The results here would serve as the critical foundation stone to establish the high-speed cell manipulation system of second generation.

Sorting force	CW laser (optical trapping)	Nanosecond laser impulse	Femtosecond laser impulse	
Sample	Whole blood sample	White blood cell (B cell)	Polymer beads	Mouse myoblast cell
Throughput (events/s)	830	45,000	100,000	
Purity (%)	>90 %	45%	>99%	--
Success rate (%)	>90 %	>90 %	>99%	27.5%
Cell viability (%)	--	--	--	71.5%
Ref.	J. Guo et al., Biomed. Opt. Express 2017.	Y. Chen et al., Analyst, 2013.	(Under preparation)	

Table 1. The manipulating performance of our current cell manipulation system and other existing optical manipulation systems

In conclusion, our current system has showed a strong manipulation potential of high throughput to be 100,000 events/s, which is higher than other existing method in Table 1. Although we did not evaluate the purity for cell manipulation yet, the 100% purity of particle manipulation still support a potential of high purity for cell manipulation. Unfortunately, the success rate is much lower than other methods since the force weakening by the cell softness. This means that the manipulating performance is largely decreased when the maximum throughput (100,000) is multiplied by the low success rate (27.5%). For this low success rate issue, two solutions were proposed. One is to narrow the waste port channel for lower requirement of flow line shift, which has not been explored yet but seems to be a feasible solution in our future work. The other is to employ new micro-structures to enhance the manipulating force for meeting the requirement of flow line shift, which has been investigated preliminarily in chapter 7 and showed a great potential. This second solution not only solves the success rate issue but also broadens the application possibility for our system to conduct the manipulation into the multi-channel (Fig. 36 (b)) for complex composition of realistic sample. In addition, our system showed the cell viability of 70%, which is a little bit lower than that (>90%) of manipulation methods of mechanical, electric and magnetic. As we noticed the cell damage is highly relative to the contact of cavitation bubble, the new strategy proposed in chapter 7 is believed to improve the cell viability in the future because

of the manipulating process by the jet flow instead of the impulsive force from the cavitation bubble.

Even though more adjustments and improvements are still required to become feasible for practical applications, there are tremendous potentials of our optical manipulation system indicated in this work. One of the potentials is the throughput of our system to be estimated as high as 100,000 events/s, not to mention the maximum throughput in principle to be 1,000,000 events/s which is limited by the pulse repetition rate of a femtosecond laser (pulse number per second). As the enhancing of the manipulating force by the designed micro-structures is suggested in the chapter 7, this not only facilitates the establishment of our current high-speed cell manipulation system but also provides a possibility to make a further elevation of manipulation throughput by recruiting a femtosecond laser with an even higher repetition rate. For example, a femtosecond laser without assistance of an amplifier could provide a higher repetition rate than 1 MHz but a weak impulsive force with a much lower pulse energy. This concerning can be eliminated by our proposed micro-structures through enhancing the manipulating force. Therefore, taking a typical fs-laser oscillator with 80 MHz repetition rate for instance, the theoretical manipulating throughput could even be estimated up to 80,000,000 events/s, which indicates the immense potentiality of our proposed manipulation method. With such high potential of manipulating throughput, our manipulation system would boost the progress of single cell research in the future.

In addition to the throughput potential, the versatility potential of the fs-laser allows it be applied to not only cell manipulation but also cell treatment. For example, photo-injection has been widely explored for introduction of targeted molecules into single cells with pulsed lasers [110, 111]. With the assistance of microfluidic chip, photo-injection could be conducted more efficiently. Even optical modification of intracellular organisms with the fs-laser [112, 113] could be realized in the microfluidic chip as the increasing controllability of cell aligning with the growing micro-fluidic techniques. With the versatility of the fs-laser, our manipulation system could serve as a cell treatment system with high throughput through a minimum setup adjustment. This would highly raise the value of our system with multi-functions.

References

1. El-Ali, J.; Sorger, P. K.; & Jensen, K. F. "Cells on chips", *Nature* **442**, 403–411 (2006).
2. Dittrich, P. S.; Tachikawa, K.; & Manz, A. "Micro total analysis systems: Latest advancements and trends", *Analytical chemistry*, **78**, 3887–3908 (2006).
3. Swain, P. S.; Elowitz, M. B.; & Siggia, E. D. "Intrinsic and extrinsic contributions to stochasticity in gene expression", *Proceedings of the National Academy of Sciences*, **99**, 12795–12800 (2002).
4. Longo, D.; & Hasty, J. "Dynamics of single-cell gene expression", *Molecular systems biology*, **2**, 64 (2006).
5. Newman, J. R.; Ghaemmaghami, S.; Ihmels, J.; Breslow, D. K.; Noble, M.; DeRisi, J. L.; & Weissman, J. S. "Single-cell proteomic analysis of S. cerevisiae reveals the architecture of biological noise", *Nature*, **441**, 840–846 (2006).
6. Eldar, A.; & Elowitz, M. B. "Functional roles for noise in genetic circuits", *Nature*, **467**, 167–173 (2010).
7. Zhu, J.; & Paul, W. E. "CD4 T cells: fates, functions, and faults" *Blood*, **112**, 1557–1569 (2008).
8. Ferell, J. E.; & Machleder, E. M.; "The biochemical basis of an all-or-nonr cell fate switch in Xenopus Oocytes", *Science*, **280**, 895–898 (1998).
9. Yun, H.; Bang, H.; Min, J.; Chung, C.; Chang, J. K.; & Han, D. C. "Simultaneous counting of two subsets of leukocytes using fluorescent silica nanoparticles in a sheathless microchip flow cytometer", *Lab on a Chip*, **10**, 3243–3254 (2010).
10. Gross, A.; Schoendube, J.; Zimmermann, S.; Steeb, M.; Zengerle, R.; & Koltay, P. "Technologies for Single-Cell Isolation", *International journal of molecular sciences*, **16**, 16897–16919 (2015).
11. Johnstone, K. I. "Single Organisms", *Methods in microbiology*, **1**, 455 (1969).
12. Fröhlich, J.; & König, H. "New techniques for isolation of single prokaryotic cells", *FEMS microbiology reviews*, **24**, 567–572 (2000).
13. Eriksson, E.; Sott, K.; Lundqvist, F.; Sveningsson, M.; Scrimgeour, J.; Hanstorp, D.; Goksor, M.; & Granéli, A. "A microfluidic device for reversible environmental changes around single cells using optical tweezers for cell selection and positioning", *Lab on a Chip*, **10**, 617–625 (2010).
14. Ashkin, A. "Forces of a single-beam gradient laser trap on a dielectric sphere in the ray optics regime", *Biophysical journal*, **61**, 569-582 (1992).
15. Ashkin, A. ; Dziedzic, J. M.; & Yamane, T. "Optical trapping and manipulation

of single cells using infrared laser beams", *Nature*, **330**, 769 (1987).

16. Umehara, S.; Wakamoto, Y.; Inoue, I.; & Yasuda, K. "On-chip single-cell microcultivation assay for monitoring environmental effects on isolated cells", *Biochemical and biophysical research communications*, **305**, 534–540 (2003).
17. Asbury, C. L.; Fehr, A. N.; & Block, S. M. 2003 "Kenesin moves by an asymmetric hand-over-hand mechanism", *Science*, **302**, 2130–2134 (2003).
18. Ashkin, A.; Schütze, K.; Dziedzic, J. M.; Euteneuer, U.; & Schliwa, M.. "Force generation of organelle transport measured in vivo by an infrared laser trap", *Nature*, **348**, 346 (1990).
19. Roux, A.; Cuvelier, D.; Nassoy, P.; Prost, J.; Bassereau, P.; & Goud, B.. "Role of curvature and phase transition in lipid sorting and fission of membrane tubules", *The EMBO journal*, **24**, 1537–1545 (2005).
20. Boukobza, E.; Sonnenfeld, A.; & Haran, G. "Immobilization in surface-tethered lipid vesicles as a new tool for single biomolecule spectroscopy", *The Journal of Physical Chemistry B*, **105**, 12165–12170 (2001).
21. Chiou, P. Y.; Ohta, A. T.; & Wu, M. C; "Massively parallel manipulation of single cells and microparticles using optical images", *Nature*, **436**, 370 (2005).
22. Ozkan, M.; Wang, M.; Ozkan, C.; Flynn, R.; Birkbeck, A.; & Esener, S. "Optical manipulation of objects and biological cells in microfluidic devices", *Biomedical Microdevices*, **5**, 61–67 (2003).
23. Lincoln, B.; Schinkinger, S.; Travis, K.; Wottawah, F.; Ebert, S.; Sauer, F.; & Guck, J. "Reconfigurable microfluidic integration of a dual-beam laser trap with biomedical applications", *Biomedical microdevices*, **9**, 703–710 (2007).
24. Flynn, R. A.; Birkbeck, A. L.; Gross, M.; Ozkan, M.; Shao, B.; Wang, M. M.; & Esener, S. C. "Parallel transport of biological cells using individually addressable VCSEL arrays as optical tweezers", *Sensors and Actuators B: Chemical*, **87**, 239–243 (2002).
25. Birkbeck, A. L.; Flynn, R. A.; Ozkan, M.; Song, D.; Gross, M.; & Esener, S. C. "VCSEL arrays as micromanipulators in chip-based biosystems", *Biomedical Microdevices*, **5**, 47–54 (2003).
26. Huh, D.; Gu, W.; Kamotani, Y.; Grotberg, J. B.; & Takayama, S. "Microfluidics for flow cytometric analysis of cells and particles", *Physiological measurement*, **26**, R73 (2005).
27. Yang, Z.; Yu, B.; Zhu, J.; Huang, X.; Xie, J.; Xu, S.; Yang, X.; Wang, X.; Yung, B. C.; Lee, L. J.; et al. "A microfluidic method to synthesize transferrin-lipid

nanoparticles loaded with siRNA LOR-1284 for therapy of acute myeloid leukemia", *Nanoscale*, **6**, 9742–9751 (2014).

28. Primiceri, E.; Chiriaco, M. S.; Rinaldi, R.; & Maruccio, G. “Cell chips as new tools for cell biology–results, perspectives and opportunities” *Lab on a Chip*, **13**, 3789-3802 (2013).
29. Li, P. C.; & Harrison, D. J. "Transport, manipulation, and reaction of biological cells on-chip using electrokinetic effects", *Analytical Chemistry*, **69**, 1564–1568 (1997).
30. Mehling, M.; & Tay, S. "Microfluidic cell culture", *Current opinion in Biotechnology*, **25**, 95–102 (2014).
31. Hejazian, M.; & Li, W.; Nguyen, N.-T. "Lab on a chip for continuous-flow magnetic cell separation", *Lab on a Chip*, **15**, 959–970 (2015).
32. Volpatti, L. R.; & Yetisen, A. K. "Commercialization of microfluidic devices", *Trends in biotechnology*, **32**, 347–350 (2014).
33. Siegel, D. L.; Chang, T. Y.; Russell, S. L.; & Bunya, V. Y. "Isolation of cell surface-specific human monoclonal antibodies using phage display and magnetically-activated cell sorting: applications in immunohematology", *Journal of immunological methods*, **206**, 73–85 (1997).
34. Umehara, S.; Wakamoto, Y.; Inoue, I.; & Yasuda, K. "On-chip single-cell microcultivation assay for monitoring environmental effects on isolated cells", *Biochemical and biophysical research communications*, **305**, 534–540 (2003).
35. Enger, J.; Goksör, M.; Ramser, K.; Hagberg, P.; & Hanstorp, D. "Optical tweezers applied to a microfluidic system", *Lab on a Chip*, **4**, 196–200 (2004).
36. Karniadakis G. E.; & Beskok, A. "Micro Flows: Fundamentals and Simulation (Book)", *Springer*, (2002).
37. Hunt, T. P.; Issadore, D.; & Westervelt, R. M. "Integrated circuit/microfluidic chip to programmably trap and move cells and droplets with dielectrophoresis", *Lab on a Chip*, **8**, 81–87 (2008).
38. Neale, S. L.; Ohta, A. T.; Hsu, H. Y.; Valley, J. K.; Jamshidi, A.; & Wu, M. C. "Trap profiles of projector based optoelectronic tweezers (OET) with HeLa cells", *Optics express*, **17**, 5231–5239 (2009).
39. Thomas, R. S.; Morgan, H.; & Green, N. G. "Negative DEP traps for single cell immobilisation", *Lab on a Chip*, **9**, 1534–1540 (2009).
40. Chiou, P. Y.; Ohta, A. T.; & Wu, M. C. "Massively parallel manipulation of single cells and microparticles using optical images", *Nature*, **436**, 370 (2005).

41. Han, K. H.; & Frazier, A. B. "Lateral-driven continuous dielectrophoretic microseparators for blood cells suspended in a highly conductive medium", *Lab on a Chip*, **8**, 1079–1086 (2008).
42. Kim, U.; Qian, J.; Kenrick, S. A.; Daugherty, P. S.; & Soh, H. T. "Multitarget dielectrophoresis activated cell sorter", *Analytical chemistry*, **80**, 8656–8661 (2008).
43. Yang, J.; Huang, Y.; Wang, X. B.; Becker, F. F.; & Gascoyne, P. R. "Differential analysis of human leukocytes by dielectrophoretic field-flow-fractionation", *Biophysical journal*, **78**, 2680–2689 (2000).
44. Hu, X.; Bessette, P. H.; Qian, J.; Meinhart, C. D.; Daugherty, P. S.; & Soh, H. T. "Marker-specific sorting of rare cells using dielectrophoresis", *Proceedings of the National Academy of Sciences of the United States of America*, **102**, 15757–15761 (2005).
45. Malachowski, K.; Jamal, M.; Jin, Q.; Polat, B.; Morris, C. J.; & Gracias, D. H. "Self-folding single cell grippers", *Nano letters*, **14**, 4164–4170 (2014).
46. Kawai, M.; Nogami, T.; Takano, K.; Okumura, A.; Nakazato, K.; Ikeuchi, M.; & Matsushita, S. "Single-cell Trapping Using Microwell Arrays Fabricated from Self-assembled Particle Monolayers", *Molecular Crystals and Liquid Crystals*, **603**, 248–255 (2014).
47. Irimia, D.; & Toner, M. "Cell handling using microstructured membranes", *Lab on a Chip*, **6**, 345–352 (2006).
48. Hümmer, D.; Kurth, F.; Naredi-Rainer, N.; & Dittrich, P. S. "Single cells in confined volumes: Microchambers and microdroplets", *Lab on a Chip*, **16**, 447–458 (2016).
49. Van Delinder, V.; & Groisman, A. "Perfusion in microfluidic cross-flow: Separation of white blood cells from whole blood and exchange of medium in a continuous flow", *Analytical Chemistry*, **79**, 2023–2030 (2007).
50. Di Carlo, D.; Wu, L. Y.; & Lee, L. P. "Dynamic single cell culture array", *Lab on a Chip*, **6**, 1445–1449 (2006).
51. Lin, L. Y.; Chu, Y. S.; Thiery, J. P.; Lim, C. T.; & Rodriguez, I. "Microfluidic cell trap array for controlled positioning of single cells on adhesive micropatterns", *Lab on a Chip*, **13**, 714–721 (2013).
52. Jimenez, M.; Miller, B.; & Bridle, H. L. "Efficient separation of small microparticles at high flowrates using spiral channels: application to waterborne pathogens", *Chemical Engineering Science*, **157**, 247-254 (2017).

53. Che, J.; Yu, V.; Garon, E. B.; Goldman, J. W.; & Di Carlo, D. "Biophysical isolation and identification of circulating tumor cells", *Lab on a Chip*, **17**, 1452–1461 (2017).
54. Dhar, M.; Lam, J. N.; Walser, T.; Dubinett, S. M.; Rettig, M. B.; & Di Carlo, D. "Functional profiling of circulating tumor cells with an integrated vortex capture and single-cell protease activity assay", *Proceedings of the National Academy of Sciences*, **115**, 9986–9991 (2018).
55. Bruus, H.; Dual, J.; Hawkes, J.; Hill, M.; Laurell, T.; Nilsson, J.; & Wiklund, M. "Forthcoming Lab on a Chip tutorial series on acoustofluidics: Acoustofluidics—exploiting ultrasonic standing wave forces and acoustic streaming in microfluidic systems for cell and particle manipulation", *Lab on a Chip*, **11**, 3579–3580 (2011).
56. Shi, J. J.; Ahmed, D.; Mao, X.; Lin, S. C. S.; Lawit, A.; & Huang, T. J. "Acoustic tweezers: Patterning cells and microparticles using standing surface acoustic waves (SSAW)", *Lab on a Chip*, **9**, 2890–2895 (2009).
57. Ding, X.; Lin, S. C. S.; Lapsley, M. I.; Li, S.; Guo, X.; Chan, C. Y.; & Huang, T. J. "Standing surface acoustic wave (SSAW) based multichannel cell sorting", *Lab on a Chip*, **12**, 4228–4231 (2012).
58. Evander, M.; Johansson, L.; Lilliehorn, T.; Piskur, J.; Lindvall, M.; Johansson, S.; Almqvist, M.; Laurell, T.; & Nilsson, J. "Noninvasive acoustic cell trapping in a microfluidic perfusion system for online bioassays", *Analytical chemistry*, **79**, 2984–2991 (2007).
59. Hultstrom, J.; Manneberg, O.; Dopf, K.; Hertz, H. M.; Brismar, H.; & Wiklund, M. "Proliferation and viability of adherent cells manipulated by standing-wave ultrasound in a microfluidic chip", *Ultrasound in medicine & biology*, **33**, 145–151 (2007).
60. Yeo, L. Y.; Chang, H. C.; Chan, P. P.; & Friend, J. R. "Microfluidic devices for bioapplications", *Small*, **7**, 12–48 (2011).
61. Ding, X.; Lin, S. C. S.; Kiraly, B.; Yue, H.; Li, S.; Chiang, I. K.; Jinjie, S.; Stephen, J. B.; & Huang, T. J. "On-chip manipulation of single microparticles, cells, and organisms using surface acoustic waves", *Proceedings of the National Academy of Sciences*, **109**, 11105–11109 (2012).
62. Ha, B. H.; Lee, K. S.; Destgeer, G.; Park, J.; Choung, J. S.; Jung, J. H.; Jennifer, H. S.; & Sung, H. J. "Acoustothermal heating of polydimethylsiloxane microfluidic system", *Scientific reports*, **5**, 11851 (2015).
63. Wang, X.; Chen, S.; Kong, M.; Wang, Z.; Costa, K. D.; Li, R. A.; & Sun, D.

"Enhanced cell sorting and manipulation with combined optical tweezer and microfluidic chip technologies", *Lab on a Chip*, **11**, 3656–3662 (2011).

64. Eriksson, E.; Sott, K.; Lundqvist, F.; Sveningsson, M.; Scrimgeour, J.; Hanstorp, D.; Goksor, M.; & Granéli, A. "A microfluidic device for reversible environmental changes around single cells using optical tweezers for cell selection and positioning", *Lab on a Chip*, **10**, 617–625 (2010).
65. Applegate Jr, R. W.; Squier, J.; Vestad, T.; Oakey, J.; Marr, D. W.; Bado, P.; Mark, A. D.; & Said, A. A. "Microfluidic sorting system based on optical waveguide integration and diode laser bar trapping", *Lab on a Chip*, **6**, 422–426 (2006).
66. Wu, T. H.; Gao, L.; Chen, Y.; Wei, K.; & Chiou, P. Y. "Pulsed laser triggered high speed microfluidic switch", *Applied Physics Letters*, **93**, 144102 (2008).
67. Chen, Y.; Wu, T. H.; Kung, Y. C.; Teitell, M. A.; & Chiou, P. Y. "3D pulsed laser-triggered high-speed microfluidic fluorescence-activated cell sorter", *Analyst*, **138**, 7308–7315 (2013).
68. Strickland, D.; & Mourou, G. "Compression of amplified chirped optical pulses", *Optics communications*, **55**, 447–449 (1985).
69. Maine, P.; Strickland, D.; Bado, P.; Pessot, M.; & Mourou, G. "Generation of ultrahigh peak power pulses by chirped pulse amplification", *IEEE Journal of Quantum electronics*, **24**, 398–403 (1988).
70. Zhang, H.; Lu, S. B.; Zheng, J.; Du, J.; Wen, S. C.; Tang, D. Y.; & Loh, K. P. "Molybdenum disulfide (MoS 2) as a broadband saturable absorber for ultra-fast photonics", *Optics express*, **22**, 7249–7260 (2014).
71. Kemp, M. C.; Taday, P. F.; Cole, B. E.; Cluff, J. A.; Fitzgerald, A. J.; & Tribe, W. R. " Security applications of terahertz technology", *Proceedings of International Society for Optics and Photonics In Terahertz for Military and Security Applications*, **5070**, 44–53 (2003).
72. Gordon, J. P. "Interaction forces among solitons in optical fibers", *Optics letters*, **8**, 596–598 (1983).
73. Stegeman, G. I.; & Segev, M. "Optical spatial solitons and their interactions: universality and diversity", *Science*, **286**, 1518–1523 (1999).
74. Fork, R. L.; Shank, C. V.; Hirlimann, C.; Yen, R.; & Tomlinson, W. J. "Femtosecond white-light continuum pulses", *Optics letters*, **8**, 1–3 (1983).
75. Gattass, R. R.; & Mazur, E. "Femtosecond laser micromachining in transparent materials", *Nature photonics*, **2**, 219 (2008).
76. Zipfel, W. R.; Williams, R. M.; & Webb, W. W. "Nonlinear magic: multiphoton

microscopy in the biosciences", *Nature biotechnology*, **21**, 1369 (2003).

77. Townes, C. H. "Optical masers and their possible applications to biology", *Biophysical journal*, **2**, 325–329 (1962).
78. Denk, W.; Strickler, J. H.; & Webb, W. W. "Two-photon laser scanning fluorescence microscopy", *Science*, **248**, 73–76 (1990).
79. Nuzzo, V.; Plamann, K.; Savoldelli, M.; Merano, M.; Donate, D.; Albert, O.; Rodriguez, P. F. G.; Mourou, G.; & Legeais, J. -M. "In situ monitoring of second-harmonic generation in human corneas to compensate for femtosecond laser pulse attenuation in keratoplasty", *Journal of Biomedical Optics*, **12**, 064032–064011 (2007).
80. Han, M.; Zickler, L.; Giese, G.; Walter, M.; Loesel, F. H.; & Bille, J. F. "Second-harmonic imaging of cornea after intrastromal femtosecond laser ablation", *Journal of biomedical optics*, **9**, 760–767 (2004).
81. Bessis, M. ; Gires, F. ; Mayer, G.; & Nomarski, G. "Irradiation des organites cellulaires a l'aide d'un LASER a rubis," *Comptes Rendus Hebdomadaires des Seances de l'Academie. des Sciences*, **255**, 1010 (1962).
82. Saks, N. M.; & Roth, C. A. "Ruby laser as a microsurgical instrument", *Science*, **141**, 46–47 (1963).
83. Amy, R. L.; & Storb, R. "Selective mitochondrial damage by a ruby laser microbeam: an electron microscopic study", *Science*, **150**, 756–758 (1965).
84. Berns, M. W.; Olson, R. S.; & Rounds, D. E. "In vitro production of chromosomal lesions with an argon laser microbeam", *Nature*, **221**, 74–75 (1969).
85. Zaret, M. M.; Breinin, G. M.; Schmidt, H.; Ripps, H.; Siegel, I. M.; & Solon, L. R. "Ocular lesions produced by an optical maser (laser)", *Science*, **134**, 1525–1526 (1961).
86. Goldman, L.; Blaney, D. J.; Jun, D. J. K.; Richfield, D.; & Franke, E. K. "Pathology of the effect of the laser beam on the skin", *Nature*, **197**, 912–914 (1963).
87. Goldman, L.; Hornby, P.; Meyer, R.; & Goldman, B. "Impact of the laser on dental caries", *Nature*, **203**, 417 (1964).
88. F. Fankhauser, and S. Kwasniewska, Lasers in Ophthalmology—Basic, Diagnostic, and Surgical Aspects: A Review (Kugler Publications, The Hague, Netherlands, 2003).
89. Fankhauser, F.; & Kwasniewska, S. "Lasers in Ophthalmology: basic, diagnostic, and surgical aspects: a review (Book)", *Kugler Publications* (2003).

90. Tanzi, E. L.; Lupton, J. R.; & Alster, T. S. "Lasers in dermatology: Four decades of progress", *Journal of the American Academy of Dermatology*, **49**, 1–31 (2003).
91. Ossoff, R. H.; Coleman, J. A.; Courey, M. S.; Duncavage, J. A.; Werkhaven, J. A.; & Reinisch, L. "Clinical applications of lasers in otolaryngology - head and neck surgery", *Lasers in Surgery and Medicine*, **15**, 217–248 (1994).
92. Docchio, F.; Sacchi, C. A.; & Marshall, J. "Experimental investigation of optical breakdown thresholds in ocular media under single pulse irradiation with different pulse durations", *Lasers Light Ophthalmol*, **1**, 10 (1986).
93. Sacchi, C. A. "Laser-induced electric breakdown in water", *Josa b*, **8**, 337–345 (1991).
94. Vogel, A.; Linz, N.; Freidank, S.; & Paltauf, G. "Femtosecond-laser-induced nanocavitation in water: implications for optical breakdown threshold and cell surgery", *Physical review letters*, **100**, 038102 (2008).
95. Noack, J.; Hammer, D. X.; Noojin, G. D.; Rockwell, B. A.; & Vogel, A. "Influence of pulse duration on mechanical effects after laser-induced breakdown in water", *Journal of Applied Physics*, **83**, 7488–7495 (1998).
96. Vogel, A.; & Venugopalan, V. "Mechanisms of pulsed laser ablation of biological tissues", *Chemical reviews*, **103**, 577–644 (2003).
97. Vogel, A.; Noack, J.; Hüttman, G.; & Paltauf, G. "Mechanisms of femtosecond laser nanosurgery of cells and tissues", *Applied Physics*, **81**, 1015–1047 (2005).
98. Hosokawa, Y.; Yashiro, M.; Asahi, T.; & Masuhara, H. "Photothermal conversion dynamics in femtosecond and picosecond discrete laser etching of Cu-phthalocyanine amorphous film analysed by ultrafast UV–VIS absorption spectroscopy", *Journal of Photochemistry and Photobiology A: Chemistry*, **142**, 197–207 (2001).
99. Iino, T.; & Hosokawa, Y. "Direct measurement of femtosecond laser impulse in water by atomic force microscopy", *Applied physics express*, **3**, 107002 (2010).
100. Hosokawa, Y.; Iguchi, S.; Yasukuni, R.; Hiraki, Y.; Shukunami, C.; & Masuhara, H. "Gene delivery process in a single animal cell after femtosecond laser microinjection", *Applied Surface Science*, **255**, 9880–9884 (2009).
101. Okano, K.; Hsu, H. Y.; Li, Y. K.; & Masuhara, H. "In situ patterning and controlling living cells by utilizing femtosecond laser", *Journal of Photochemistry and Photobiology C: Photochemistry Reviews*, **28**, 1–28 (2016).
102. Nagrath, S.; Sequist, L. V.; Maheswaran, S.; Bell, D. W.; Irimia, D.; Ulkus, L.; Ryan, P. "Isolation of rare circulating tumour cells in cancer patients by

microchip technology", *Nature*, **450**, 1235 (2007).

103. Alix-Panabières, C. ; & Pantel, K. "Challenges in circulating tumour cell research", *Nature Reviews Cancer*, **14**, 623 (2014).
104. Dean, M.; Fojo, T.; & Bates, S. "Tumour stem cells and drug resistance", *Nature Reviews Cancer*, **5**, 275 (2005).
105. Qi, X.; Carberry, D. M.; Cai, C.; Hu, S.; Yuan, Z.; Rubinsztein-Dunlop, H.; & Guo, J. "Optical sorting and cultivation of denitrifying anaerobic methane oxidation archaea", *Biomedical optics express*, **8**, 934–942 (2017)
106. Iino, T., & Hosokawa, Y. "Controllability of femtosecond laser-induced impulse in water evaluated by local force measurement system using atomic force microscopy", *Journal of Applied Physics*, **112**, 066106 (2012).
107. Noack, J.; & Vogel, A. "Laser-induced plasma formation in water at nanosecond to femtosecond time scales: calculation of thresholds, absorption coefficients, and energy density", *IEEE journal of quantum electronics*, **35**, 1156–1167 (1999).
108. Fukumura, H.; & Masuhara, H. "The mechanism of dopant-induced laser ablation. Possibility of cyclic multiphotonic absorption in excited states", *Chemical physics letters*, **221**, 373–378 (1994).
109. Schmitt, F. J.; Renger, G.; Friedrich, T.; Kreslavski, V. D.; Zharmukhamedov, S. K.; Los, D. A.; & Allakhverdiev, S. I. "Reactive oxygen species: re-evaluation of generation, monitoring and role in stress-signaling in phototrophic organisms", *Biochimica et Biophysica Acta (BBA)-Bioenergetics*, **1837**, 835–848 (2014).
110. Antkowiak, M.; Torres-Mapa, M. L.; Dholakia, K.; & Gunn-Moore, F. J. "Quantitative phase study of the dynamic cellular response in femtosecond laser photoporation", *Biomedical optics express*, **1**, 414–424 (2010).
111. He, H.; Kong, S. K.; Lee, R. K. Y.; Suen, Y. K.; & Chan, K. T "Targeted photoporation and transfection in human HepG2 cells by a fiber femtosecond laser at 1554 nm", *Optics letters*, **33**, 2961–2963 (2008).
112. Tirlapur, U. K.; König, K.; Peuckert, C.; Krieg, R.; & Halbhuber, K. J. "Femtosecond near-infrared laser pulses elicit generation of reactive oxygen species in mammalian cells leading to apoptosis-like death", *Experimental cell research*, **263**, 88–97 (2001).
113. Tsen, K. T.; Tsen, S. W. D.; Sankey, O. F.; & Kiang, J. G. "Selective inactivation of micro-organisms with near-infrared femtosecond laser pulses", *Journal of Physics: Condensed Matter*, **19**, 472201 (2007).

Achievements

Journal publications

1. **Zhen-Yi Hong**, Takanori Iino, Hiroki Hagihara, Takanori Maeno, Kazunori Okano, Ryohei Yasukuni, Yoichiroh Hosokawa, "Cell damage evaluation of mammalian cells in cell manipulation by amplified femtosecond ytterbium laser", *Applied Physics A*, 124:268 (2018) — Relative to chapter 5
2. **Zhen-Yi Hong**, Yaxiaer Yalikun, Takanori Iino, Kazunori Okano, Dino Di Carlo, Ryohei Yasukuni and Yoichiroh Hosokawa, "Additive Structure in Microfluidic Channel to Optimize Laser-induced Impulse Loaded on Flowing Micro-objects", (To be submitted to *Applied Physics Express* in 2019) — Relative to chapter 7

Related journal publications

1. Lin Hui-Jen, **Zhen-Yi Hong**, Lee Yaw-Kuen and Liau Ian, "Fluorescent tracer of dopamine enables selective labelling and interrogation of dopaminergic amacrine cells in the retina of living zebrafish", *Royal Society of Chemistry Advance,* **6**, 71589-71595 (2016) — Relative to chapter 1
2. **Zhen-Yi Hong**, Yalikun Yaxiler, Takanori Iino, Kazunori Okano, Dino Di Carlo, Ryohei Yasukuni, Yoichiroh Hosokawa, "Femtosecond Laser-Activated High-Speed Manipulation Of Microparticles In Microfluidic Chip With Assistance of Modified Channel Structure", *Proceeding of International Conference on Miniaturized Systems for Chemistry and Life Sciences (μTAS)* (To be submitted in 2019) — Relative to chapter 7
3. Takanori Iino, Hiroki Hagihara, Takanori Maeno, Takeshi Yamakawa, **Zhen-Yi Hong**, Kazunori Okano, Sang Wook Lee, Keisuke Goda, and Yoichiro Hosokawa, "On-chip microfluidic fluorescence-activated cell sorting at 100,000 cells per second" (To be submitted to PNAS in 2019) — Relative to chapter 4

Peer reviewed international conference publications

1. "Additive Structure in Microfluidic Channel to Optimize Laser-induced Impulse Loaded on Flowing Micro-objects"
   Zhen-Yi Hong, Yalikun Yaxiler, Takanori Iino, Kazunori Okano, Dino Di Carlo, Ryohei Yasukuni, Yoichiroh Hosokawa
   2018 International Conference on Miniaturized Systems for Chemistry and Life Sciences (μTAS), Kaohsiung, Taiwan (Nov. 2018) [Poster, Acceptance rate 74%]

International conference publications
(Oral/Poster)

1. "High-speed sorting of micro-objects in microfluidics by Yb femtosecond laser"
   Zhen-Yi Hong, Hiroki Hagihara, Takanori Maeno, Takanori Iino, Kazunori Okano, Yoichiroh Hosokawa
   2016 77th Japan Society of Applied Physics (JSAP) Autumn Meeting (JSAP-OSA Joint Symposia), Niigata, Japan (Sep. 2016) [Oral]

2. "Development of high-throughput cell sorting utilizing femtosecond laser impulse: Evaluation of switching performance "
   Zhen-Yi Hong, T. Iino, H. Hagihara, T. Maeno, K. Okano, and Y. Hosokawa
   2017 Annual Meeting of the Physical Society of the Republic of China (PSROC), Taipei, Taiwan (Jan. 2017) [Oral]

3. "Development of high-throughput cell sorting system utilizing femtosecond laser impulse"
   Zhen-Yi Hong, Takanori Iino, Hiroki Hagihara, Takanori Maeno, Kazunori Okano, Ryohei Yasukuni, Yoichiroh Hosokawa
   2017 The 18th International Symposium on Laser Precision Microfabrication (LPM), Toyama, Japan (Jul. 2017) [Oral]

4. "Viability evaluation of cells in femtosecond laser driven cell sorter"
   Zhen-Yi Hong, Takanori Iino, Hiroki Hagihara, Takanori Maeno, Kazunori Okano, Ryohei Yasukuni, Yoichiroh Hosokawa
   International Conference of Laser Ablation (COLA) 2017, Marseille, France (Sep. 2017) [Poster]

International conference publications

(Co-auther)

1. "Development of High-Throughput Cell Sorting by Femtosecond Laser Impulse: Selection of Targeted Fluorescent Beads"
   Hiroki Hagihara, **Zhen-Yi Hong**, Takanori Maeno, Takanori Iino, Kazunori Okano, Yoichiroh Hosokawa
   Annual Meeting of the Physical Society of the Republic of China 2017 (PSROC 2017), Tamsui, Taiwan (Jan. 2017) [Poster]

2. "Development of Acoustic Cell Arrangement System in High-Speed Microfluidic Channel"
   Tomoyuki Suzuki, Daichi Fujita, **Zhen-Yi Hong**, Takanori Iino, Yoichiroh Hosokawa
   Annual Meeting of the Physical Society of the Republic of China 2017 (PSROC 2018), Taipei, Taiwan (Jan. 2018) [Poster]

Domestic presentation

(Oral/Poster)

1. "Dynamics of Micro-objects Caused by Femtosecond Laser-Induced Impulses in High-Speed Fluid: Evaluation of cell sorting system with microbeads"
   Zhen-Yi Hong
   The 1st TM Network Workshop in Goda ImPACT Program Meeting, Yamagata (Aug. 2016) [Oral]

2. "High-speed manipulation of micro-objects in microfluidics driven by femtosecond-laser induced impulses"
   Zhen-Yi Hong, Hiroki Hagihara, Takanori Maeno, Takanori Iino, Kazunori Okano, Yoichiroh Hosokawa
   GIST-NCTU-NAIST International Joint Symposium (GNN) 2016, NAIST (Nov. 2016) [Oral, Awarded with 2nd prize]

3. "Femtosecond Laser-Induced Jet Flow for Particle Manipulation in Microfluidic Chip with Assistance of Micro-Structure"
   Zhen-Yi Hong, Yalikun Yaxiler, Kazunori Okano, Dino Di Carlo, Yoichiroh Hosokawa

The 79th JSAP Autumn Meeting of Japan Society of Applied Physics 2018 (JSAP), Nagoa (Sep. 2018) [Oral]

4. "Femtosecond Laser-Induced Jet Flow for Particle Manipulation in Microfluidic Chip with Assistance of Micro-Structure"
   Zhen-Yi Hong, Yalikun Yaxiler, Kazunori Okano, Dino Di Carlo, Yoichiroh Hosokawa
   Symposium of PHC-JSPS Sakura Program, NAIST (Oct. 2018) [Oral]

Domestic presentation

(Co-auther)

1. ″フェムト秒レーザー誘起衝撃力を用いた高速細胞分取システムの性能評価″
   萩原宏規、飯野敬矩、洪振益、前野貴則、岡野和宣、細川陽一郎,
   第 77 回応用物理学会秋季学術講演会、朱鷺メッセ(新潟県)、2016 年 9 月

2. ″フェムト秒レーザー誘起衝撃力を用いた高精細な細胞分取システムの開発″
   萩原宏規、洪振益、前野貴則、飯野敬矩、岡野和宣、細川陽一郎
   応用物理学会関西支部 平成 28 年度第 2 回講演会「光・ナノ・バイオの融合 基礎～応用：エネルギーから医療まで」、関西学院大学（兵庫県）、2016 月 10 月

Award

1. GIST-NCTU-NAIST International Joint Symposium 2016 Oral presentation award (2nd prize)
   "High-speed manipulation of micro-objects in microfluidics driven by femtosecond-laser induced impulses"
   Zhen-Yi Hong, Hiroki Hagihara, Takanori Maeno, Takanori Iino, Kazunori Okano, Yoichiroh Hosokawa
   Nov. 28-29, 2016

Acknowledgements

It has been three years for me to do my research in the Bio-process Engineering Laboratory, Material Sciences, Nara Institute of Science and Technology. I still remembered the process how I joined this sweet group luckily. I received an invitation for enrollment interview for NAIST from *Yoichiroh Hosokawa* sensei under the assistance of *Kazunori Okano* sensei. In the whole process of interview preparation, Hosokawa sensei always kindly provided reference materials and required interview information by emails, and even held pre-interview practicing for me, which really took a long time. In assistance of Hosokawa sensei and all the group members, I relieve my stress and passed the interview. Moreover, as my first travelling abroad, Okano sensei gave me the full accompanying for the entire journey from my home country to Japan back and forth. In the welcome party after the interview, all the group members impressed my with their great friendliness, which truly broke the ice wall and diminished my worrying to be an international student.

Time really flies, especially happy time. I would like to begin by thanking my supervisor *Yoichiroh Hosokawa* sensei for the opportunity to work in his group and for all the support and guidance he has given me; particularly, for always making time from his busy schedule to help me out when needed.

I would also like to thank *Jun Ohta* sensei, *Hiroshi Daimon* sensei and *Hironari Kamikubo* sensei, my advisors in these three years for all the great suggestions and questions that inspired me what should be modified in my research plan.

I would also like to give special thanks to Professor *Dino Di Carlo* in Bioengineering department, University of California, Los Angeles for offering me a precious opportunity of two-month lab stay and assisting me to design my microfluidic chip with great advices.

I would also like to thank *Yalikun Yaxiaer* sensei for kindly helping on the fabrication of microfluidic chips and answering the entire relative question. Not only troubleshooting for experimental problems, Yalikun Yaxiaer sensei made me realize deeper about the qualification as a researcher, which let me evaluate my own potential in the academic field more concretely.

I would also like to thank *Takanori Iino* sensei for always kindly teaching how to prepare lots of trivial research materials such as research grant applications and presentation materials. Also for guiding me how to have long-term research planning and cooperate with others through effective communications.

I would also like to thank *Ryohei Yasukuni* sensei for helping me out when I encountered a ineffective communications on my researches. Great advices always led me out of the hard time.

I would also like to thank *Takeo Katayama* sensei for always kindly helping me on those trivial daily-life problems as an international student and often cheering me up as I felt down no matter because of research bottlenecks or personal issues.

I would also like to thank *Kazunori Okano* sensei to help me build up relationship with group members and give me a hand as my seat neighbor whenever I got a trouble.

I would also like to thank *Takanori Maeno* sensei to provide your skill support for cells culturing and biological experiments. In addition, the office was always lighted up thanks to your brimming happiness.

I would also like to thank *Sohei Yamada* sensei to refer great advices for my defense presentation.

I would also like to those graduates: *Hiroki Hagihara*, *Keisuke Fukita*, *Daiki Minamino*, *Tei Watanabe*, *Daichi Fujita* and *Yuuki Osikawa*. They always gave me supports of all kinds, no matter to my research or daily life. Particularly, thank to *Hiroki Hagihara* for not only being my daily-life tutor in the first few months after my arriving NAIST, but also for great cooperation on the researches together.

Also many thanks to *Keiko Tada* san, secretary in my group, for helping my deal with all the massive paper works.

At last, a great appreciation to *NAIST International Scholar program* for offering such a scholarship and *Nakatani Foundation* to support my attendance of academic conferences.